CHARACTERIZATION OF MICROFLUIDIC SHEAR-DEPENDENT IMMUNOCAPTURE AND ENRICHMENT OF CANCER CELLS FROM BLOOD CELLS WITH DIELECTROPHORESIS

A Dissertation

Presented to the Faculty of the Graduate School

of Cornell University

in Partial Fulfillment of the Requirements for the Degree of

Doctor of Philosophy

by

Chao Huang

August 2014

CHARACTERIZATION OF MICROFLUIDIC SHEAR-DEPENDENT
IMMUNOCAPTURE AND ENRICHMENT OF CANCER CELLS FROM BLOOD
CELLS WITH DIELECTROPHORESIS

Chao Huang, Ph.D.

Cornell University 2014

In this work, we investigate the effects of dielectrophoresis (DEP) on microfluidic im-
munocapture of prostate cancer and pancreatic cancer cells. We make novel measure-
ments of these cancer cells' DEP response, and characterize the combination of DEP and
immunocapture techniques as a function of shear stress in a Hele-Shaw flow cell with
interdigitated electrodes. At the same applied electric field frequency, we demonstrate
enhanced capture of cancer cells by attracting them to immunocapture surfaces with
positive DEP and reduced nonspecific adhesion of peripheral blood mononuclear cells
(PBMCs) by repelling them from immunocapture surfaces with negative DEP. Using
an exponential capture model, we show that immunocapture performance is dependent
on the applied DEP force sign and magnitude, cell and immunocapture surface chem-
istry, and shear stress experienced by cells flowing in the capture device. These data
inform the simulation of cancer cell and blood cell capture probabilities to design fu-
ture hybrid DEP and immunocapture device geometries with improved rare cell capture
performance.

BIOGRAPHICAL SKETCH

Chao "Charlie" Huang was born in Nanjing, China in 1988, and at the age of 3, immigrated with his family to North America, where they eventually settled in Seattle, WA after his father completed his Ph.D. and began a career as a telecommunications electrical engineer. In 2002, Charlie enrolled in the University of Washington's Early Entrance Program, and completed his B.S. in Bioengineering with College Honors and a minor in Mathematics from the University of Washington in 2008. During his undergraduate studies, Charlie worked on silver nanostructure synthesis and osteocyte network modeling research projects with Professors Younan Xia and Ted S. Gross, respectively, and also developed an interest in microfluidics through coursework with Professors Albert Folch and Paul Yager. Keen to design microfluidic technologies for biomedical applications, Charlie joined Professor Brian J. Kirby's research group at Cornell University in Ithaca, NY in late 2008 to pursue his Ph.D. in Biomedical Engineering, and in 2010, was awarded a National Science Foundation Graduate Research Fellowship to support his research on dielectrophoretic cancer cell capture.

Outside of his academic endeavors, Charlie has long had a deep passion for playing and writing music. He has played guitar and keyboards in amateur rock bands, and more recently, transitioned to working on music/video production with MIDI instruments on his own YouTube channel, which has attracted a sizeable subscriber base. In addition, having previously lived in Montreal, QC where he was effectively required by law to play ice hockey, Charlie still enjoys lacing up the skates every once in a while.

After completing his doctorate, Charlie will join Lawrence Livermore National Laboratory in Livermore, CA as a postdoctoral research staff member in the Materials Engineering Division. He is looking forward to working on a wide range of exciting research projects, as well as amazing weather and delicious Chinese food in California, as the second Dr. Huang in his family.

ACKNOWLEDGEMENTS

Above all, I need to thank my father, Jifu Huang, and mother, Jun Gao, for their unwavering support and sacrifices made to provide me with the numerous opportunities that I have had throughout my life. I am truly lucky to have such dedicated and hardworking parents as mentors and role models.

I would like to thank my Ph.D. advisor, Professor Brian J. Kirby, for his academic and professional guidance over the past 6 years. It has been an exciting, challenging, and rewarding experience working in his lab, and he has made countless efforts to help me grow and improve as an engineer, scientist, and academic professional. I would also like to thank my thesis committee members, Professors Susan Daniel and Robert S. Weiss, for their expertise and insight in clarifying scientific concepts and shaping the direction of my research. I have been very fortunate to have such a supportive and reliable thesis committee. In addition, I would like to thank Belinda Floyd, Marcia Sawyer, and Professor Peter Doerschuk for making everything run smoothly on the administrative side.

I would not have come close to completing my doctorate without the help and friendship of my colleagues at Cornell. Nitya Arasanipalai, Alex Barbati, Mike Bono, Tim Lannin, Erica Pratt, Steven Santana, Jim Smith, Fredrik Thege, and Professor Ben Hawkins from the Kirby Lab have all contributed immensely to my research, education, and professional development. Thank you for all of your brutally honest comments during lab meeting presentations! I must also thank Mo Chen, Piku Ghosh, Meng Li, Ming Li, Phong Nguyenle, Xavier Serey, Natasha Udpa, and Xiaohua Yang for commiserating with me over how tough graduate school, life, and especially the job search can be.

Finally, I would not be who and where I am today without all of my professors, advisors, and longtime friends from the University of Washington. I owe much gratitude to the Early Entrance Program staff for offering me a once-in-a-lifetime opportunity, and

TABLE OF CONTENTS

LIST OF TABLES

LIST OF FIGURES

ix

CHAPTER 1

INTRODUCTION

The isolation of circulating tumor cells (CTCs) from cancer patient blood is of particular interest to cancer researchers, as the enumeration of CTCs can serve as a prognostic indicator of cancer and predictor of patient survival [24, 55, 31, 28]. In addition, genetic and pharmacological evaluation of CTCs can lead to a better understanding of cancer metastasis as well as improved drug therapies [91, 156, 79, 132, 188]. Despite the rarity of CTCs in blood—as few as 1–100 CTCs per 10^9 blood cells—microfluidic "immunocapture" methods that immobilize cells via antibody or aptamer chemistry have reported high capture efficiencies; however, these methods are currently limited by low capture purities due to nonspecific adhesion of leukocytes to capture surfaces [126]. A high capture purity of CTCs is desirable because it can facilitate numerous subsequent biological analyses by reducing the amount of time and money that is potentially wasted on analyzing contaminating blood cells. For example, the yield from analyses that require single-cell sequencing, such as RNA sequencing to identify distinct CTC gene expression patterns [131, 188, 10, 79] and copy number variation analysis to characterize CTC provenance [136, 114, 125], is improved proportionally with increasing purity. Because existing immunocapture techniques, as well as others, are not able to deliver high CTC capture purities [126], in this thesis, we explore dielectrophoretic phenomena as an alternative or complementary method to isolate CTCs with high purity.

Dielectrophoresis (DEP) refers to the net electromigration of induced dipoles owing to interactions with an electric field gradient [122]. The DEP force is a direct function of particle or cellular properties such as size, charge, conductivity, and permittivity, and accesses a wide range of characteristics through the frequency-dependent dielectric properties of particle or cellular morphology and composition [72, 78]. For a more detailed

description of DEP physics and modeling, the reader is referred to Chapter 3. Briefly, when a particle is more polarizable than its suspending medium in a non-uniform electric field, positive DEP (pDEP) occurs, in which the particle is attracted to regions of high electric field gradients. In contrast, when the particle is less polarizable than its suspending medium, negative DEP (nDEP) occurs, in which the particle is repelled from regions of high electric field gradients. As such, DEP enables electrically controllable manipulation of particulate mineral, chemical, and biological analytes (e.g., mammalian cells) within a fluid suspending medium [109]. DEP is particularly well suited for use in microfluidic devices, as small electrodes that produce the electric field gradients may be integrated easily by inexpensive fabrication methods [167]. These DEP-activated devices have a wide range of research applications in the purification, enrichment, and characterization of environmental, biological, and clinical components [52]. For cancer cell isolation applications, specifically, previous research has shown that in certain applied electric field frequency ranges, a majority of cancer cell populations exhibit a pDEP response whereas blood cells exhibit a nDEP response [7, 43, 149], which can lead to high-purity separation. However, for rare cell capture applications, DEP methods are often limited by low capture efficiency and throughput, as it is difficult to bring rare cells in close proximity to electrodes where the DEP response is strongest [126].

Given that existing immunocapture techniques typically report high capture efficiencies but low capture purities, and DEP methods have the potential for high-purity separation by cancer cells' pDEP and blood cells' nDEP responses but are limited by low capture efficiencies in rare cell capture applications, we hypothesize that DEP can complement existing immunocapture techniques by acting only near capture surfaces where the electric fields are strongest and antibody interactions occur. Specifically, DEP can act to attract cancer cells to immunocapture surfaces by pDEP and also repel contaminating blood cells by nDEP [7, 185, 63, 43], therefore potentially increasing the capture

purity. To assess the feasibility and outcomes of combining DEP and immunocapture techniques, we design microfluidic DEP characterization devices to investigate and optimize relevant experimental parameters (e.g., electric field magnitude, frequency, antibody concentration, fluid flow conditions). The primary goals of this thesis are to (1) make novel measurements of cancer cells' DEP response to inform DEP separation parameters, and (2) characterize how DEP enhances or diminishes the immunocapture of cancer cells and blood cells, respectively, as a function of shear stress. These data inform the design of future hybrid DEP and immunocapture devices for CTC capture with high efficiency *and* purity, which will facilitate subsequent functional and genetic analyses of captured CTCs to elucidate cancer progression and develop improved treatment options.

In **Chapter 2**, we present a survey of literature of rare cell capture studies using either DEP or non-electrokinetic techniques. We evaluate these studies based on a panel of performance criteria, make suggestions for future improvements, and discuss how a combination of these techniques can potentially lead to enhanced capture performance.

In **Chapter 3**, we make novel measurements of the DEP response of a cultured prostate cancer cell line, LNCaP, and present a hybrid DEP and immunocapture Hele-Shaw flow cell system to characterize the effects of DEP on immunocapture with a highly prostate cancer-specific antibody, J591, as a function of antibody concentration, DEP magnitude and electric field frequency, and shear stress experienced by cells flowing in a typical immunocapture device geometry.

In **Chapter 4**, we extend our characterization work and demonstrate that LNCaPs can be enriched from peripheral blood mononuclear cells (PBMCs) with DEP. Specifically, we show that at the same applied electric field frequency, capture of LNCaPs is enhanced by attracting them to immunocapture surfaces with positive DEP, and nonspe-

cific adhesion of PBMCs is reduced by repelling them from immunocapture surfaces with negative DEP.

Finally, in **Chapter 5**, we characterize shear-dependent immunocapture of a panel of pancreatic cancer cell lines (Capan-1, PANC-1, and BxPC-3) that do not have an organ-specific biomarker and are typically captured with anti-EpCAM [133, 161]. We make novel measurements of pancreatic cancer cells' DEP response, demonstrate their enrichment from PBMCs with DEP, and use an exponential capture model to evaluate immunocapture performance as a function of applied DEP force sign and magnitude, cell surface EpCAM expression level, and shear stress experienced by cells flowing in the capture device. Importantly, we show that DEP can enhance the capture of cancer cells independent of their surface antigen expression levels, indicating that DEP methods may be especially useful for isolating cancer cells that are less likely to be captured by traditional immunocapture techniques.

The characterization data on combining DEP with immunocapture techniques presented in this thesis can be used in computational fluid dynamics studies [46, 153] to predict capture probabilities of cancer and blood cells under the influence of DEP in existing immunocapture geometries [45, 79, 161]. These simulation results will inform the design of future hybrid DEP and immunocapture rare cell capture devices with improved capture performance.

CHAPTER 2

RARE CELL CAPTURE IN MICROFLUIDIC DEVICES

2.1   Abstract

This article reviews existing methods for the isolation, fractionation, or capture of rare cells in microfluidic devices. Rare cell capture devices face the challenge of maintaining the efficiency standard of traditional bulk separation methods such as flow cytometers and immunomagnetic separators while requiring very high purity of the target cell population, which is typically already at very low starting concentrations. Two major classifications of rare cell capture approaches are covered: (1) non-electrokinetic methods (e.g. immobilization via antibody or aptamer chemistry, size-based sorting, and sheath flow and streamline sorting) are discussed for applications using blood cells, cancer cells, and other mammalian cells, and (2) electrokinetic (primarily dielectrophoretic) methods using both electrode-based and insulative geometries are presented with a view towards pathogen detection, blood fractionation, and cancer cell isolation. The included methods were evaluated based on performance criteria including cell type modeled and used, number of steps/stages, cell viability, and enrichment, efficiency, and/or purity. Major areas for improvement are increasing viability and capture efficiency/purity of directly processed biological samples, as a majority current studies only process spiked cell lines or pre-diluted/lysed samples. Despite these current challenges, multiple strides have been made in the development of devices for rare cell capture and the subsequent

elucidation of new biological phenomena; this article serves to highlight this progress as well as the electrokinetic and non-electrokinetic methods that can potentially be combined to improve performance in future studies.

2.2 Introduction

The isolation, fractionation, and capture of cells from suspensions has a wide range of applications, from the detection of bacteria [95, 180] to the enumeration of cancer cells [43, 14, 113]. The benefits and limitations of flow cytometers, immunomagnetic separators and other macro-sized sorting equipment have been studied extensively in experimentation and in review [117, 15, 84] when compared to the abilities of microdevices. This article focuses on devices and techniques with potential to analyze cells that are typically found at low concentrations in suspension; such devices are currently used, or have the potential to be used, for applications in environmental pathogen detection [86, 187] and cancer cell isolation from patient blood samples [45]. The discussion is divided into sections that detail two major classifications of microfluidic approaches, non-electrokinetic and electrokinetic, followed by a summary of performance criteria by which these methods are evaluated; studies that focused on quantifying these performance specifications are highlighted in tables at the end of the article. While rare cell capture is the ultimate motivation of this paper, many of the described methods exist only as proof-of-concept studies. Thus, this article serves to highlight both the progress made in using microfluidic devices for rare cell capture and the techniques that may contribute to rare cell capture in the near future.

2.3 Non-electrokinetic methods

This section focuses upon non-electrokinetic methods of cell isolation, capture, or fractionation from a suspension. As such, it lends itself naturally to organization by sorting technique. Each sorting methodology is further subdivided into cell separations of interest: blood cell fractionation, cancer cells, other mammalian cells, and prokaryotes and viruses.

Blood cell fractionation, as defined here, focuses on isolation of cell types native to circulation. Most of the studies described here revolve around the capture or elimination of white blood cells (WBCs). WBCs are of value in many diagnostic assays and studies of disease progression, but they must first be separated from the bulk blood suspension. However, WBC concentrations are low as compared to red blood cells (RBCs), roughly 1 to 1000 [112, 166]. Conversely, for the purpose of leukemia treatments, blood transfusions, etc, it is vital to eliminate WBCs as a source of contaminantion [144].

Studies for the isolation of cancer cells focus upon approximating, or capturing, circulating tumor cells(CTCs), which can be found in the circulation of cancer patients [113, 45, 157]. CTCs have been used as prognostic indicators of patient survival [29] as well as representative tissue for genetic analyses [157]. CTCs are 10^6 rarer than WBCs, making their capture particuarly challenging [113, 1, 45].

Non-electokinetic microfluidic techniques have also been applied to study other mammalian cells. Applications are quite disparate, ranging from sorting of cells based on stages of cell cycle [19] to isolation of fetal nucleated red blood cells (nRBCs) from maternal blood [61, 106, 107].

2.3.1 Immobilization via antibody or aptamer chemistry

The microfluidic devices discussed in this section take advantage of biochemical interactions to enhance rare cell capture or fractionation. Immunocapture is a technique frequently used in the extraction of cells, viruses, and proteins from suspension. It employs anti-sera to target biological agents of interest. In rare cell isolation, immunocapture presents an opportunity to separate cells with extremely high specificity from a suspension, in a viable state. In practice, this technique is analogous to microscale affinity chromatography for cells possessing unique markers or characteristics [120].

Blood cell fractionation

Chang et al. studied the effect of microfludic structures on white blood cell (WBC) adhesion using different pillar geometries and orientations. They compared square and rhombic arrays with square and ellipsoidal micropillars, respectively. The micropillars were physisorbed with E-selectin to identify different leukocyte model cell lines (in cell media) via adhesive rolling speeds. Cell rolling velocities were two times as high in rhombic arrays, resulting in 130- to 160-fold enrichment, as opposed to 200-fold enrichment in square arrays. By comparing microarray geometries under identical flow and immunocapture conditions, Chang et al. demonstrated that the type of pillar geometry alone influenced cell adhesion mechanics and, by extension, isolation [13].

In contrast, Murthy et al. focused upon the effects of shear stress on leukocyte adhesion mechanics. They studied the effects of shear stress using a Hele-Shaw flow cell with a device geometry that created a linear variation in shear stress along its axis (see Figure 2.1C). The researchers used anti-CD5, anti-CD19, and PEG to isolate T- and B-lymphocytes from a heterogeneous PBS suspension. Non-target cells were depleted
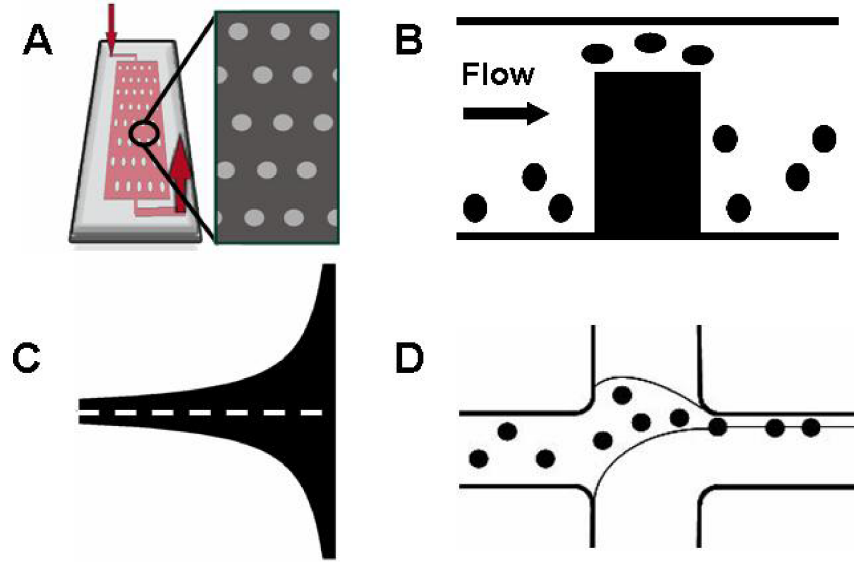
Figure 2.1: (A) Schematic of an micro-pillar device's architecture. Adapted from [45]. (B) Schematic of a Weir microfilter's operation. Adapted from [70]. (C) Example of a Hele-Shaw flow cell where the dotted line is the region of linearly increasing shear. (D) Schematic of a sheath-flow based separation system. Adapted from [180].

from heterogeneous mixtures, resulting in suspensions that were 97% pure [112]. Sin et al. extended this work to blood, and studied the effects of suspension density on cell binding and the time-scale of cell-antibody kinetics. Within three minutes they obtained 100% and 75% pure suspensions of T-lymphocytes and B-lymphocytes, respectively [151]. Wang et al. also captured T-lymphocytes using anti-CD3-coated micropillars. They surrounded their pillars with segmented curved walls to increase the range of shear stresses experienced by the cells. Using this technique, they were able to isolate T-lymphocytes spiked in blood with 80% efficiency [177]. These studies, in combination, demonstrated that the fluid mechanics of microfluidic devices influence efficient immobilization in addition to antibody/apatamer specificity.

Cancer cells

Many microfludic devices take advantage of the 3D structure of channels to increase the surface area available to be coated with the antibody or aptamer of choice. Du et al. demonstrated the efficacy of this technique in straight microchannels by differentially capturing human mammary epithelial cells and breast cancer cells by use of epithelial membrane antigen (EMA) and epithelial growth factor receptor (EGFR) [37]. The sensitivity of capture to antibody dilution alone was also demonstrated using the same device geometry. Using this isolation technique, their capture rates from a PBS suspension ranged up to 30%. Xu et al. used DNA aptamers within an S-shaped microfluidic device [181] to capture cancer cells from PBS. Using aptamers targeted to various leukemia and lymphoma cell lines lines, their device efficiencies ranged from 50-83% with 88-97% purity. Recent work by Wang, et al. on silicon nanopillars (SiNPs) indicated that the topology of the microdevice itself may contribute greatly to the efficiency of rare cell capture. Comparing EpCAM functionalized SiNPs and flat surfaces, there was approximately 6-fold increase in capture efficiency, from 4-14% to 45-65% [171].

Cancer cells have also been captured from blood-based systems. Liu et al. used nickel micro-pillars to immobilize functionalized superparamagnetic beads to create a capture zone within their microfludic devices. Using magnetic fields, they then immobilized and released an immortalized lung cancer cell line mixed with human RBCs. This method produced 133-fold enrichment with 62-74% capture efficiency [95]. Adams et al. observed cell margination along the walls of linear channels when working with whole rabbit blood. They hypothesized that this reduced the rate of cell-antibody interactions in their devices [1]. This phenomenon was no longer seen when straight-walled channels were exchanged for sinusoidally varying ones. In combination with

anti-epithelial growth factor receptor (EpCAM) antibodies, Adams et al. achieved immortalized breast cancer cell capture efficiencs of 97%. The device was translated to the capture of model prostate cancer cells spiked in PBS, using anti-prostate specific membrane antigen(PSMA) aptamers with an efficiency of 90% [34].

While the prior studies worked with model cell lines spiked in buffer solution [37, 181, 34, 171] or blood systems [95, 1, 113, 45], this method has also been used for cancer patient blood samples [113, 45]. Nagrath et al. used a dense array of micropillars coated in EpCAM to increase the number of cell-antibody interactions for a given suspension volume. Using this approach, they isolated lung, prostate, pancreatic and other cell lines from blood samples with average effiency and purity of 65% and 50% respectively [113]. Recently, Gleghorn et al. used computational modeling to design micro-pillar arrays such that cell-antibody interactions were size-dependent. Using microdevices functionalized with anti-PSMA antibodies, prostate cancer cells were captured at efficiences of 85-97% with purities of 68% [45] (see Figure 2.1A).

Other mammalian cells

Plouffe et al. used previously discussed microfluidic devices [112, 151] to selectively isolate endothelial cells (ECs) and smooth muscle cells (SMCs) from suspension. They coated their devices with peptides (REDV and VAPG) targeted to ECs and SMCs, and investigated binding to target cells as a function of shear stress. Using these peptide sequences, they differentially isolated ECs and SMCs from homogenous and heterogenous suspensions with purities of 86% and 83%, respectively [120]. Plouffe et al. further demonstrated the feasibility of peptide-based capture systems by using a 3-stage isolation system to deplete heterogenous suspensions of ECs, SMCs and fibroblasts [121]. Using this system, they were able to achieve 96% to 99% depletion of the three different

cell types with over 97% viability of non-immobilized cells. Their work agreed with results on shear-dependent cell capture discussed previously [112, 151], showing this relationship to be true regardless of cell type.

2.3.2 Size-based sorting

Size-based sorting affords the ability to capture target cells without knowledge of the target cell's biochemical characteristics. This is an attractive option if the target cell's size is extreme in relation to its medium and also if the cell's properties are not well understood. Many approaches have been used to attempt size-sensitive isolation, ranging from size-dependent transport through small geometries to size-dependent particle pathlines in open obstacle arrays [68, 165, 166, 144, 151, 30, 70].

Blood cell fractionation

Much research has been done to develop microfludic platforms to fractionate blood components, particuarly WBCs, based on size. Sethu et al. developed a microfluidic diffusive filter for WBC depletion from whole human blood. The system allowed biconcave red blood cells (RBCs) egress from the main device while larger WBCs were retained. The filtration elements were placed on the sides of the main channel, to minimize clogging by distributing RBC egress points along the length of the channel rather than focusing it in one area. To maintain equivalent volumetric flow rates in each segment, they used a flared geometry designed using Hele-Shaw analysis.Using this diffusive filter technique, over 97% WBC depletion was achieved [144].

Ji et al. reviewed various other microfludic filtration techniques for the application

of WBC depletion. They found that pillar filters and cross-flow filters had high WBC depletion rates and could be used to process large sample volumes [70]. VanDelinder et al. also investigated cross-flow filters for WBC depletion, but also observed that RBC clogging hindered performance. They subsequently attempted WBC isolation using repeated microfluidic array geometries, achieving 98% WBC retention from human blood with no RBC lysis [165, 166].

Davis et al. and Inglis et al. used microfludic devices featuring pillars. Rather than using the pillars to create microfludic slits to obstruct larger cell flow, they used the micropillars to create particle-size-dependent pathlines such that target cells were sorted into predetermined outlet ports based on size alone [30, 68]. Using this technique, Davis et al. depleted lymphocytes and monocytes from blood with 100% efficiency and Inglis et al. were able to separate lymphocytes from diluted blood suspensions with 73% effieciency.

Cancer cells

Zheng et al. developed paralyene microfilters for the isolation of immortalized prostate cancer cell lines. Using pressure-driven flow to force cell suspensions through the filter, their cell recoveries ranged from 87% to 89% [191]. Cells retained on the microfilters were lysed for genomic analysis. Chen et al. used a combination of experimental results and physical modeling to develop a weir filter to selectively isolate cancer cells based upon their deformability [14] (see Figure 2.1B). Using a filter fabricated specifically for their model lung adenocarcinoma cells, they were able to achieve over 99.9% capture efficiency from diluted human blood samples.

Other mammalian cells

Mohamed et al. also used pillar filters for the goal of isolating fetal nucleated red blood cells (fNRBCs) from maternal blood [107].The pillars were placed to create succesively narrower channels in the device such that cell capture between pillars was a function of size and deformability. RBCs and fNRBCs were isolated from goose blood and cord blood samples, respectively. Mohamed et al. reported no significant clogging using this staged pillar technique; however, blood samples were diluted pre-isolation. Huang et al. separated NRBCs based on size-dependent pathlines as described previously [30, 68]. Their device successfully eliminated over 99% of RBCs; NRBCs were further purified from contaminating WBCs by use of magnetic separation. Huang et al. sucessfully enriched NRBCs by a factor of 10- to 20 more than previously reported techniques [61].

2.3.3 Sheathflow and streamline sorting

These devices take advantage of the fluid flow associated with the imposition of certain geometries or parallel fluid flows of different flow rates to passively sort or segregate target cells (see Figure 2.1D). This is another label-free and chemistry-free method of cell isolation that is most commonly used when size differences between cells is significant.

Blood cell fractionation

SooHoo et al. used a microfluidics-based aqueous two-phase system (ATPS) to enrich leukocytes from blood suspension. Using one stream of polyethylene glycol (PEG) and one of dextran (DEX), with Zap-oglobin as the lysing agent, they achieved 100% RBC depletion from human blood samples [154]. Zheng et al. developed devices based on

T-shaped bifurcated channels to separate WBCs from RBCs. By adjusting the length of the T-channel, and the vertical distance between upstream and downstream side walls, cells were directed to different stream lines based on size alone. They were able to separate WBCs from diluted blood with 97% efficiency. However, they found that RBC orientation heavily influenced the segregation of small WBCs from RBCs [192].

Other mammalian cells

Kuntaegowdanahalli et al. used spiral microchannels to segregate cells based on size across the width of their devices. Using a five-loop system, they sorted neuroblastoma cells from glioma cells with 80% efficiency [85]. The cells were then placed in culture and exhibited 90% viability after sorting. Lin et al. used multiple sheath flows in parallel to sort yeast cells from suspension. They used two streams of unequal flow rate to achieve a focusing effect and were able to separate yeast cells with 87.7% efficiency and 94.1% purity [93].

In contrast, Choi et al. used a series of slanted microfluidic channels of periodically varying heights to sort cells by cell-cycle phase. The slanted obstacles generated streamlines that diverted cells transverse to the flow, towards the wall of the device. There, the cell-obstacle interactions diverted larger cells out of the transverse streamlines, keeping them near the wall, while smaller cells diverged from the wall [19]. They achieved lateral separation of G_0/G_1 phase and G_2/M phase monocyte model cells with over 4-fold G_2/M cell enrichment.

Prokaryotes and viruses

Wu et al. used sheath flows to sort *E. coli* from blood. High concentrations (greater than 10^8cells/ml) of *E. coli* cells were spiked into diluted human RBCs and were enriched 300-fold over the course of separation. They demonstrated a sorting efficiency of 62% and purity of 99.87%. The bacteria were expanded in culture and exhibited over 95% viability [180].

2.4 Electrokinetic methods

Electrokinetic methods comprise those methods that use electric fields to actuate cells. In microfluidic devices, the two most widespread electrokinetic techniques for manipulating cells are electrophoresis and dielectrophoresis. Electrophoresis refers to net migration due to the action of an electric field on the net fixed charge of a particle. This technique has been used to study cells at the membrane level [104], and methods such as capillary electrophoresis and microfluidic free-flow electrophoresis have been developed to separate different populations of biomolecules, viruses, bacteria, and eukaryotic cells [81, 162]. However, as the net charge of a cell's electrical phenotype is often not specific enough to distinguish between a mixture of different cells, electrophoresis has been used minimally as a cell separation technique and is not suited for applications in rare cell capture. Thus, this review will focus primarily on dielectrophoretic techniques.

Dielectrophoresis (DEP) refers to the net migration of polarized particles owing to interactions with an electric field gradient, and depends on cell wall, membrane, and cytoplasmic electrical properties [72, 78]. The DEP force is a direct function of these electrical properties as well as cell size, the electrical properties of the fluid medium,

and the magnitude and frequency of the applied electric field; the dependence on this wealth of parameters makes DEP an attractive tool for distinguishing between different cell types [167, 52]. DEP response is classified into two regimes: when particles are more polarizable than the medium, positive DEP results and the particles are attracted to stronger field regions; conversely, when particles are less polarizable than the medium, negative DEP results and the particles are repelled from stronger field regions; the frequency at which the DEP force switches from one regime to the other (i.e. when the force is zero) is termed the "crossover frequency" [72, 109]. The sign and magnitude of the DEP force provides the basis for DEP cell separation techniques, and this review will cover the most common device geometries used for these techniques. The scope of this review on DEP methods will be limited to those used for capture, separation, or concentration of bulk cell populations; DEP methods for single cell capture or manipulation are covered in other reviews [167, 52, 5, 73, 189]. The DEP methods are organized by the type of device geometry used; each section includes a brief description of the physics associated with the technique and a summary of how it is applied to separate different cell types with a view towards pathogen detection, blood fractionation, or cancer cell isolation. Many DEP experiments have used model systems to characterize geometric performance, or as mockups of rare cell capture experiments. Thus, this section includes many devices that do not capture rare cells, but whose performance informs the potential for rare cell capture with DEP.

2.4.1 Electrode-based DEP

Microfabricated electrodes are the most common and practical method for creating the non-uniform electric fields necessary for DEP. While potential limitations to the use of electrode-based DEP include fouling and electrolysis at low electric field frequencies as

well as increased fabrication time and cost required for more complex electrode configurations, a majority of DEP techniques use microfabricated electrodes owing to their simplicity and flexibility in implementation. The following sections will cover the most common and simple device geometries used for cell separation.

Interdigitated array (IDA) electrodes

Interdigitated arrays consist of spatially alternating sets of grounded and energized electrodes that create non-uniform electric field regions and trap particles against a flow via positive DEP (Figure 2.2A). IDA electrodes are one of the most commonly used electrode configurations because their use entails minimal design parameters (electrode length and width, inter-electrode distance, and channel depth) and experimental parameters (flow rate, electric field magnitude and frequency), and yields analytical solutions for electric fields and particle motion [158]. IDA electrodes are typically used for "binary" cell separation; an electric field is applied to capture the target cells from a mixture of two or more cell types via positive DEP, the non-target cells are minimally affected by the field or repelled via negative DEP and are flushed out of the device, and finally the field is turned off to release the target cells for separate collection. Through DEP characterization, a frequency regime can be selected in which one cell type is attracted to the electrodes (positive DEP) while another cell type is repelled into the regions separating the electrodes (negative DEP). Rare cell capture requires that all non-target cells be repelled, which can be demanding if the suspension is complex.

IDA electrodes have been used to separate or concentrate bacteria for potential applications in pathogen sensing. Typical cell concentrations used for these studies lie in the range of 10^5 to 10^9 cells/mL. Efforts to detect foodborne pathogens such as those in the genus *Literia* include separation of live and heat-treated *L. innocua* with 90%

18
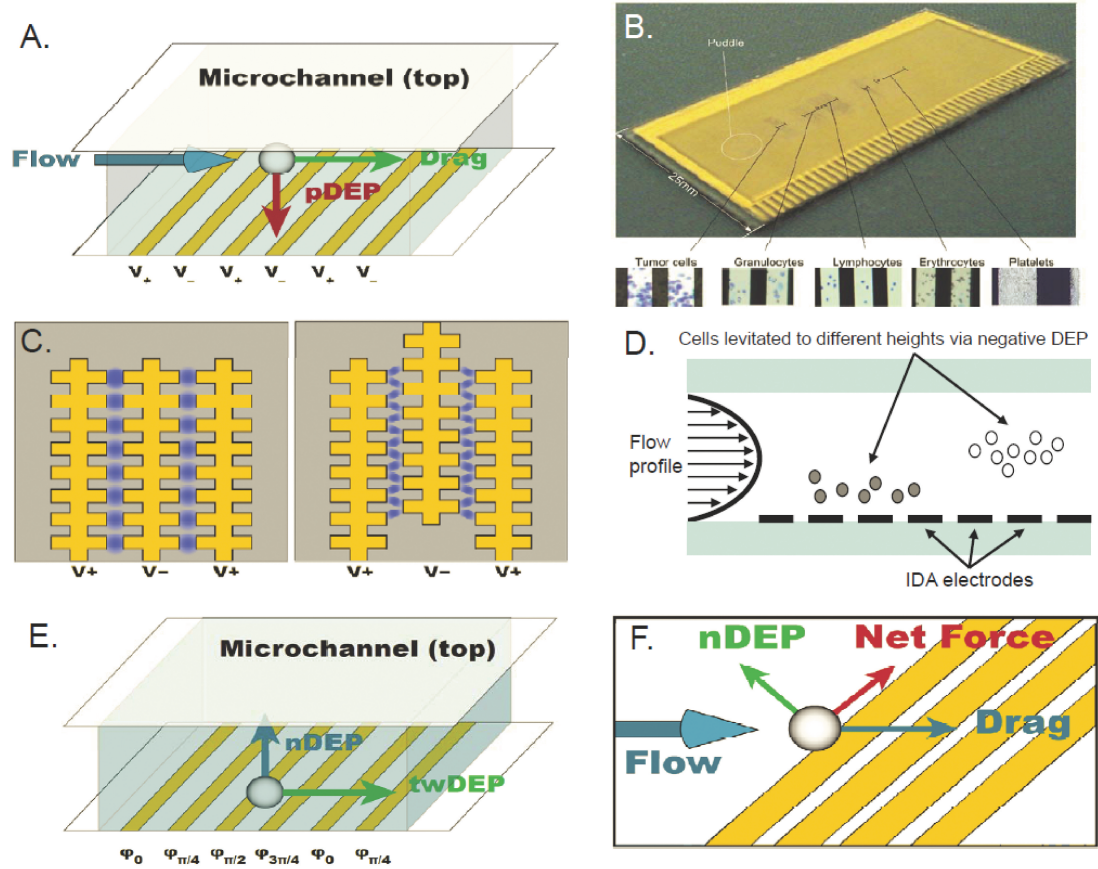
Figure 2.2: (A) Interdigitated array (IDA) electrodes. (B) Electrosmear slide showing fractionation tumor cells and blood components. Reproduced from [25]. (C) Castellated IDA electrodes. (D) DEP field-flow fractionation operates by levitating cells against gravity to different heights in the channel via negative DEP, allowing separation to be achieved based on their differing flow velocities. (E) Configuration and forces in a twDEP electrode array. (F) Summation of forces near an angled electrode.

efficiency; as the cell membrane becomes permeable upon death, large changes in conductivity can result in differences in the DEP response of live and dead cells [92]. Researchers have also used positive DEP to attract a mixture of *Listeria* and *Escherichia* species to antibody-coated electrodes and selectively capture only *L. monocytogenes* (i.e. immunocapture) with 87-92% efficiency [187, 80]. To aid efforts in detecting environmental pathogens, researchers have demonstrated concentration of *Bacillus subtilis* spores (a surrogate bacteria used for research on *Bacillus anthracis*, i.e., anthrax) from airborne environmental samples containing diesel particulate matter with up to 60%

purity; appropriate frequency ranges for separation were selected based on crossover frequency measurements [39]. Additionally, Gadish et al. concentrated *B. subtilis* by integration of a chaotic mixer to bring the spores into closer proximity with the IDA electrodes and enrich the sample ninefold [41], and Liu et al. captured *B. anthracis* with 90% efficiency for impedance measurements in order to detect viable spores electrically by their germination [97].

IDA electrodes have also been used for blood fractionation. Cristofanilli et al. used an "electrosmear" slide that was coated to promote cell adhesion and patterned with IDA electrodes to which different electric field frequencies were applied along the length of the device [25]. Near the inlet port, a low frequency was applied to levitate all cells via negative DEP to avoid adhesion to the slide, and as the blood sample obtained from a murine aspiration biopsy was flowed further along the device, different constituents of blood as well as biopsied tumor cells from a cancer line grown in nude mice were pulled toward and adhered to the electrodes via positive DEP in different regions of the slide, based on their previously characterized dielectric properties (Figure 2.2B) [25].

Castellated IDA electrodes

Castellated electrode arrays consist of interdigitated electrodes with width variation along their length, which create alternating regions of high and low electric field magnitude at the tips of the electrodes and the regions separating each electrode, respectively (Figure 2.2C). The advantage of castellated electrodes is the localization of high electric field regions, which can be used to trap or concentrate flowing cells in the device effectively. The procedure for cell separation using castellated electrodes is the same as that used with straight IDA electrodes; this procedure has been used for binary separation of a mixture of two bacteria types, including yeast, *E. coli*, and *Micrococcus lysodeikti-*

cus [101], as well as for separation of viable and non-viable yeast cells [102]. Optical absorbance of DEP trapping was measured to calculate the effective conductivity of the cells and predict their DEP response.

Castellated IDA electrodes have been used for cell separation between bacteria and blood cells for applications in pathogen detection, with typical cell concentrations of 10^6 to 10^7 cells/mL; researchers have demonstrated separation of *M. lysodeikticus* from erythrocytes based on their differing dielectric properties [172]. Isolation of erythrocytes infected with malaria pathogen from healthy erythrocytes was also achieved with 90% efficiency owing to the sharp increase in membrane conductivity of erythrocytes hosting malarial parasites [42]. In addition, Huang et al. demonstrated simultaneous separation of multiple bacteria (*Bacillus cereus, E. coli, L. monocytogenes*) from diluted blood with up to 97% efficiency using size-based DEP separation and post-separation PCR analysis [64].

Castellated IDA electrodes have also been used for applications in cancer cell isolation. Becker et al. characterized the dielectric parameters of cultured breast cancer cells, lymphocytes, and erythrocytes using particle electrorotation techniques, and subsequently trapped the breast cancer cells from a suspension of diluted blood, demonstrating up to 95% purity in captured cancer cells [7]. More recently, Tai et al. developed an automatic platform for separation of viable and non-viable cultured human lung cancer cells based on differing dielectric properties with 81-84% efficiency and nucleus collection for nuclear protein extraction [159]. While castellated IDA electrodes are similar in function and application (e.g. binary sorting) to straight IDA electrodes, their ability to create alternating regions of high and low electric field magnitude makes them better suited for concentrating samples or patterning particles at a specific location than straight IDA electrodes. As is the case for straight IDA electrodes, the challenge associ-

ated with castellated IDA electrodes is in finding a frequency or set of frequencies such that only the rare cells are attracted to the electrodes.

IDA electrodes for flow-field fractionation

In DEP flow-field fractionation (DEP-FFF), IDA electrodes are fabricated on the bottom of a device channel, and flowing particles of differing dielectric properties are levitated against gravity via negative DEP. The levitated particles equilibrate to different heights in the channel owing to the distinct DEP force on different types of particles, and these differing heights allow separation to be achieved by sequential collection based on different flow velocities due to the parabolic velocity distribution of low-Reynolds-number Poiseuille flow (Figure 2.2D). The velocities of different cells can be characterized by measuring cell elution fractograms as a function of frequency [63]. The main advantage of DEP-FFF is its ability to achieve continuous-flow separation of bioparticles with size and/or dielectric differences under a constantly applied electric field, therefore avoiding the need for activation and deactivation of the field as required by binary sorting devices.

DEP-FFF has been used often as a technique to separate different cell types in blood, with cell concentrations ranging from 10^5 to 10^7 cells/mL. Researchers have demonstrated separation of erythrocytes from latex beads and characterization of their different levitation heights [135], as well as binary separation of human leukocyte subpopulations (T-, B-lymphocytes, monocytes, and granulocytes) based on differing membrane dielectric properties with 87-98% purity, which can be used for clinical applications in differential analysis of leukocytes [184]. More recently, Hashimoto et al. performed selective capture of neutrophils and eosinophils from a mixed leukocyte suspension with 80% efficiency by deflecting the target cells away from the IDA electrodes and toward an antibody-coated layer on the opposite wall [51]. DEP-FFF also has been used ex-

tensively for the separation and isolation of cancer cells. In particular, the Gascoyne research group has demonstrated separation of cultured human leukemia cells from diluted blood after characterizing the cells by DEP levitation experiments [62], separation of cultured human breast cancer cells from whole blood based on measured differences in cell size and membrane capacitance [185, 43], and separation of cultured human breast cancer cells from normal T-lymphocytes and hematopoietic CD34+ stem cells [63, 176], all with efficiencies and/or purities over 90%.

In more recent years, DEP-FFF has been used for a larger variety of applications as well as in different device geometries. These applications include separation of cells with high and low embryogenic potential in suspension cultures of carrot based on their differences in size and cytoplasm density [38], toxicity testing by dielectric characterization of cultured human leukemia cells with membrane dissimilarities due to exposure to various toxic agents [127], and enrichment of a progenitor cell population in a mixture of cell debris and erythrocytes from freshly harvested adipose tissue [168]. Finally, vertical IDA electrodes have been fabricated on the sidewalls of the device channel (as opposed to horizontal electrodes on the bottom of the channel) to achieve lateral separation through separate outlets. This device geometry has been used to separate mammalian cells of different sizes [171] and viable from non-viable yeast cells [9], as well as to enrich *Babesia bovis*-infected erythrocytes sevenfold [9]. Unlike trapping on straight or castellated IDA electrodes, DEP-FFF allows cells to be separated based on the magnitude of the DEP response rather than just the sign of the response, and rare cell capture can be achieved in theory if the DEP response of a cell can be distinguished within the sensitivity of the device.

IDA electrodes for traveling-wave DEP

IDA electrodes have been used for a technique called traveling-wave DEP (twDEP) to fractionate bioparticles. The electrodes are independently driven with different electric field phases, and particles are levitated against gravity owing to negative DEP (Figure 2.2E). Fractionation is achieved by varying the electric field phases to drive the particles transverse to the direction of flow at different velocities. Cui and Morgan detailed the design and fabrication of a twDEP device and demonstrated particle motion using polystyrene latex particles [26]. The main advantage of twDEP is that fractionation may be achieved based on the particles' differing velocities alone; there is no need to drive fluid flow or to trap or concentrate particles via positive DEP.

Building on the successful implementation of twDEP on polystyrene beads, a number of biological separations have been achieved. Bacteria separation has been demonstrated by use of viable and non-viable yeast cells [160, 83]; as well, blood fractionation has been demonstrated by separating T-lymphocytes and erythrocytes by applying multiple frequencies to direct the cells to move in opposite directions such that they were collected separately through different outlets [98]. twDEP has also been used for applications in pathogen detection; a spiral electrode array was characterized and used for a 1000-fold enrichment of malaria-infected erythrocytes from normal erythrocytes with 90% purity [175, 42]. Application of the traveling field caused normal erythrocytes to be trapped at the electrode edges via positive DEP, while infected cells were levitated via negative DEP and carried to the center of the spiral [42]. More recently, Cheng et al. developed a high-throughput 3D twDEP device used for focusing and sorting particles, and demonstrated its ability to separate bacteria and blood cells based on DEP mobility magnitude as well as direction [17]. Other recent studies used twDEP for characterization of cultured lymphoma and myeloma cells for potential applications in rare

cell capture [12] and the development of a DEP pump for blood delivery in microfluidic devices [90].

Angled electrodes

Angled electrodes are most often used for binary separation of bioparticles or to create localized particle pathlines due to the particles' negative DEP mobilities. As the particles approach an electrode, the negative DEP force that acts on them can exceed drag forces, resulting in a net force parallel to the electrodes. Particles then travel along the length of the electrode until drag forces exceed the DEP force, at which point the particles can flow past the electrodes (Figure 2.2F). Displacing particles transverse to the direction of flow allows angled electrodes to preferentially direct particles to different outlets or focus them into concentrated streams.

Angled electrodes have been used to sort and concentrate various bacterial samples. Cheng et al. designed a device with 3D electrode gates to focus and separate yeast and *E. coli* into different outlets, after which surface-enhanced Raman scattering was used to detect bacteria concentration and evaluate efficiency [16]. Kim et al. tagged *E. coli* with different sized microspheres and used angled electrodes to separate the two target cell types into different outlets, after which capture efficiency and purity was evaluated using flow cytometry [75]. More recently, a magnetic separation module was incorporated into the device to capture magnetically-tagged cells and separate them from unlabeled non-target cells, which improved the device's ability to separate multiple cell types [77]. Vahey and Voldman developed a separation method termed "isodielectric separation," which uses a diffusive mixer to establish an electrical conductivity gradient across the width of a channel containing angled electrodes [164]. DEP forces vary along the length of the electrodes, which direct and separate viable and non-viable yeast cells across

the device in the direction of decreasing conductivity until they reach their respective isodielectric points, where there is no net force [164].

Angled electrodes have also been used for binary sorting of mammalian and blood cells. To address the need for a noninvasive method for sorting cell populations according to their cell-cycle phase, Kim et al. separated cultured human breast cancer cells based on their differing sizes due to their cell cycle phase [?]. Angled electrodes were also used to demonstrate a low-stress platelet size-based DEP separation technique by separating platelets from diluted whole blood with 95% purity [124].

2.4.2 Insulative DEP

Insulative DEP techniques rely on constrictions or expansions in channel geometry to generate electric field non-uniformities and deflect or trap bioparticles via negative DEP. While this approach places limits on the frequencies and geometries used, the main advantage of insulative DEP is that no internal electrodes are used. This leads to simpler device fabrication, reduced propensity for fouling, and the possibility of using a DC field for electrokinetic particle transport as well as trapping via DEP [87].

Angled and curved constrictions

The simplest geometry in an insulative DEP device is a perpendicular insulative constriction in the device channel. Kang et al. demonstrated size-based separation of live cells by using rectangular constrictions to deflect larger cells (white blood cells and cultured mammalian breast cancer cells) via negative DEP to a different trajectory than smaller blood components (red blood cells, platelets) [74]. Binary sorting is achieved

by fabricating two outlet channels for the separate trajectories.

Extending the basic principles of rectangular constrictions, angled constrictions have also been used to separate and concentrate bioparticles. The DEP force acting perpendicular to the constriction depends on the angle that the constriction forms with the channel. If this DEP force is smaller than the drag force, then particles will flow past the constriction unaffected; if, however, the DEP force exceeds the drag force, then the particles are stopped at and deflected parallel to the constriction. Angled constrictions have been used to demonstrate size-based separation of *B. subtilis* from polystyrene particles [6]. Curved constrictions, in which the angle of constriction varies continuously across the channel, have also been used to separate different sized particles (Figure 2.3A) [54].

Post arrays

DEP trapping using an array of insulating posts was reported by Cummings and Singh, who investigated various geometric variables that affect the electric field, including post shape, distance between posts, and array angle to the applied field [27]. Using an array of circular posts etched in a glass substrate, researchers at Sandia National Laboratories have demonstrated trapping of polystyrene beads [105] and separation of live and dead *E. coli* based on their differing magnitudes in negative DEP response (Figure 2.3B) [87]. The group later demonstrated separation and concentration of any two pairs of *E. coli*, *B. subtilis*, *B. cereus*, and *Bacillus megaterium* [88], as well as tobacco mosaic virus [86]. A direct application of this technique is for the detection of microbes in drinking water, which is hindered by current analytical instruments that require significant concentration of microbes in order to detect them [86].

27
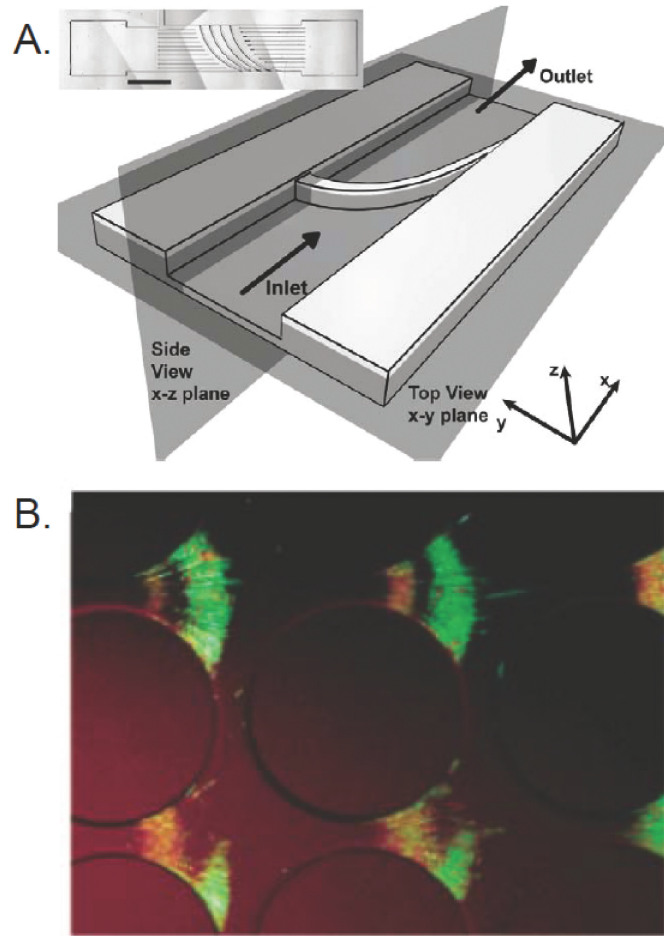
Figure 2.3: (A) Schematic of curved constriction in channel depth. Inset: top view of device fabricated in Zeonor 1020R polymer substrate. Reproduced from [54]. (B) Trapping of live (green) and dead (red) *E. coli* with separation of populations using insulative post array. Reproduced from [87].

Other geometries

A variety of other device geometries have been designed for bioparticle separation and isolation using insulative DEP. Chou et al. used an array of constrictions to trap and concentrate single- and double-stranded DNA [20]. Pysher et al. designed channel walls with a sawtooth pattern to produce spatially resolved separation of live and dead *E. coli* and *B. subtilis* [128]. More recently, Church et al. fabricated a serpentine channel to filter *E. coli* from yeast cells [22], Cho et al. positioned plastic membranes with

honeycomb-shaped pores between electrodes to trap and release *E. coli* in the flow channel [18], and Shafiee et al. developed a "contactless" DEP technique to isolate live/dead cultured human leukemia cells by using thin insulating barriers to separate the electrodes used to apply the electric field from the sample channel, thus preventing potential issues such as contamination and bubble formation [147].

2.4.3   Prospects for DEP rare cell capture

The preceding sections on electrode-based and insulative DEP techniques introduced the most common device geometries that researchers have used to separate different populations of cells. Those studies that focused on quantifying experimental performance criteria such as efficiency, enrichment, and/or purity are summarized in Table 2. Overall, DEP methods are advantageous because they do not require a biochemical labeling step to achieve continuous-flow separation. Additionally, it is possible to achieve DEP cell separation without *a priori* knowledge of the different cells' properties. For binary separation using IDA electrodes, only the frequency range in which the cells experience DEP forces opposite in sign needs to be known; for methods that use angled electrodes or insulative constrictions and techniques such as DEP-FFF and twDEP, only the cells' relative DEP response magnitudes is required to achieve separation of several cell types. As such, DEP offers the ability to isolate single cells (because of its sensitivity to cellular dielectric properties) as well as the possibility for separation of cell populations in which not all cell types have been characterized. In the latter case, DEP potentially can be used to screen for cells with unknown membrane phenotypes, which can facilitate research on bacterial species such as *Mycobacterium tuberculosis*, whose pathogenicity is closely tied to membrane composition [134].

Using only DEP techniques for rare cell capture in pathogen detection or tumor cell isolation, however, is challenging; studies have reported significant decreases in cell capture efficiency or purity as target cell concentrations became more dilute [43, 39, 42, 64]. While numerous DEP methods for cell separation of artificial samples have been reviewed in this article, we are not aware of a study that demonstrates strictly dielectrophoretic capture of pathogens from environmental (air or water) samples or capture of viable tumor cells from whole blood of cancer patients. In the future development of rare cell capture microfluidic devices, it may be beneficial to merge DEP methods with techniques such as magnetic-activated cell sorting [75, 77] or immunocapture [187, 51]. Such hybrid techniques combine the actuation of DEP with the chemical-specificity of immunocapture techniques; a system could be developed in which the applied electric field is tuned low enough to cause no physiological harm to target cells while inducing a strong enough DEP force to cause or prevent interactions with immunocapture surfaces. These synergistic effects have the potential to minimize problems associated with immunocapture techniques (e.g. nonspecific binding) and yield higher performance in rare cell capture efficiency and purity compared to using DEP techniques alone.

2.5 Performance criteria

In the previous sections, we have described a variety of different methods to isolate a multitude of rare cell types. In this section, we quantitatively compare these disparate studies with a unified set of performance criteria. Comparing the literature systematically identifies the strengths and weakness of the field as a whole and provides insights into future research directions. In the following paragraphs, we define performance metrics by which the literature will be evaluated (see Tables 2.1 and 2.2) and draw con-

clusions upon analyzing these criteria. Italics are used to highlight headings in these tables.

When comparing different rare cell capture devices, it is important to distinguish between the *cell type modeled* (e.g. cells obtained from biological samples) and the *cell type used* (often an immortalized cell line). This is imperative when the target cell's biological characteristics are not well understood, e.g. circulating tumor cells. While the use of well-understood model cell lines eases the characterization of device performance, their relations to clinical samples are not always well defined. Likewise, the *carrier media* used for experimentation is often chosen to simplify device characterization. Many rare cells that are targeted for isolation exist in dense biological suspension when *in vivo*, e.g. blood. However, many such fluids present other cellular material that confound quantification of performance for example, changing viscous or conductivity properties . For this reason, rare cells are often captured from diluted biological solutions or even buffer solutions. For devices that use DEP methods, the conductivity of the media and the cell concentrations used are also important as these parameters affect the DEP force and capture efficiency or purity, respectively.

A number of qunatitative metrics can be used to describe device performance. *Efficiency* is the most commonly used measure of performance in rare cell isolation literature. Efficiency is defined as the fraction of successfully isolated/fractionated cells with respect to the total number of target cells introduced into the device. High-efficiency microfludic cell isolation devices are often operated at higher volumetric flowrates than high-purity ones, resulting in increased throughput [45, 144]. Another common metric is *enrichment*, the multiplicative factor by which the number of rare cells per unit volume is increased. In contrast is depletion, where non-target cells are captured within the device, leaving a more pure subpopulation at the outlet [121, 120]. *Purity* is the num-

31

ber of target cells captured divided by the total captured cell population. Purity is an important metric for measuring the selectivity of a device, but its optimization usually results in lower efficiencies and throughputs. However, high purity samples are desirable for a variety of biomolecular assays and tools. Equally important is the *viability* of cells post-capture. Some devices define viability as the percentage of cells left in a functional state post-capture and others post-culture *ex-vitro*. When comparing results from different methods, it is also important to compare the *number of steps/stages* involved. The possibility of increased performance with multi-stage processing versus the simplicity of device operation are major concerns for devices designed for clinical applications. However, the number of steps/stages was not included for devices that employ DEP methods, as a majority of those listed in Table 1 had similar procedures that include dielectric characterization, cell staining, on-chip capture or fractionation, and post-process cell counting. Given the data in Tables 2.1 and 2.2 organized under the headings described in previous paragraphs, we can make a number of observations about rare cell capture in microdevices.

Table 2.1: Non-electrokinetic cell fractionation and isolation studies (abbreviated version from [126]). Acronyms: IC = Immunocapture, SBS = Size-based Sorting, ShF = Sheath Flow, StF = Streamline Focusing, BC = Breast Cancer, CC = Cervical Cancer, LC = Lung Cancer, PC = Prostate Cancer.

Application	Cell modeled	Cell used	Media	Processing	Efficiency	Enrichment	Purity	Analysis	Reference
Blood cell fractionation	B-lymphocytes, T-lymphocytes	Raji, Molt-3	PBS	staining	97%	na	na	anti-CD5, anti-CD19, PEG IC	[112]
	BC, PC, CC, Lymphoblast	MCF7, PC3, HeLa, Daudi	DMEM, Blood	staining, enumeration	80%	na	na	EpCAM IC	[177]
	B-lymphocytes, T-lymphocytes	Raji, Molt-3	PBS	staining, enumeration	na	na	na	anti-CD5, anti-CD19 IC	[151]
	Myeloid cells	HL-60, U-937	RPMI-1600	labeling, enumeration	na	130–200x	na	E-selectin IC	[13]
	Leukocytes	Leukocytes	Whole human blood	enumeration, lysing	na	na	97%	SBS	[144]
	Leukocytes	Leukocytes	Whole human blood	labeling, enumeration	98%	na	na	SBS	[166]
	Leukocytes	Leukocytes	Diluted human blood	enumeration	70–95%	na	na	SBS	[70]
	Leukocytes	Leukocytes	Diluted human blood	flow cytometry, staining, lysing, enumeration	99.6%	na	na	SBS	[30]
	Lymphocytes, monocytes	CD4+ cells, CD14+ cells, J45 lymphocytes	Diluted human blood	labeling, enumeration	73%	na	na	SBS	[68]
	Leukocytes	Leukocytes	Diluted human blood	lysing, enumeration	na	100x	na	ShF	[154]
	Leukocytes	Leukocytes	Diluted human Blood	dilution, enumeration	97%	na	na	StF	[192]
Cancer cells	Normal breast cell, BC	HME, TTU-1	PBS	enumeration, staining	30%	na	na	EMA, EGFR IC	[37]
	Leukemia, lymphoma	CCRF-CEM, Ramos, Toledo	Modified PBS	cytometry, staining, enumeration	50–83%	135x	88-97%	Scg8, TD05, Sgd5 IC	[181]
	BC	MCF7	Whole rabbit blood	check	97%	na	na	EpCAM IC	[1]
	PC	LNCaP	PBS	enumeration, staining	90%	na	na	PSMA, EpCAM IC	[34]
	BC	MCF7	DMEM	staining, enumeration, SEM	45-60%	na	na	EpCAM IC	[171]
	LC	SPC-A-1	Diluted human blood	enumeration	99.9%	na	na	SBS	[14]
	LC	A549	Human RBCs	staining, enumeration	62–74%	133x	na	WGA IC	[95]
	LC, PC, BC, Bladder cancer	NCI-H1650, PC3-9, SKBr-3, T-24	PBS	staining, enumeration	65%	na	na	EpCAM IC	[113]
	LC	NCI-H1650	Whole human blood	staining, enumeration	60%	na	na	EpCAM IC	[113]
	PC	LNCaP	PBS	labeling, enumeration	97%	na	na	PSMA IC	[45]

Continued on next page

33

Table 2.1 – continued from previous page

Application	Cell modeled	Cell used	Media	Processing	Efficiency	Enrichment	Purity	Analysis	Reference
	PC	LNCaP	Whole human blood	labeling, enumeration	85%	na	68%	PSMA IC	[45]
	PC	PC CTCs	Whole human blood	labeling, enumeration	na	na	62%	PSMA IC	[45]
	LC, PC, Pancreatic cancer, Colon cancer	LC, PC, Pancreatic CTC, Colon CTC	Whole human blood	staining, enumeration	na	na	42–67%	EpCAM IC	[113]
	PC	LNCaP	PBS	labeling, enumeration, electrolysis, PCR	87–89%	na	na	SBS	[191]
	PC	LNCaP	Whole human blood	labeling, enumeration, electrolysis, PCR	89%	na	na	SBS	[191]
Other mammalian cells	Endothelial cells, smooth muscle cells	H5V, A7r5	PBS	labeling, enumeration, staining	na	na	86%; 83%	REDV/VAPG Peptide IC	[120]
	Endothelial cells, smooth muscle cells, fibroblasts	H5V, A7r5, 3T3-6	PBS	labeling, enumeration, staining	na	na	96-99%	REDV/VAPG/ RGDS Peptide IC	[121]
	Neural stem cells	SH-SY5Y, C6	PBS	staining, enumeration, flow cytometry	89%	na	na	SBS	[85]
	G_2/M myeloid cells	U937	10mM sodium borate	flow cytometry	na	4x	na	StF	[19]
	Nucleated RBC	Nucleated RBC	Diluted human blood	filtration, dilution, staining	na	10–20x	na	StF	[61]
Prokaryotes & viruses	E. coli	E. Coli	Diluted human RBCs	staining, enumeration, SDS page	62%	300x	99.87%	ShF	[180]

34

Table 2.2: Electrokinetic cell fractionation and isolation studies (abbreviated version from [126]).

Application	Cell modeled	Cell used	Media	Processing	Efficiency	Enrichment	Purity	Technique	Reference
Pathogen detection	L. monocytogenes	L. innocua	DI water	Cell counting	90%	na	na	IDA	[92]
	L. monocytogenes	L. monocytogenes	DI water	Cell counting	87–92%	na	na	IDA + immunocapture	[187]
	B. anthracis	B. subtilis	DI water	Measure absorbance	na	9x	na	IDA	[41]
	B. anthracis	B. subtilis	DI water	Hemocytometer	na	na	≤60%	IDA	[39]
	B. anthracis	B. anthracis	DI water	Cell counting	90%	na	na	IDA	[97]
	Plasmodium falciparum	Malaria-infected erythrocytes	Sucrose buffer	Cell counting	90%	50–200x	na	Castellated	[42]
	na	B. cereus, E. coli, L. monocytogenes	Mannitol + PBS	PCR amplification	≤97%	na	na	Castellated	[64]
	na	E. coli	DI water	Cell counting	90+%	3000x	na	iDEP	[86]
	na	E. coli	PBS	Cell counting	66%	na	na	iDEP	[18]
Cancer cell isolation	Lung cancer	A549-luc-C8	DMEM buffer	Flow cytometry	81–84%	na	na	Castellated	[159]
	Breast cancer	MDA231	Sucrose buffer	Cell counting	na	na	95%	Castellated	[7]
	Breast cancer	MDA-435	Sucrose buffer	Cell counting	na	na	98%	FFF	[185]
	Breast cancer	MDA-435, -468, -231	Sucrose buffer	Cell counting	≤92%	na	na	FFF	[43]
	Breast cancer	MDA-435, CD34+ stem cells	Sucrose buffer	Flow cytometry	na	na	96–99%	FFF	[63]
	Breast cancer	MDA-231	PBS	Flow cytometry	na	4.4x	96%	Angled electrodes	[?]
	Leukemia	THP-1	Sucrose buffer	Cell counting	90+%	na	na	Contactless DEP	[147]
Blood fractionation or enrichment	Leukocytes	Leukocytes	Sucrose buffer	Flow cytometry	na	na	87–98%	FFF	[184]
	Leukocytes	Leukocytes	GIT medium	Cell counting	80%	na	na	FFF + immunocapture	[51]
	Leukocytes	Leukocytes	Sucrose buffer	Flow cytometry	55–75%	na	92–99%	FFF	[176]
	Malaria	Erythrocytes infected with B. bovis	PBS	Cell counting	na	7x	na	FFF	[9]
	Malaria	Erythrocytes infected with P. falciparum	Sucrose buffer	Cell counting	na	1000x	90%	twDEP	[42]
	Platelets	Concentrated platelets + whole blood	Sucrose buffer	Flow cytometry	na	5.3x	95%	Angled electrodes	[124]

2.6 Discussion and conclusions

Multiple strides have been made in the enrichment, fractionation, and capture of rare cells. The devices outlined in this review have been successfully used for the enrichment of bacteria to the genetic analyses of cancer cells [180, 157]. Microfluidic devices for rare cell capture have elucidated new biological phenomena and afforded multiple avenues of further scientific investigation. Current devices have been successfully implemented in the enumeration of rare cells ranging from NRBCs to CTCs [61, 113, 45]; however the lack of a single microfluidic device that can isolate pure cell populations with high efficiency limits the number of molecular and genetic tools that can be used on these populations.

Additionally, few cell capture studies directly process biological samples [113, 45, 165, 166]. In contrast, most devices spike cell lines into buffer solution [13, 112, 151, 120, 191, 85, 19, 34, 181, 121], or pre-diluted/lysed blood samples [192, 30, 61, 180]. Importantly, in devices that employ DEP methods, efficiency and purity performance is low when target cell concentrations are dilute [39, 42, 64, 43], thus making rare cell capture using DEP techniques alone extremely difficult. In addition, many more cell capture devices approximate the *ex vivo* target with a model equivalent [181, 34, 92, 41, 39, 7, 185, 63] rather than capture of the actual *in vivo* target [166, 144, 187, 97]. Most use of undiluted *ex vivo* targets is for WBC fractionation, with few exceptions for other rare cell types [113, 61, 45].

Similarly, the viability of cells after the capture process is not a well-quantified area, but one that is a crucial performance evaluation metric for rare cell capture devices. Mechanical stresses from shear, either from electric-(i.e. DEP forces), contact- (i.e. from pillar filters) or fluid-induced forces (i.e. obstacle-based arrays) can lead to gene upreg-

ulation or even induce an apoptotic response [178, 115]. Directly tied to cell viability is cell release and culture post-capture. Some attempts have been made to elute rare cells from devices [181, 1, 34, 95, 190, 191, 180], especially those using affinity-based methods (i.e. immunocapture) [1, 34]. Although a majority of devices that employ DEP methods do not quantify post-process viability, other researchers have established that exposure to electric fields from microfabricated electrodes used for DEP techniques often does not alter cell viability [174, 57]. Electric field magnitudes and frequencies used for these devices are listed in the *Experimental Parameters* column of Table 2. Ultimately, in situations where the target cell can be as few as 1 per billion non-target cells (e.g. bacteria, viruses, CTCs), cell expansion in culture will be a critical step in obtaining enough material for further experimentation.

For future studies and biological applications, the major areas for improvement are ability to elute cells in an undamaged state, increased cell survivability, and systems capable of delivering both high capture efficiency and purity. The development of such a platform could be facilitated by incorporating both electrokinetic and non-electrokinetic methods to create hybrid systems, as in recent efforts [187, 51, 75, 77]. Combining the sensitivity of DEP cell manipulation with the robustness of immunocapture has the potential to improve rare cell capture efficiency and purity, and such hybrid systems have scientific value and applicability across a variety of biological fields.

CHAPTER 3

CHARACTERIZATION OF A HYBRID DIELECTROPHORESIS AND IMMUNOCAPTURE MICROFLUIDIC SYSTEM FOR CANCER CELL CAPTURE

3.1 Abstract

The capture of circulating tumor cells (CTCs) from cancer patient blood enables early clinical assessment as well as genetic and pharmacological evaluation of cancer and metastasis. Although there have been many microfluidic immunocapture and electrokinetic techniques developed for isolating rare cancer cells, these techniques are often limited by a capture performance tradeoff between high efficiency and high purity. We present the characterization of shear-dependent cancer cell capture in a novel hybrid dielectrophoresis (DEP)-immunocapture system consisting of interdigitated electrodes fabricated in a Hele-Shaw flow cell that was functionalized with a monoclonal antibody, J591, which is highly specific to prostate-specific membrane antigen (PSMA)-expressing prostate cancer cells. We measured the positive and negative DEP response of a prostate cancer cell line, LNCaP, as a function of applied electric field frequency, and showed that DEP can control capture performance by promoting or preventing cell interactions with immunocapture surfaces, depending on the sign and magnitude of the applied DEP force, as well as on the local shear stress experienced by cells flowing in the device. This work demonstrates that DEP and immunocapture techniques can work syn-

ergistically to improve cell capture performance, and it will aid in the design of future hybrid DEP-immunocapture systems for high-efficiency CTC capture with enhanced purity.

3.2 Introduction

Circulating tumor cells (CTCs) are cells that have been shed into the circulatory system from a tumor source, and are believed to contribute to cancer metastasis [3, 99]. The enumeration of CTCs isolated from cancer patient blood samples can serve as a prognostic indicator of cancer and predictor of patient survival [24, 55, 31, 28]. In addition, genetic and pharmacological evaluation of CTCs can lead to a better understanding of cancer metastasis as well as improved drug therapies [91, 156, 79, 132, 188]. However, CTCs are rare—as few as one cell per 10^8 blood cells [129, 82]. The only system for detecting CTCs that is approved by the U.S. Food and Drug Administration, CellSearch® (Veridex, LLC), requires immunomagnetic tagging and cell fixation, which inhibits further biological analyses on captured CTCs. Given this drawback, the isolation of *viable* CTCs from cancer patient blood presents a technical challenge for those who wish to study them.

Researchers have developed a variety of techniques for isolating rare cancer cells from blood [126, 99, 118]. Examples of microfluidic approaches include micropillar arrays [113, 45, 79], chaotic mixers [155, 170], filters [191, 94], and devices with other micro- and nanostructured surfaces [1, 35, 65, 66, 171]. Of those techniques that are capable of processing whole blood, immunocapture methods have shown the greatest potential for capturing rare cancer cells with high efficiency (62–95%) [113, 155, 45, 170]. Studies that used the epithelial cell-adhesion molecule (EpCAM) to capture lung,

prostate, pancreatic, and colorectal CTCs have reported a wide range of capture purities (9–67%) [113, 155, 170]. Our group has combined immunospecificity with optimization of cell adhesion and transport mechanisms to create Geometrically Enhanced Differential Immunocapture (GEDI) [152], and reported a capture purity of 62% with prostate CTCs by use of a monoclonal antibody, J591, that is highly specific to prostate-specific membrane antigen (PSMA) [45]. The main contributing factor to CTC capture impurities is the nonspecific adhesion of leukocytes to immunocapture surfaces. Thus, although immunocapture techniques typically produce high CTC capture efficiencies from whole blood, capture purity can still potentially be improved to facilitate subsequent biological studies on the CTCs.

Whereas microfluidic immunocapture techniques rely on surface immunological interactions to isolate rare cancer cells, electrokinetic techniques such as dielectrophoresis primarily rely on differences in the cell populations' electrical properties [52]. Dielectrophoresis (DEP) refers to the net migration of polarized particles due to interactions with an electric field gradient, and operates in two regimes: when a particle is more polarizable than its suspending medium, positive DEP occurs and the particle is attracted to stronger field regions; conversely, when a particle is less polarizable than the medium, negative DEP occurs and the particle is repelled from stronger field regions [72, 109]. The sign and magnitude of the DEP force is dictated by the real part of the Clausius-Mossotti factor, which describes the relationship between the electrical properties of the particle and the medium as a function of the applied AC electric field frequency [78]. This relationship forms the basis for the majority of DEP cell separation and isolation techniques [167].

Although numerous microfluidic DEP methods for cancer cell capture in artificial samples exist, there has not been a study that demonstrates DEP capture of viable CTCs

from whole blood of cancer patients [126]. A majority of DEP cancer cell isolation techniques use model cancer cell lines spiked in buffer media or diluted blood; such techniques include DEP flow-field fractionation (DEP-FFF) [43, 148, 48, 179], insulative and contactless DEP [8, 147, 56, 137], and streamline separations using angled electrodes [76, 2, 108, 182]. These studies separate cancer cells from other blood constituents based on their differences in DEP response in a specific applied frequency range. This binary separation mechanism makes DEP an attractive tool for cell separation, as DEP requires no biochemical treatment or labeling to achieve high capture efficiency and purity. However, to date, studies using DEP methods for CTC capture have only reported high capture performance for model cancer cell lines spiked in preprocessed blood with concentrations ranging from one cancer cell per 10^4–10^6 blood cells [43, 148, 56, 137, 2, 182, 179]. The commercially licensed ApoStream[TM] (ApoCell) system, which uses DEP-FFF, has reported capture efficiencies in the range of 50–80% for ovarian and breast cancer cell lines spiked in peripheral blood mononuclear cells (PBMCs) with concentrations as low as one cancer cell per 10^6 blood cells, but noted that efficiency decreased after running samples through the system multiple times to increase capture purity [48]. DEP capture performance has also been shown to decrease drastically with concentrations lower than one cancer cell per 10^6 blood cells [43]. Thus, although the use of DEP methods often produces high purities for cell separation, their application for CTC capture from whole blood is currently limited by low throughput and efficiency.

Given that DEP and immunocapture techniques both have unique advantages as well as areas for improvement, the development of a platform capable of high capture efficiency *and* purity could be facilitated by incorporating both methods [126]. In this study, we characterized the performance of a hybrid DEP-immunocapture system by quantifying cell adhesion to immunocapture surfaces as a function of the local shear stress

41

experienced by cells. This characterization of the shear-dependence of immunocapture was performed in a Hele-Shaw flow cell using a prostate cancer cell line, LNCaP, and the monoclonal antibody, J591, which is highly specific to PSMA [96, 142]. We show that, depending on the applied electric field frequency, DEP effects can control the capture performance of prostate cancer cells by attracting them to or repelling them from immunocapture surfaces. To our knowledge, this is the first reported study of a hybrid DEP-immunocapture characterization system for cancer cell capture, and our results inform the design of future hybrid DEP-immunocapture devices for high-purity CTC isolation.

3.3 Materials and methods

3.3.1 Hele-Shaw flow cell design

To optimize a microfluidic immunocapture system, the flow conditions that affect cell capture performance must be characterized. Such characterization is often difficult or expensive to perform in typical immunocapture devices, given their 3D topologies, cost of fabrication, and sample processing time. A Hele-Shaw flow cell, depicted in Figure 3.1, was designed to facilitate the analysis of flow conditions, specifically shear stress, and its effect on the immunocapture of LNCaPs. The device exhibits Stokes flow owing to its small channel depth and attendant low Reynolds number. As the device's width and length are large, its velocity field is approximately equivalent to a solution of a 2D irrotational, incompressible stagnation point flow [163].

Our Hele-Shaw flow cell is similar to but refined relative to previous designs [142, 145, 112, 163]. The device geometry includes sidewalls that are sections of rectangular
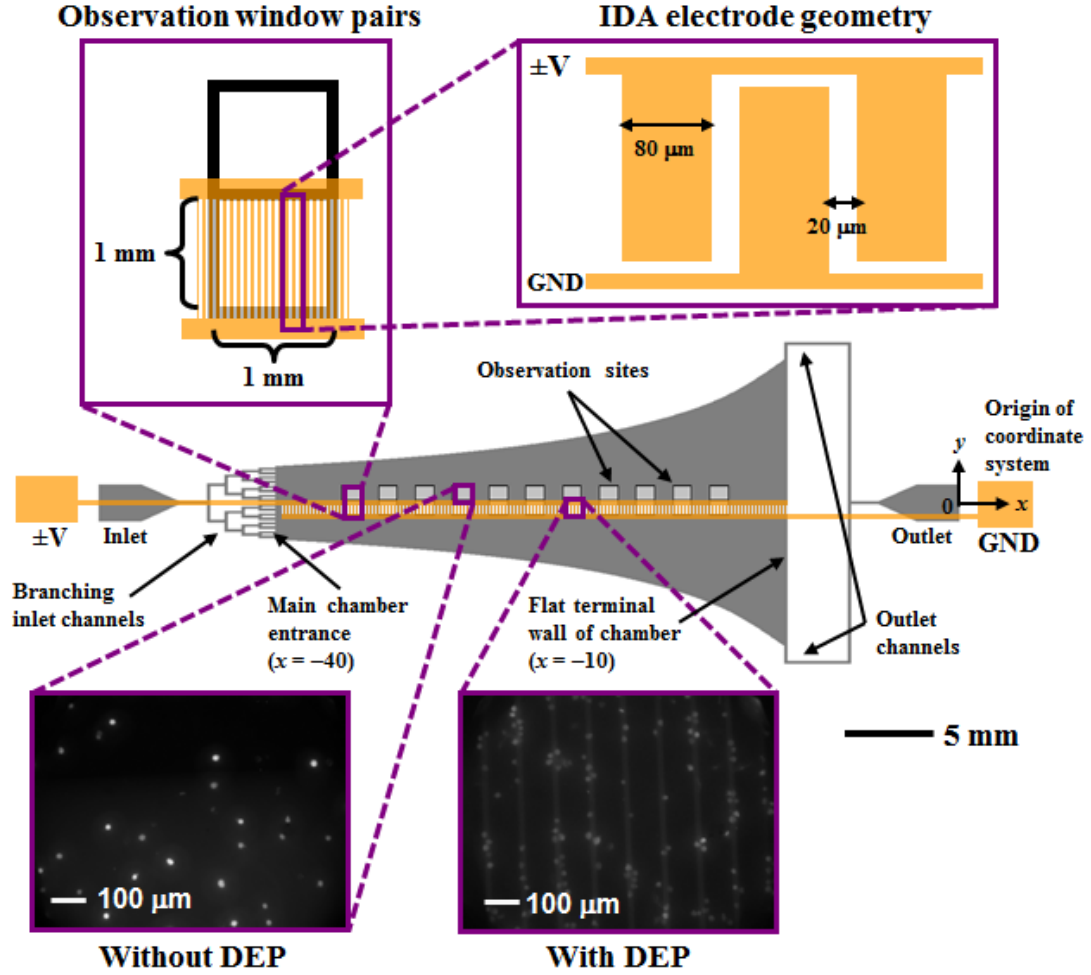
Figure 3.1: Schematic of the Hele-Shaw flow cell and its interdigitated array (IDA) electrodes with lead connections to an applied voltage ($\pm$V) and ground (GND). Inset images show details of the IDA electrode geometry and fluorescently labeled LNCaPs captured with and without DEP effects on the immunocapture surface immobilized with the antibody J591 at various observation sites (corresponding to a range of shear stresses). Captured cells in each pair of observation windows were enumerated and compared at all observation sites. The main chamber was 30 mm long, with an initial width of $w_0 = 5$ mm at its entrance and a flat wall at its terminal end. The channel height was 48 μm, and the branching inlet and outlet channels were 156 μm wide. The width, w, at any x along the curved channel was $w = -(40 \text{ mm})w_0/x$, given a coordinate system with an origin 40 mm to the right of the main chamber entrance. The shear stress in the main chamber ranged from 0 to 0.029 Pa, as shown in Figure 3.2.

43
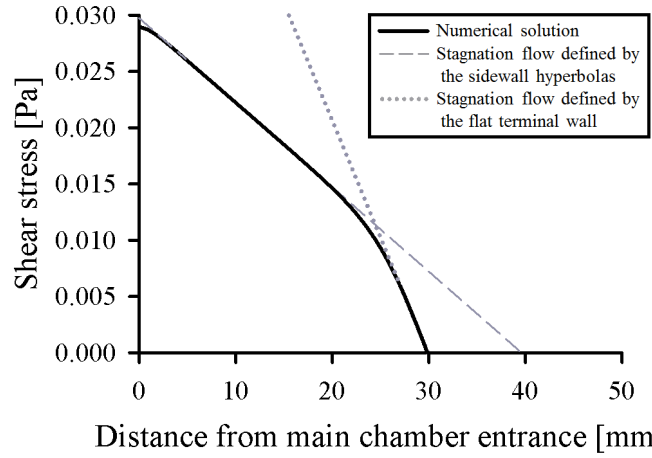
Figure 3.2: Shear stress at the immunocapture surface of the Hele-Shaw flow cell's central axis as a function of distance from the entrance to the main chamber (solid line). 2D variation in shear stress was calculated from a 2D potential flow simulation using COMSOL Multiphysics®, and a Poiseuille distribution was assumed in the height coordinate. The bilinear variation in shear stress results from the transition between (1) a stagnation flow defined by the sidewall hyperbolas with a theoretical stagnation point 40 mm from the main chamber entrance (dashed line), and (2) a stagnation flow defined by the flat terminal wall with a stagnation point 30 mm from the main chamber entrance (dotted line), as depicted in Figure 3.1.

hyperbolas [163], which replicate the far field of a stagnation flow impinging on the coordinate origin of the hyperbolas. However, because the outlet boundaries of such a stagnation flow are impractical to implement, we use two point outlets [145] and terminate the hyperbolas 10 mm from their coordinate origin (Figure 3.1). On the device's central axis, this flow asymptotes to a different stagnation flow, one whose coordinate origin is at the flat terminal wall. This geometry leads to a bilinear variation in shear stress along the length of the device's central axis. Figure 3.2 shows this variation in shear stress as a function of distance from the entrance to the device's main chamber (i.e., the output of the branching inlet channels).

The Hele-Shaw flow cell allows for characterization of cell adhesion as a function of shear stresses corresponding to those experienced by cells in immunocapture de-

vices [112, 142, 79]. To compare immunocapture performance of LNCaPs with and without DEP effects, interdigitated array (IDA) electrodes were fabricated along the length of the Hele-Shaw flow cell on only one side of its central axis (Figure 3.1). Branching inlet channels into the main chamber entrance ensure that entering cells are uniformly distributed across the chamber width. Approximately half of LNCaPs in the central axis region flow over the IDA electrodes and are affected by a DEP force when the electrodes are energized, whereas the other half of the cell population is unaffected by DEP. In this way, the immunocapture of LNCaPs with and without DEP effects can be directly compared as a function of shear stress.

3.3.2 Device fabrication

The Hele-Shaw flow cell was fabricated by bonding a channel defined in polydimethyl-siloxane (PDMS) to glass. All photolithography and thin-film deposition work was performed at the Cornell NanoScale Science and Technology Facility (CNF). Device masters were fabricated by spin-coating silicon wafers with MicroChem SU-8 2000 to create a film thickness of 48 μm. The photoresist was exposed at 12 mW/cm^2 for 40 seconds using an EV620 Contact Aligner on soft-contact mode, then developed in MicroChem SU-8 Developer for 2 minutes and rinsed with acetone, isopropyl alcohol (IPA), and deionized water (DI H$_2$O). The wafers were then coated with 1H,1H,2H,2H-perfluorooctyltrichlorosilane (Sigma-Aldrich) to prevent PDMS adhesion.

IDA electrodes were fabricated using standard lift-off photolithography. Borofloat glass wafers were cleaned with hot piranha solution for 10 minutes and vapor-primed with hexamethyldisilazane (HMDS) for 30 minutes. The wafers were then spin-coated with Microposit S1818 photoresist at 3000 RPM for 30 seconds and baked at 115 °C

for 90 seconds. The photoresist was exposed at 12 mW/cm^2 for 60 seconds using the EV620 Contact Aligner on soft-contact mode, then developed in Microposit MF-321 for 2 minutes. Wafers were treated with oxygen plasma at 150 W and 80 °C for 60 seconds, then placed in a CVC SC4500 Combination Thermal/Electron-Gun Evaporator. A 250-nm layer of gold was deposited between 20-nm layers of chromium. Lift-off was performed in Microposit Remover 1165 for 12 hours, after which wafers were diced on a K&S 7100 Dicing Saw. The resulting IDA electrode devices were cleaned with Cyantek Nano-Strip for 20 minutes immediately before bonding to PDMS.

PDMS was prepared using a Sylgard$^®$ 184 Silicone Elastomer Kit with a 5:1 ratio of elastomer base to curing agent, and baked with the Hele-Shaw device master in an oven at 60 °C for 12 hours. The PDMS was then removed from the master, and inlet and outlet holes were punched with a Harris Uni-Core 1.5-mm biopsy punch. Both the patterned PDMS channel and glass with IDA electrodes were rinsed with acetone, IPA, and DI H$_2$O, dried with an air gun, cleaned in a Harrick Plasma Cleaner for 60 seconds, bonded together, and baked in an oven at 60 °C for 12 hours. IDA electrodes were then connected externally to wires with MG Chemicals 8331 Silver Conductive Epoxy, and inlet and outlet ports were connected to Tygon S-54-HL Microbore tubing.

3.3.3 Antibody functionalization

Immunocapture experiments were conducted with the humanized monoclonal biotinylated antibody J591 (manufactured by Lonza Biologics plc for BZL Biologics Inc.). This antibody has been shown to have high specificity for PSMA [96], and its use in the analysis of immunocapture performance of LNCaPs was characterized over a range of concentrations and shear stresses [142]. Additionally, J591 has been used to demon-

strate high-efficiency immunocapture of prostate CTCs from prostate cancer patient blood samples [45, 79]. The glass surface of the Hele-Shaw flow cell was functionalized to immobilize the antibody using MPTMS-GMBS-NeutrAvidin-biotin chemistry following previously reported protocols [45, 142].

3.3.4 Cell culture maintenance

All experiments were conducted with LNCaPs, an immortalized PSMA-expressing prostate cancer cell line, purchased from the American Type Culture Collection. LNCaPs were cultured in Corning CellBIND T75 culture flasks at 37 °C in a 5% CO_2 humidified environment. Cells were cultured in RPMI-1640 supplemented with 10% fetal bovine serum and 1% penicillin-streptomycin (Mediatech). To prepare for experiments, cells were trypsinized from the culture flasks, enumerated in a Hausser Scientific hemacytometer, and resuspended in one of three buffer solutions to a specified cell suspension density (see next section).

3.3.5 DEP characterization of LNCaPs

The expression for the time-averaged DEP force on a spherical particle in an infinite domain with homogeneous and isotropic complex permittivities is [109, 78]:

$$\langle \mathbf{F}_{\text{DEP}} \rangle = \pi \varepsilon_{\text{m}} a^3 \Re(\tilde{f}_{\text{CM}}) \nabla (\mathbf{E}_0 \cdot \mathbf{E}_0) \tag{3.1}$$

$$\tilde{f}_{\text{CM}} = \frac{\tilde{\varepsilon}_{\text{p}} - \tilde{\varepsilon}_{\text{m}}}{\tilde{\varepsilon}_{\text{p}} + 2\tilde{\varepsilon}_{\text{m}}} \tag{3.2}$$

where a is the particle radius, $\mathbf{E}_0$ is the externally applied electric field magnitude, and $\Re(\tilde{f}_{\text{CM}})$ denotes the real part of the Clausius-Mossotti factor. $\tilde{\varepsilon} = \varepsilon - i\sigma/\omega$ is the com-

plex permittivity, ε is the permittivity, σ is the electrical conductivity, ω is the angular frequency of the applied electric field, $i = (-1)^{1/2}$, and the subscripts p and m denote the particle and the medium, respectively. When $\Re(\tilde{f}_{CM}) > 0$, positive DEP (pDEP) occurs; conversely, when $\Re(\tilde{f}_{CM}) < 0$, negative DEP (nDEP) occurs. The frequency at which $\Re(\tilde{f}_{CM}) = 0$, i.e., when the particle transitions from nDEP to pDEP (or vice versa), is called the "crossover" frequency. In our fabricated devices, the electric field above a pair of IDA electrodes (Figure 3.1) can be approximated by assuming that the gap between the electrodes is differentially small. The resulting expressions for the electric field and the DEP force on the particle are [139, 53]:

$$\mathbf{E} = \frac{V}{\pi}\frac{\hat{\theta}}{r} \tag{3.3}$$

$$\langle\mathbf{F}_{DEP}\rangle = \frac{a^3\varepsilon_m}{3\pi r^3}\Re(\tilde{f}_{CM})V^2\hat{r} \tag{3.4}$$

where $\hat{\theta}$ and $\hat{r}$ are unit vectors in cylindrical coordinates, r is the radial distance from the center of the electrode gap, and V is the applied potential.

The most common DEP approach for isolating cancer cells from blood relies on a binary separation mechanism in which cancer cells and blood cells are actuated in different directions using pDEP and nDEP, respectively, in a specific applied frequency range [43, 56, 48]. To determine what frequency range to use for DEP separation of LNCaPs, we measured their crossover frequency and characterized their DEP response as a function of applied frequency. These experiments used a separate device consisting of IDA electrodes patterned on glass and bonded to a straight channel defined in PDMS with a depth of 50 μm and a width of 250 μm. This device (henceforth referred to as the IDA electrode device) was fabricated using the same protocol for the Hele-Shaw flow cell as described in a previous section, and the IDA electrodes had the same dimensions as detailed in Figure 3.1. The IDA electrode device was not functionalized with J591, allowing for immediate release of trapped LNCaPs when the electric field was turned

off, and for several DEP characterization experiments to be performed serially in the same device.

In characterizing the DEP response of LNCaPs, three different buffer solutions were used: (1) an isotonic sugar in DI H_2O solution consisting of 9.5% sucrose, 0.3% dextrose, and 0.1% Pluronic F68 (Sigma-Aldrich) with $\sigma_m = 0.7$ mS/m (similar to that used by other researchers [43, 48]), henceforth referred to as the low-conductivity sugar solution, (2) the same sugar solution with KCl added to produce $\sigma_m = 70$ mS/m, henceforth referred to as the high-conductivity sugar solution, and (3) phosphate buffered saline (PBS) diluted 20 times by volume in the low-conductivity sugar solution also to produce $\sigma_m = 70$ mS/m, henceforth referred to as the diluted PBS solution. To determine the crossover frequency range of LNCaPs, the cells were labeled with Calcein AM dye (Molecular Probes), resuspended in each of the three buffer solutions at a density of 1×10^6 cells/mL, drawn into a plastic syringe (Becton Dickinson), manually flowed through the IDA electrode device, and visualized on a Nikon LV100 upright microscope. The electrodes were energized by an Agilent 33200A function generator at 6 V and frequencies ranging from 10 kHz to 10 MHz. At each applied frequency, we observed whether the LNCaPs were attracted to (pDEP) or repelled from (nDEP) the electrodes, and determined the frequency range in which the cells were unaffected by the DEP force (i.e., crossover frequency).

We measured the relative magnitude of the pDEP response of LNCaPs as a function of frequency using a previously reported automated DEP characterization process [53]. To summarize, LNCaPs were labeled with Calcein AM, suspended at 1×10^6 cells/mL in each of the three buffer solutions, and flowed through the IDA electrode device at a rate of 0.2 mL/hr using a Chemyx Fusion 400 syringe pump. Voltages ranging from 2 to 8 V and frequencies ranging from 40 kHz to 10 MHz were applied, and cell trapping

on the first five electrodes was visualized on the Nikon LV100 upright microscope and quantified by fluorescence intensity using a custom LabVIEW (National Instruments) interface. A "trapping potential" was extrapolated for each applied frequency using a series of postprocessing analyses in MATLAB (MathWorks). This trapping potential, V_{trap}, was defined as the minimum voltage needed to trap a threshold number of cells (as quantified by fluorescence intensity) to be considered a pDEP response, and was related to the magnitude of the DEP force by $C_0 \Re(\tilde{f}_{\text{CM}}) = 1/V_{\text{trap}}^2$ (following Equation 3.4), where C_0 denotes an arbitrary constant related to the flow rate and electrode geometry [53]. Therefore, we report our DEP characterization data in terms of C_0/V_{trap}^2 as a function of frequency to describe the proportionate DEP response of LNCaPs.

The pDEP characterization data was fit to a function for $\Re(\tilde{f}_{\text{CM}})$ by modeling the LNCaP cell as a single-shelled dielectric sphere. Because the interaction between the electric field and the cell occurs primarily at the cell membrane [167], we modeled the electrical properties of the cell in terms of a specific membrane capacitance, C_{membrane}, in addition to the cytoplasmic electrical properties [40]. The effective permittivity of the particle, $\tilde{\varepsilon}_{\text{p}}$, in Equation 3.2 is then replaced by an effective permittivity for the cell, $\tilde{\varepsilon}_{\text{cell}}$, that is a function of both C_{membrane} and the cytoplasmic permittivity and conductivity [72]:

$$\tilde{\varepsilon}_{\text{cell}} = \frac{C_{\text{membrane}} \, a \, \tilde{\varepsilon}_{\text{cytoplasm}}}{C_{\text{membrane}} \, a + \tilde{\varepsilon}_{\text{cytoplasm}}} \qquad (3.5)$$

Under our experimental conditions ($\sigma_{\text{m}} \leq 0.7$ mS/m and applied frequencies below 10 MHz), varying the cytoplasmic permittivity and conductivity did not significantly change the magnitude of $\Re(\tilde{f}_{\text{CM}})$. Therefore, we fixed their values to $50\varepsilon_0$ ($\varepsilon_0 = 8.85 \times 10^{-12}$ F/m) and 1000 mS/m, respectively, which are within the range of previously reported values for cancer cells [7, 141]. The cell radius was fixed at 10 μm (the

size of a typical LNCaP cell), leaving C_{membrane} and C_0 as the only free parameters in the $\Re(\tilde{f}_{\text{CM}})$ fit for the $C_0/V_{\text{trap}}{}^2$ vs. applied frequency data.

3.3.6 Immunocapture of LNCaPs with DEP effects

To simulate the range of local shear stresses that cells experience in immunocapture devices and to characterize cell adhesion as a function shear stress, LNCaPs were flowed through the Hele-Shaw flow cell and captured cells were enumerated along the length of the device. For all immunocapture experimental conditions, two separate concentrations of antibody in solution were tested (i.e., incubated in the device): 5 μg/mL and 10 μg/mL. The cells were labeled with Calcein AM, suspended at 5×10^5 cells/mL in the diluted PBS solution ($\sigma_{\text{m}} = 70$ mS/m), and flowed through the device at 0.2 mL/hr using a Chemyx Fusion 400 syringe pump for 10 minutes. Six separate conditions for the applied DEP force were tested: 6 V at 10 kHz (where nDEP is expected), and 1 V, 3 V, 4.5 V, 6 V, and 10 V at 10 MHz (where pDEP is expected). After each capture experiment, PBS was flowed through the device at 0.2 mL/hr for 10 minutes to wash away any non-adherent cells.

Fluorescent images of captured cells were taken at a 20× magnification at a series of predetermined observation sites along the length of the device, as shown in Figure 3.1. Cell count values were collected for 11 unique shear stress regions with at least three experimental replicates. For all shear stresses, the reported value corresponds to the shear stress at the immunocapture surface of the device in the center of the imaged area. Because streamlines in the Hele-Shaw flow cell diverge, the effective input density of cells is variable and must be corrected for. Thus, the reported captured cell densities are the number of cells imaged in a 1-mm^2 region immediately to either side of the central

axis of the device (i.e., with and without IDA electrodes) multiplied by a correction factor that is inversely proportional to the shear stress (shown in Figure 3.2) and streamline density, which corrected for the diverging streamlines in the device. These normalized captured cell densities of immunocapture with and without DEP effects were then compared at each reported shear stress.

3.4 Results and discussion

3.4.1 DEP characterization of LNCaPs

To determine the AC electric field frequency-dependent DEP response of LNCaPs, we characterized their relative DEP magnitude and crossover frequency regions in a low and high-conductivity sugar solution as well as in PBS diluted in the low-conductivity sugar solution. The trapping potential was measured and the proportionate DEP response was calculated as a function of frequency, shown in Figures 3.3(a) and 3.3(b), respectively. We found that for the applied electric fields that were tested (10 kHz to 10 MHz, up to 10 V), the cells exhibited no measurable pDEP response in both sugar solutions and PBS with $\sigma_m > 100$ mS/m. Therefore, we minimally diluted both buffer solutions to 70 mS/m, which is two to seven times higher than conductivities used in the majority of DEP cancer cell capture studies [7, 63, 43, 141]. We obtained similar DEP characterization data for the high-conductivity sugar solution and diluted PBS solution, which suggests that diluted PBS is an appropriate substitute for the isotonic sugar solution. PBS was chosen as a model for whole blood because both have similar osmolarities, ion concentrations, and conductivities (approximately $\sigma_m = 1000$ mS/m). Although blood is generally classified as a shear-thinning fluid with a higher viscosity
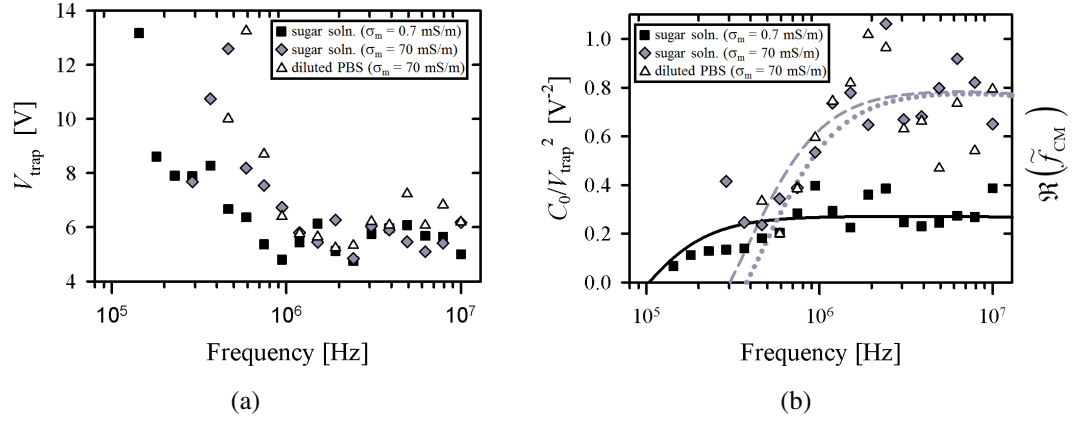
Figure 3.3: Trapping potential (V_{trap}), 3.3(a), and proportionate DEP response (C_0/V_{trap}^2), 3.3(b), as a function of applied cyclic frequency for LNCaPs suspended in three buffer solutions: (1) an isotonic sugar solution with $\sigma_m = 0.7$ mS/m (squares), (2) the same sugar solution with KCl added to produce $\sigma_m = 70$ mS/m (diamonds), and (3) PBS diluted 20 times by volume in the low-conductivity sugar solution to also produce $\sigma_m = 70$ mS/m (triangles). Each value represents the mean of 3 to 7 experimental replicates. Error bars are omitted for clarity; standard error of the mean values ranged from 0.2 to 4.6 V for V_{trap} and 0.008 to 0.2 V^{-2} for C_0/V_{trap}^2. Curve fits for $\mathfrak{R}(\tilde{f}_{\text{CM}})$ in 3.3(b) were calculated using Equations 3.2 and 5.3. Fit parameters were $C_{\text{membrane}} = 0.15$ mF/m^2 and $C_0 = 0.13$ for the low-conductivity sugar solution (solid line), $C_{\text{membrane}} = 5$ mF/m^2 and $C_0 = 0.05$ for the high-conductivity sugar solution (dashed line), and $C_{\text{membrane}} = 4$ mF/m^2 and $C_0 = 0.04$ for the diluted PBS solution (dotted line).

than PBS, we expect that these hydrodynamic differences will discernibly impact the capture performance on a 2D immunocapture surface (e.g., Hele-Shaw flow cell), but minimally impact a 3D immunocapture device (e.g., GEDI [45, 79]) that more heavily relies on cell-to-post collisions for high-efficiency capture. Because we have demonstrated that cancer cells can be actuated by DEP in minimally diluted PBS, we expect to obtain similar results in minimally diluted blood, which can potentially result in a significantly higher throughput than current DEP devices used for rare cancer cell capture from blood.

The DEP response of LNCaPs measured in this work is qualitatively similar to that of cancer cells measured by other research groups [43, 141, 179]. Figure 3.3(a)

shows that in the tested frequency range, the trapping potential decreased with increasing frequency, i.e., less voltage was needed to trap cells at higher frequencies. This trend suggests that the DEP response of the cells was stronger at higher frequencies, as confirmed in the proportionate DEP response data shown in Figure 3.3(b). A decrease in solution conductivity corresponded to a shift to lower frequencies in both the V_{trap} data and the $\Re(\tilde{f}_{\text{CM}})$ curve fits; this shift was most clearly demonstrated in our crossover frequency measurements: approximately 300 kHz for $\sigma_{\text{m}} = 70$ mS/m and 100 kHz for $\sigma_{\text{m}} = 0.7$ mS/m. Despite this shift in frequency response, the trapping potential remained in the same range for both conductivities (Figure 3.3(a)), suggesting that the maximum value of $\Re(\tilde{f}_{\text{CM}})$ was comparable in both cases. Wu et al. reported similar trends in their capture voltage spectrum data for colorectal cancer cells, and obtained crossover frequencies in the same range using sucrose buffer solutions with $\sigma_{\text{m}} = 50$ mS/m and $\sigma_{\text{m}} = 100$ mS/m [179].

The curve fits for $\Re(\tilde{f}_{\text{CM}})$ in Figure 3.3(b) were calculated by modeling the LNCaP cell as a single-shelled dielectric sphere with a frequency-dependent DEP response primarily dictated by a specific membrane capacitance, C_{membrane} [40]. In the high-conductivity cases, the pDEP response and crossover frequency regions were fit well; the magnitude and frequency dependence, as well as the fit value for C_{membrane}, were similar to those previously reported for other cancer cells [63, 141, 110]. Yang et al. reported on DEP separation of LNCaPs from colorectal cancer cells, but used a higher conductivity media ($\sigma_{\text{m}} = 300$ mS/m) at which LNCaPs experienced nDEP even in the MHz range [182]. Although we did not perform DEP characterization experiments at this conductivity, our model does predict similar nDEP behavior in those high conductivity and frequency ranges.

In the low-conductivity sugar solution, however, the best fit for C_{membrane} and the

measured crossover frequency resulted in a predicted $\Re(\tilde{f}_{CM})$ that was lower in magnitude than the other curve fits; this difference was not seen in the trapping potential values measured for both conductivities. Thus, the single-shell dielectric model seems able to describe only some aspects of the data. Despite this drawback, the model accurately predicted the DEP response of cancer cells suspended in media with $\sigma_m > 1$ mS/m (as experimentally verified in this study and others [43, 56, 141]), a range that includes whole blood, the suspending medium of most direct relevance for any CTC capture system. In this study, we measured the proportionate frequency-dependent pDEP response of LNCaPs, their crossover frequency, and predicted nDEP frequency range. Importantly, we obtained the strong pDEP response of LNCaPs by only diluting PBS by 20 times (in contrast to typical 100–1000 fold dilutions done by other researchers [43, 56, 48]). These results inform the design of future hybrid DEP-immunocapture systems for CTC isolation that, if multiplexed, have the potential to produce comparable capture efficiencies to existing immunocapture techniques (e.g., GEDI [45, 79]), with enhanced capture purity from the addition of DEP effects.

3.4.2   Immunocapture of LNCaPs with DEP effects

To study the effect of antibody concentration on immunocapture with and without DEP, we performed capture experiments in a microfluidic device of uniform, shallow depth (i.e., a Hele-Shaw flow cell) that was functionalized with two J591 incubating solution concentrations: 5 μg/mL and 10 μg/mL. In both cases, a range of voltages and frequencies were applied, and captured LNCaPs in regions up to 1 mm to either side of the device's central axis (i.e., regions with and without IDA electrodes) were enumerated across a range of shear stresses. Figure 3.4 shows the calculated mean ratio of captured cell density with and without DEP effects across the entire range of shear

stresses. As expected, there were fewer cells captured when a nDEP force was applied (ratio lower than 1), and more cells captured with an increasing pDEP force (ratio close to 1 when 1 V was applied, and growing with increasing applied voltage). In comparing the two antibody incubating solution concentrations, when nDEP was applied at 10 kHz, fewer cells were repelled from the immunocapture surface in the 10 μg/mL case, thus resulting in a higher ratio of captured cell density with and without DEP. Furthermore, DEP-enhanced immunocapture at 10 MHz saturated for voltages above 4.5 V with 10 μg/mL, whereas capture performance continued to improve up to 6 V with 5 μg/mL. These results suggest that the immunocapture surface was saturated with antibody in the 10 μg/mL case (consistent with our previously reported results [142]). Although we demonstrated that the two antibody concentrations resulted in similar trends of immunocapture with and without DEP effects, the difference in capture performance is more evident with the lower concentration. Therefore, we only further analyzed and present data from the 5 μg/mL case.

The captured cell density was quantified over a range of shear stress values for two applied frequencies (one of each chosen to induce pDEP or nDEP) and a series of increasing applied voltages; these values are listed in Table 3.1. We also performed experiments at 10 MHz with 10 V, but found that the pDEP force was so strong that nearly all LNCaPs were captured at the first few electrodes nearest to the inlet, invalidating the weak-capture assumption required to interpret the data. The 10 V data is thus omitted. Figure 3.5 shows representative cases of captured cell density with pDEP (10 MHz, 6 V), nDEP (10 kHz, 6 V), and no DEP applied. The observed trend of immunocapture with no DEP effects as a function of shear stress is consistent with those previously reported for LNCaPs [142]. In general, the number of captured cells increased with increasing applied voltage (i.e., pDEP force), and decreased with increasing shear stress. Immunocapture was enhanced by pDEP at 10 MHz, and was diminished by nDEP at
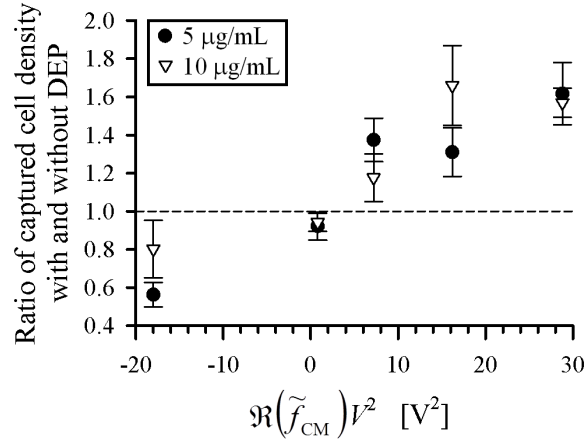
Figure 3.4: Ratio of captured cell density (normalized for streamline divergence) with and without DEP effects under various applied electric field frequency and voltage conditions for two J591 incubating solution concentrations: 5 μg/mL (circles) and 10 μg/mL (triangles). Ratios were averaged over captured cell density values across all shear stresses listed in Table 3.1. The no-DEP condition had 22 experimental replicates for the 10 μg/mL case and 15 replicates for the 5 μg/mL case; all other conditions had 3 to 7 replicates. Error bars represent standard error of the mean of ratios calculated at 11 shear stress values. The abscissa is plotted as $\Re(\tilde{f}_{CM})V^2$, which is proportional to the DEP force (Equation 3.4), to differentiate between nDEP and pDEP conditions. V was the applied voltage, and the values of $\Re(\tilde{f}_{CM}) = -0.5$ at 10 kHz and $\Re(\tilde{f}_{CM}) = 0.8$ at 10 MHz were obtained from the curve fits shown in Figure 3.3(b).

10 kHz. This trend is observed over nearly the entire shear stress range; at the two highest shear stress values, however, the captured cell densities with and without DEP were comparable, suggesting that immunocapture performance was both poor and unaffected by DEP above a threshold shear stress. Although we present a quantitative comparison of immunocapture with and without DEP effects as a function of shear stress, the underlying mechanisms of shear-dependent cell adhesion and rolling have been described using more complex models by other researchers [49, 11].

To our knowledge, this is the first reported study of DEP effects on the immunocapture of cancer cells. Our results provide insight on the experimental conditions (e.g., applied voltage range, antibody concentration, flow parameters and device geometries that control shear stress) needed to optimize DEP-guided immunocapture performance.

From a technology standpoint, this work was completed with a device that was designed to generate shear-dependent adhesion data [142]; we focused on characterization of cell physicochemical response rather than clinical and translational implementation of high-efficiency rare cell capture, which we have reported previously [79]. Our data on shear-dependent cell adhesion with the addition of DEP effects can be incorporated into computational fluid dynamics simulations of cancer and blood cell trajectories in 3D immunocapture devices to better predict capture performance and inform the design of future high-purity CTC capture systems that can facilitate subsequent clinical studies [45, 152].

Table 3.1: Captured cell density (normalized for streamline divergence) with a J591 incubating solution concentration of 5 μg/mL under various applied electric field frequency and voltage conditions as a function of shear stress. Captured cell density is reported as mean $\pm$ standard deviation. The no-DEP condition had 15 experimental replicates; all other conditions had 3 replicates.

Shear stress [Pa]	Captured cell density [cells/mm^2]					
	No DEP	10 kHz, 6 V	10 MHz, 1 V	10 MHz, 3 V	10 MHz, 4.5 V	10 MHz, 6 V
0.009	123.9±70.1	44.8±20.3	151.3±140.5	147.9±105.9	263.3±80.8	227.5±146.4
0.011	71.1±35.3	34.1±36.9	93.7±87.7	133.8±66.7	142.3±37.2	195.9±147.3
0.013	53.1±25.0	18.7±6.6	64.1±50.4	104.4±51.8	85.7±17.5	103.7±58.4
0.015	44.4±24.3	13.4±8.3	35.7±25.2	79.7±46.8	49.1±9.8	63.7±18.9
0.017	33.6±13.9	15.0±4.0	24.2±12.5	49.6±22.2	41.5±22.6	61.1±25.9
0.018	23.6±11.6	14.4±7.3	19.1±3.2	35.6±20.7	29.2±5.6	36.1±17.5
0.020	21.1±7.2	10.8±0.8	15.2±10.0	27.0±2.2	22.1±3.9	37.8±8.6
0.021	18.9±6.6	10.9±5.5	12.7±11.9	19.6±11.4	21.4±10.3	28.2±4.2
0.023	17.9±7.5	13.6±1.9	17.0±7.2	20.0±8.1	20.0±1.9	27.6±1.5
0.024	18.7±8.0	16.3±8.8	12.0±7.3	17.1±7.7	17.9±7.3	17.9±5.5
0.026	17.4±6.9	16.2±9.1	18.8±8.8	16.6±7.5	14.7±4.1	11.7±5.1

Previous studies have also reported the combination of DEP with a variety of other techniques to enable cell capture, separation, or characterization. Yang et al. combined DEP and immunocapture to detect and concentrate *Listeria* and *Salmonella* cells [187, 186], Kim et al. demonstrated DEP-magnetic activated sorting of bacteria and cancer cells [76, 77], Hashimoto et al. selectively captured leukocytes using nDEP to direct cells to antibody-immobilized regions [51], and Cristofanilli et al. used DEP to separate cancer cells on an "electrosmear" slide with adhesive coating [25]. In addition, DEP has been used for anticancer drug screening [58], detection of cancer markers [130], and impedance sensing of cancer cells [21]. For applications in rare CTC capture from whole blood, however, DEP may best complement existing robust immunocapture techniques that demonstrate antigen specificity and high-efficiency capture [45]. A hybrid DEP-immunocapture system in which DEP is tuned to promote CTC interactions (by pDEP) and prevent leukocyte interactions (by nDEP) with capture surfaces can minimize problems associated with immunocapture techniques, such as nonspecific leukocyte adhesion. Such a DEP-guided immunocapture system has the potential to be used in high-impact clinical studies (e.g., genetic and pharmacological evaluation of CTCs [79]) that benefit from the platform's improved CTC capture efficiency and purity relative to either DEP or immunocapture techniques alone.

3.5   Concluding remarks

This work characterizes shear-dependent cancer cell adhesion in a novel hybrid DEP-immunocapture microfluidic system. We measured the frequency-dependent pDEP response of LNCaPs, as well as their crossover frequency and nDEP frequency ranges. We showed that, depending on the applied frequency, DEP can control the capture performance of prostate cancer cells by attracting them to or repelling them from immunocap-

60
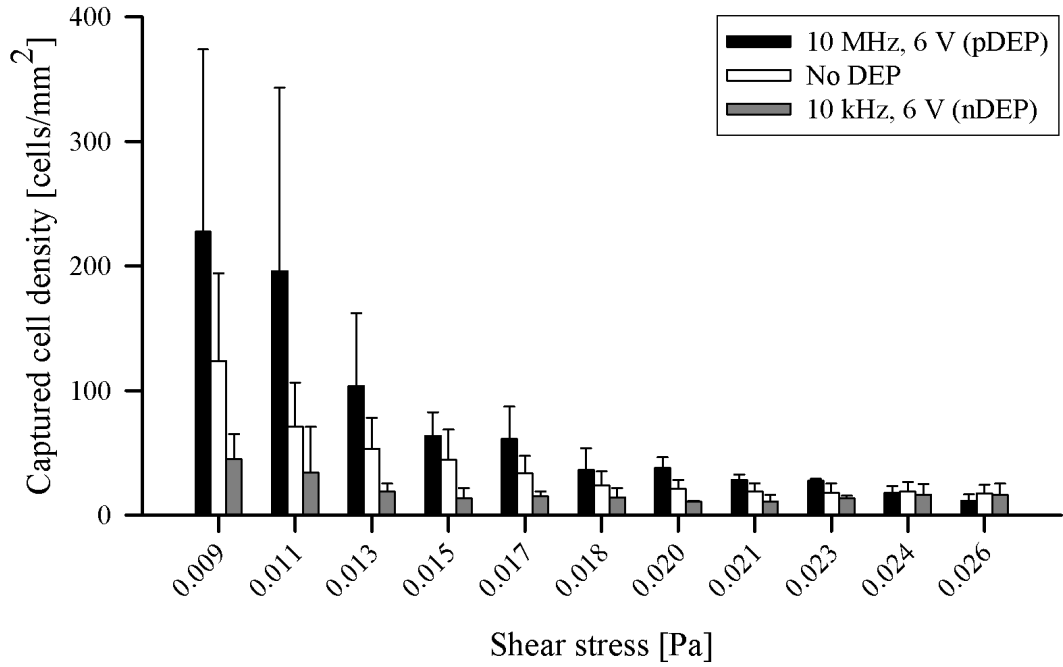
Figure 3.5: Captured cell density (normalized for streamline divergence) as a function of shear stress under representative cases of pDEP (10 MHz, 6 V; black bars), nDEP (10 kHz, 6 V; gray bars), and no DEP (white bars). Bars represent the mean captured cell density for the corresponding data listed in Table 3.1. The no-DEP condition had 15 experimental replicates; the pDEP and nDEP conditions had 3 replicates each. Error bars represent standard deviation.

ture surfaces, and that this phenomenon is dependent on local shear stresses experienced by the cells. In designing future CTC capture devices, we expect that DEP and immuno-capture techniques will work synergistically to yield higher capture performance and facilitate subsequent biological studies.

3.6 Acknowledgements

ENRICHMENT OF PROSTATE CANCER CELLS FROM BLOOD CELLS WITH A HYBRID DIELECTROPHORESIS AND IMMUNOCAPTURE MICROFLUIDIC SYSTEM

4.1   Abstract

The isolation of circulating tumor cells (CTCs) from cancer patient blood is a technical challenge that is often addressed by microfluidic approaches. Two of the most prominent techniques for rare cancer cell separation, immunocapture and dielectrophoresis (DEP), are currently limited by a performance tradeoff between high efficiency and high purity. The development of a platform capable of these two performance criteria can potentially be facilitated by incorporating both DEP *and* immunocapture. We present a hybrid DEP-immunocapture system to characterize how DEP controls the shear-dependent capture of a prostate cancer cell line, LNCaP, and the nonspecific adhesion of peripheral blood mononuclear cells (PBMCs). Characterization of cell adhesion with and without DEP effects was performed in a Hele-Shaw flow cell that was functionalized with the prostate-specific monoclonal antibody, J591. In this model system designed to make nonspecific PBMC adhesion readily apparent, we demonstrate LNCaP enrichment from PBMCs by precisely tuning the applied AC electric field frequency to enhance immunocapture of LNCaPs and reduce nonspecific adhesion of PBMCs with positive and negative DEP, respectively. Our work shows that DEP and immunocapture techniques

can work synergistically to improve cancer cell capture performance, and it informs the design of future hybrid DEP-immunocapture systems with improved CTC capture performance to facilitate research on cancer metastasis and drug therapies.

4.2   Introduction

The isolation of circulating tumor cells (CTCs)—cells that have been shed into the circulatory system from a tumor source—enables genetic and pharmacological evaluation of cancer [91, 156, 79, 132, 188]. Oftentimes, such studies require extremely pure samples of captured CTCs; this necessity presents a technical challenge, as CTCs are extremely rare—as few as one cell per 10^8–10^9 blood cells, depending on the definition of CTCs [129, 82]. Microfluidic immunocapture devices have been used successfully to capture CTCs from cancer patient blood with high efficiency, although capture purity can still potentially be improved by reducing the nonspecific adhesion of leukocytes [113, 45, 155, 170, 79]. Dielectrophoresis (DEP) is an alternative technique to using surface immunological interactions for cell capture [167, 52]; previous work on DEP separation of cancer cells is covered in other reviews [126, 67]. Examples of recent DEP techniques for isolating rare cancer cells include flow-field fractionation (DEP-FFF) [48, 150], contactless DEP [56, 137], and streamline separations by use of unique geometric features [4, 69]. Despite the advantage of not requiring biochemical labeling to achieve separation, the use of DEP techniques for CTC capture is currently limited by low throughput and efficiency owing to the rarity of CTCs in whole blood, and also by restrictions of electrode design and DEP physics [126]. Given that DEP and immunocapture techniques both have unique advantages and limitations, a combination of both techniques (e.g., applying DEP effects near immunocapture surfaces where electric fields are strongest and antibody interactions occur) can potentially lead to a platform

64

capable of high capture efficiency *and* purity to facilitate subsequent biological analyses of captured CTCs.

A majority of DEP separation methods rely on differences in the electrical properties of cancer cells and blood cells, which lead to distinct DEP responses as a function of applied AC electric field frequency. In frequency ranges where positive DEP (pDEP) occurs, cells are attracted to stronger electric field regions; conversely, when negative DEP (nDEP) occurs, cells are repelled from stronger field regions. Because cancer cells and blood cells transition from nDEP to pDEP at a different frequency (i.e., they have different "crossover" frequencies), DEP separation is typically achieved by selecting a frequency range in which cancer cells undergo pDEP and blood cells undergo nDEP to actuate the cells in different directions [43, 56, 48]. Researchers have characterized the DEP response of erythrocytes and peripheral blood mononuclear cells (PBMCs), as well as a wide variety of cultured cancer cells as a function of frequency [141, 60, 50, 138]. Of note, Shim et al. characterized the DEP crossover frequency of each NCI-60 cancer cell line and showed that all cancer types except leukemia have crossover frequencies in a range that is distinct from those of blood cells [149]. These results suggest that for solid tumors, the applied frequency can potentially be tuned to guide CTCs toward immunocapture surfaces with pDEP while repelling leukocytes and other blood contaminants with nDEP, leading to an improved capture purity [126, 60].

We have previously shown that the immunocapture of LNCaPs, a prostate cancer cell line, can be augmented by DEP; our work was the first to demonstrate DEP as a complement to existing cancer cell immunocapture techniques for improved cell capture [60]. In the current study, we characterized the adhesion of LNCaPs and PBMCs to immunocapture surfaces with and without DEP effects as a function of the local shear stress experienced by cells. This characterization was performed in a Hele-Shaw flow

cell that was functionalized with the monoclonal antibody, J591, which is highly specific to the prostate-specific membrane antigen (PSMA) expressed on LNCaPs [96, 60]. We enriched LNCaPs from PBMCs using DEP by tuning the applied frequency to differentially separate the two populations; this result demonstrates that DEP and immunocapture techniques can work synergistically to improve cancer cell capture performance. Our work informs the design of future hybrid DEP-immunocapture devices with improved CTC capture purity, which has the potential to facilitate subsequent genetic and post-translational modification studies for the development of personalized therapies for cancer patients based on analyses of their own CTCs [79, 36].

4.3 Materials and methods

4.3.1 Device design, fabrication, and antibody functionalization

A Hele-Shaw flow cell was designed to facilitate the characterization of DEP-guided immunocapture as a function of shear stresses corresponding to those experienced by cells in immunocapture devices [112, 142, 60]. Figure 4.1 depicts the Hele-Shaw flow cell with branching inlet channels to distribute entering cells uniformly across the main channel width. The sidewalls are sections of rectangular hyperbolas that replicate the far field of a stagnation flow impinging on the coordinate origin of the hyperbolas; this geometry produces a monotonically decreasing shear stress distribution along the length of the device's central axis [163]. The device geometry also generates diverging streamlines, which change the local incident cell density; these nonuniformities are known, and are corrected for when the data is analyzed. Interdigitated electrodes were fabricated on only one side of the device's central axis to directly compare cell adhesion with and
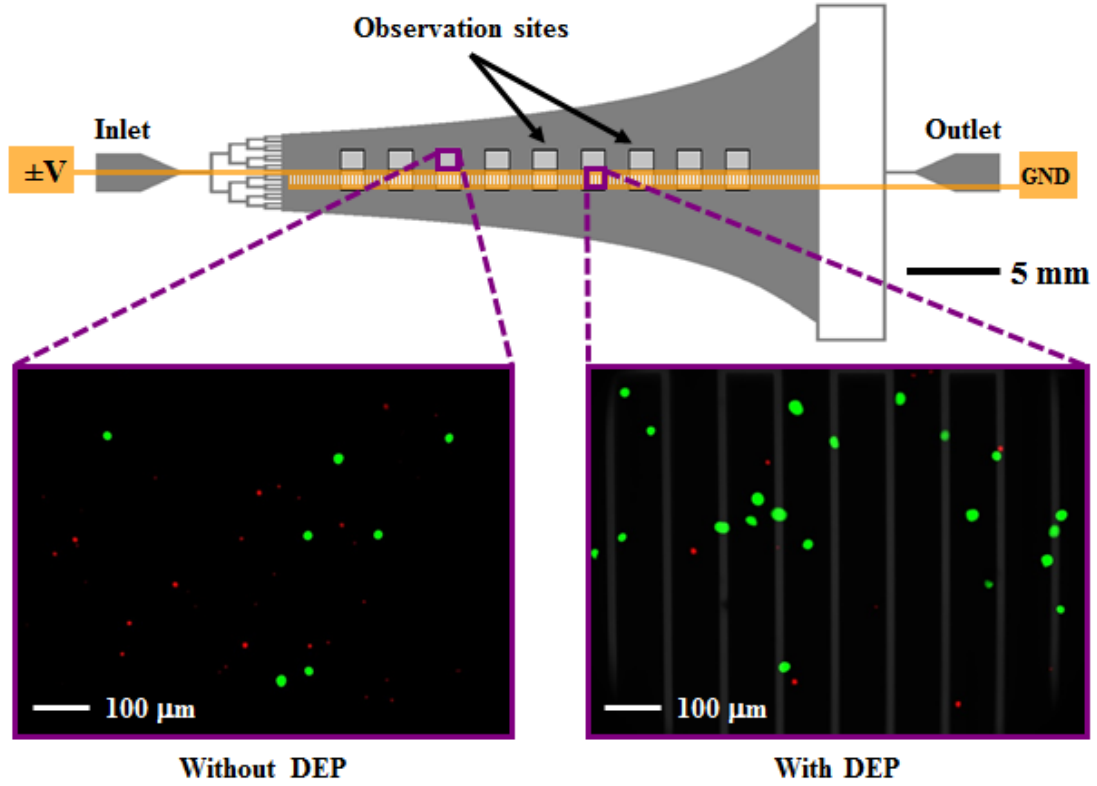
Figure 4.1: Schematic of the Hele-Shaw flow cell and its interdigitated electrodes with lead connections to an applied voltage ($\pm$V) and ground (GND). Inset images show fluorescently labeled LNCaPs (green) and PBMCs (red) adhered to the antibody-functionalized surface with and without DEP effects. These example images show that at an applied AC electric field frequency of 350 kHz, more LNCaPs and fewer PBMCs are captured with DEP as compared to without DEP. Captured cells in each pair of 1-mm^2 observation windows were enumerated and compared at a series of observation sites corresponding to a range of shear stresses. Details of the device geometry and shear stress distribution are described in our previous work [60].

without DEP effects [60].

The Hele-Shaw flow cell was fabricated with standard photolithography and thin-film deposition techniques; details of these processes are described in our previous work [60]. To summarize, the channel was defined in polydimethylsiloxane (PDMS) by use of an SU-8 master, and bonded to glass that was patterned with interdigitated electrodes. The electrodes were fabricated by depositing a 250-nm layer of gold between 20-nm layers of chromium, cleaned with Cyantek Nano-Strip, and connected externally

to wires with silver conductive epoxy. Inlet and outlet holes were created with a biopsy punch and connected to external tubing. The fully constructed Hele-Shaw flow cell was then functionalized with the humanized monoclonal biotinylated antibody, J591 (manufactured by Lonza Biologics plc for BZL Biologics Inc.), which we have previously characterized [96, 142, 60] and used for immunocapture of prostate CTCs [45, 79]. The antibody was immobilized on the device's glass surface at an incubating solution concentration of 5 μg/mL by use of MPTMS–GMBS–NeutrAvidin–biotin chemistry following previously reported protocols [45, 142].

4.3.2   Cell culture and preparation

LNCaPs, an immortalized, PSMA-expressing prostate cancer cell line, were purchased from the American Type Culture Collection, and cultured in Corning cellgro$^{®}$ RPMI 1640 supplemented with 10% fetal bovine serum and 1% penicillin-streptomycin in CellBIND T75 culture flasks at 37 $^{\circ}$C in a 5% CO_2 humidified environment. To prepare for experiments, LNCaPs were trypsinized from their flask, resuspended in phosphate-buffered saline (PBS), labeled with CellTracker^{TM} Green CMFDA (Invitrogen), and incubated for 30 minutes.

PBMCs were isolated from the blood of healthy donors with approval from the Institutional Review Board for Human Participants. Whole blood was collected in BD Vacutainer$^{®}$ CPT^{TM} Cell Preparation Tubes with Sodium Heparin^{N}, and centrifuged at 1700$\times$g for 15 minutes. PBMCs above the polyester gel were then collected in a separate conical tube, washed with PBS by centrifuging at 300$\times$g for 15 minutes twice, resuspended in PBS, labeled with CellTracker^{TM} Orange CMRA (Invitrogen), and incubated for 30 minutes.

After incubation with their respective fluorescent probes, LNCaPs and PBMCs were washed twice and resuspended in PBS diluted 20 times by volume in an isotonic sugar in deionized (DI) H_2O solution consisting of 9.5% sucrose and 0.3% dextrose with conductivity 0.07 S/m. This sugar solution is similar to that used by other researchers studying DEP separation of cancer cells [48, 150, 60], and was chosen because of the distinct DEP response that cancer cells and blood cells exhibit at the given conductivity (see next section). The final cell densities were 5×10^5 LNCaPs per mL and 2×10^6 PBMCs per mL; the two populations were mixed together before injection into the Hele-Shaw flow cell.

4.3.3 DEP characterization of cells

The sign and magnitude of the time-averaged DEP force, $\langle \mathbf{F}_{\mathrm{DEP}} \rangle$, on a spherical particle in an infinite domain with homogeneous and isotropic complex permittivities is determined by the real part of the Clausius-Mossotti factor, $\Re(\tilde{f}_{\mathrm{CM}})$:

$$\langle \mathbf{F}_{\mathrm{DEP}} \rangle = \pi \varepsilon_{\mathrm{m}} a^3 \Re(\tilde{f}_{\mathrm{CM}}) \nabla(\mathbf{E}_0 \cdot \mathbf{E}_0) \tag{4.1}$$

$$\tilde{f}_{\mathrm{CM}} = \frac{\tilde{\varepsilon}_{\mathrm{p}} - \tilde{\varepsilon}_{\mathrm{m}}}{\tilde{\varepsilon}_{\mathrm{p}} + 2\tilde{\varepsilon}_{\mathrm{m}}} \tag{4.2}$$

where a is the particle radius, $\mathbf{E} = \mathbf{E}_0 \cos(\omega t)$ is the externally applied AC electric field, ω is the angular frequency of the electric field, $\tilde{\varepsilon} = \varepsilon - i\sigma/\omega$ is the complex permittivity, $i = (-1)^{1/2}$, ε is the electrical permittivity, σ is the electrical conductivity, and the subscripts p and m denote the particle and the medium, respectively [109, 78]. The frequency at which $\Re(\tilde{f}_{\mathrm{CM}}) = 0$, i.e., when the particle transitions from nDEP to pDEP, or vice versa, is termed the crossover frequency. Although the cells under study are neither spherical, homogeneous, nor isotropic, this analysis can still be used to a good approximation because effective particle properties can be defined, facilitated by the

69

mathematical properties of the spherical harmonic solutions used in eigenfunction expansion approximations for the DEP force. In this case, $\tilde{\varepsilon}_p$ becomes an extrinsic particle property rather than an intrinsic material property [52, 78].

To determine the crossover frequency range of LNCaPs and PBMCs, the two populations were manually flowed through the Hele-Shaw flow cell and their DEP responses were observed above the interdigitated electrodes region on a Nikon LV100 upright microscope. The electrodes were energized by an Agilent 33200A function generator at 6 volts peak-to-peak (V_{pp}) and frequencies ranging from 100 kHz to 1 MHz. At each applied frequency, we recorded whether each cell population was attracted to or repelled from the electrodes by pDEP and nDEP, respectively, and we determined the frequency range in which the cells were unaffected or affected nonuniformly by the applied electric field (i.e., crossover frequency). After determining each cell population's crossover frequency, we predicted the magnitude of its DEP response as a function of frequency by modeling the cell as a single-shelled dielectric sphere [109, 78]. The effective permittivity of the particle, $\tilde{\varepsilon}_p$, in Equation 5.2, was replaced by an effective permittivity of the cell, $\tilde{\varepsilon}_{cell}$, that describes its electrical properties in terms of a specific membrane capacitance, $C_{membrane}$, and the cytoplasmic permittivity and conductivity [78, 60]:

$$\tilde{\varepsilon}_{cell} = \frac{C_{membrane}\, a\, \tilde{\varepsilon}_{cytoplasm}}{C_{membrane}\, a + \tilde{\varepsilon}_{cytoplasm}} \qquad (4.3)$$

Interactions between the cell and the electric field occur primarily at the cell membrane, although the physical and electrical properties of the membrane are often difficult to infer from experimental measurements [167, 78]. Thus, it is common to use the single-shelled dielectric model and extrapolate a specific membrane capacitance to describe the extrinsic properties of the cell [7, 43, 141]. Figure 4.2 shows the predicted DEP response of LNCaPs and PBMCs as a function of frequency using this shell model. Un-

der our experimental conditions, varying the cytoplasmic permittivity and conductivity did not significantly change the magnitude of $\Re(\tilde{f}_{CM})$, and thus their values were fixed to $50\varepsilon_0$ ($\varepsilon_0 = 8.85 \times 10^{-12}$ F/m) and 1 S/m, respectively, which are within the range of previously reported values for cancer cells and blood cells [7, 141, 50, 149]. The average cell radius was measured to be approximately 10 μm for LNCaPs and 5 μm for PBMCs. Through detailed characterization of LNCaPs' DEP response [60] and analysis of measured and predicted crossover frequencies, we selected 250 kHz and 350 kHz as the frequencies to apply in characterizing pDEP and nDEP effects on cell adhesion as a function of shear stress. As shown in Figure 4.2, both LNCaPs and PBMCs exhibit a nDEP response at 250 kHz; however, at 350 kHz, LNCaPs exhibit a pDEP response whereas PBMCs exhibit a nDEP response.

4.3.4   DEP-guided enrichment of LNCaPs from PBMCs

To characterize cell adhesion of LNCaPs and PBMCs as a function of shear stress, a mixture of the two cell populations was flowed through the Hele-Shaw flow cell and captured cells were enumerated along the length of the device. The cell mixture was drawn into a BD plastic syringe and flowed through the device at 0.2 mL/hr with a Chemyx Fusion 400 syringe pump for 5 minutes. The interdigitated electrodes were energized by an Agilent 33200A function generator at 6 V_{pp} and two different frequencies: 250 kHz and 350 kHz, with six experimental replicates each. After each capture experiment, PBS was flowed through the device at 0.2 mL/hr for 10 minutes to wash away any non-adherent cells. Fluorescent images of captured LNCaPs and PBMCs were taken at a 20$\times$ magnification with FITC and Texas Red$^{\circledR}$ / Cy3.5^{TM} Chroma filter cubes, respectively, at a series of observation sites along the length of the device, as shown in Figure 4.1. Reported captured cell densities correspond to the number of captured cells
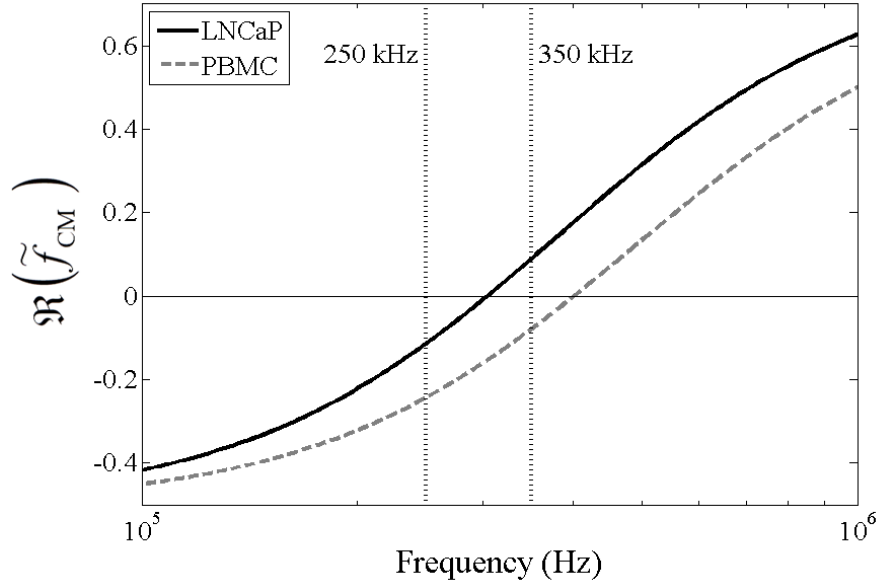
Figure 4.2: Predicted DEP response, as described by $\Re(\tilde{f}_{CM})$, of LNCaPs (solid line) and PBMCs (dashed line) as a function of applied electric field frequency. Cells were modeled as single-shelled dielectric spheres, described by Equations 5.2 and 5.3. In a diluted PBS suspending medium with $\sigma_m = 0.07$ S/m, the crossover frequency was experimentally determined to be approximately 300 kHz for LNCaPs and 400 kHz for PBMCs. These empirical measurements, combined with Equation 5.3, corresponded to specific membrane capacitance values of $C_{membrane} = 5$ mF/m^2 and $C_{membrane} = 7.5$ mF/m^2 for LNCaPs and PBMCs, respectively, in the dielectric shell model. At 250 kHz, both cell populations exhibit a nDEP response; at 350 kHz, however, LNCaPs exhibit a pDEP response whereas PBMCs still exhibit a nDEP response. Comparisons of the two frequencies' effects on DEP-guided immunocapture are shown in Figures 4.3(a) and 4.3(b).

multiplied by a correction factor (to normalize for streamline divergence in the device) in an observation window with a shear stress at the immunocapture surface in the center of the imaged area [60]. Captured cell densities of both LNCaPs and PBMCs were compared between either side of the Hele-Shaw flow cell's central axis to characterize the effect of DEP on cell adhesion at each shear stress value.

4.4 Results and discussion

The DEP-guided immunocapture performance of LNCaPs and nonspecific adhesion of PBMCs to antibody-functionalized surfaces was characterized as a function of shear stresses corresponding to those experienced by cells in immunocapture devices [142, 79, 60]. A mixture of LNCaPs and PBMCs was flowed through the Hele-Shaw flow cell and captured cells were enumerated under three experimental conditions: no DEP, 250 kHz, and 350 kHz. Figures 4.3(a) and 4.3(b) show the captured cell densities as a function of shear stress for LNCaPs and PBMCs, respectively, under these experimental conditions. Of note, the solution used for these experiments was purposely free of factors known to suppress nonspecific adhesion, which include Pluronic® surfactants [54, 53, 60] and bovine serum albumin [45, 142]. This omission maximizes nonspecific adhesion, which would be problematic for rare cell capture but is required in this study to make PBMC capture measurable at cell counts comparable to LNCaP cell counts. In rare cell capture applications, surfactants or blocking proteins are used, and the PBMC capture rate is typically much lower, but the ratio of PBMCs to target cells is still high enough that PBMCs are the primary contaminant [126]. Our experiments inform the *relative* capture of PBMCs but, because of the solutions and cell densities used, purposely study a condition that overestimates the absolute magnitude of PBMC capture.

At 250 kHz, LNCaPs exhibit a weak nDEP response whereas PBMCs exhibit a stronger nDEP response (as predicted in Figure 4.2); thus, it is expected that as the magnitude of the nDEP response increases, cells flowing past regions with energized interdigitated electrodes (as depicted in Figure 4.1) will be repelled further from the antibody-functionalized surface. Figures 4.3(a) and 4.3(b) show that under this DEP condition, LNCaP capture via immunological interactions with the antibody was not significantly affected, while significantly fewer PBMCs were captured by nonspecific
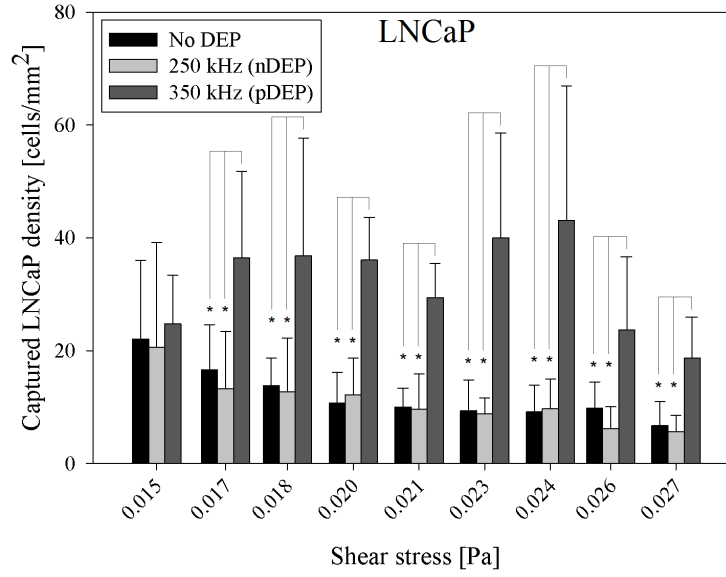
(a)
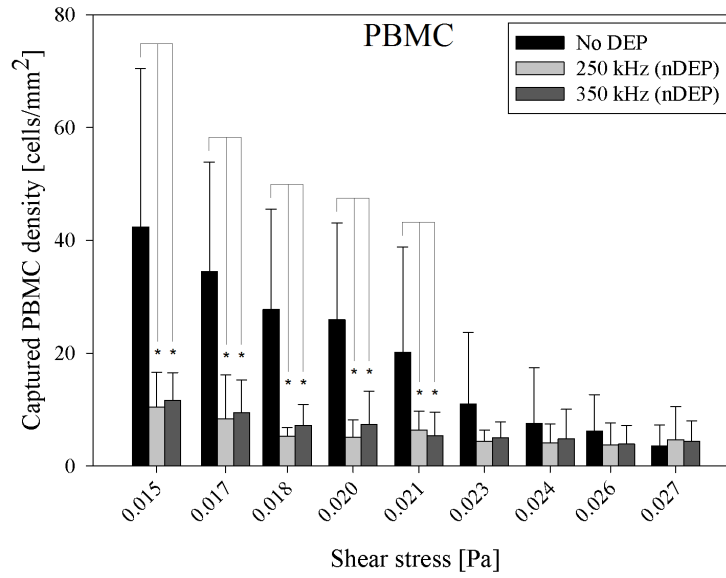
(b)

Figure 4.3: Captured cell density of LNCaPs, 4.3(a), and PBMCs, 4.3(b), as a function of shear stress under experimental conditions of no DEP (black bars; $n = 12$), 6 V_{pp} at 250 kHz (light gray bars; $n = 6$), and 6 V_{pp} at 350 kHz (dark gray bars; $n = 6$). Bars represent the mean captured cell density normalized for streamline divergence in the Hele-Shaw flow cell, and error bars represent standard deviation. A Kruskal-Wallis ANOVA test was used to compare between the experimental conditions. For the LNCaP data, asterisks (*) indicate significance of differences ($P < 0.05$) between the 350 kHz and no-DEP conditions and between the 350 kHz and 250 kHz conditions. For the PBMC data, asterisks indicate significance of differences ($P < 0.05$) between the no-DEP and 250 kHz conditions and between the no-DEP and 350 kHz conditions.

74
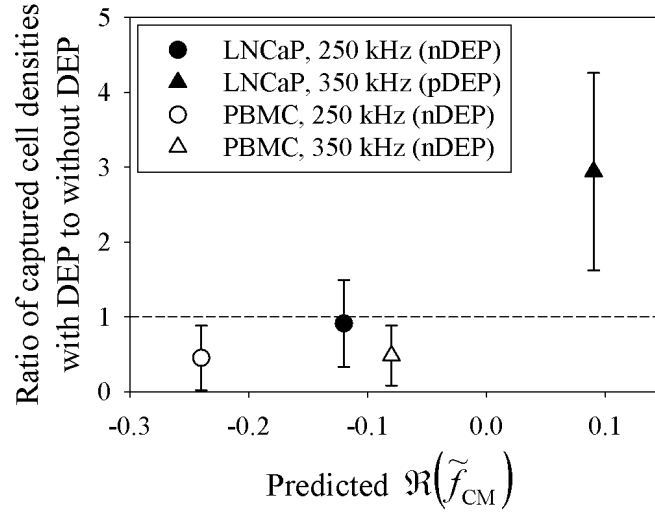
Figure 4.4: Ratios of captured LNCaP and PBMC densities with DEP to without DEP effects averaged across all reported shear stresses shown in Figure 4.3. Error bars represent standard error of the mean of ratios. Predicted $\Re(\tilde{f}_{CM})$ values were taken from the single-shelled dielectric model plotted in Figure 4.2. At 250 kHz, LNCaPs and PBMCs both exhibit a nDEP response, resulting in a calculated ratio less than 1 (i.e., fewer cells were captured with DEP as compared to without DEP). In contrast, at 350 kHz, LNCaPs exhibit a pDEP response that resulted in a ratio much larger than 1 (i.e., more LNCaPs were captured with DEP as compared to without DEP), whereas PBMCs still exhibit a nDEP response that resulted in a ratio less than 1.

adhesion as compared to conditions without DEP at a majority of reported shear stresses. The ratio of captured cell densities with DEP to without DEP averaged across all shear stresses was calculated to be 0.91 for LNCaPs and 0.45 for PBMCs under the 250 kHz condition, as shown in Figure 4.4. The ratio for LNCaPs is marginally less than 1, indicating that the cells exhibited a minimal nDEP response that resulted in negligibly fewer cells being captured as compared to without DEP. In contrast, the ratio for PBMCs is much smaller than 1, indicating that the cells exhibited a strong nDEP response that resulted in significantly fewer cells being captured as compared to without DEP. The conclusions drawn from these comparisons of captured cell densities are supported by tests of statistical significance (Figure 4.3).

At 350 kHz, LNCaPs exhibit a pDEP response whereas PBMCs exhibit a nDEP re-

sponse (as predicted in Figure 4.2); under this condition, it is expected that LNCaPs will be attracted to energized electrodes on the antibody-functionalized surface and that PBMCs will be repelled. Figures 4.3(a) and 4.3(b) show that at a majority of shear stresses, significantly more LNCaPs and fewer PBMCs were captured with DEP as compared to conditions without DEP. The ratio of captured cell densities with DEP to without DEP averaged across all reported shear stresses was calculated to be 2.94 for LNCaPs and 0.48 for PBMCs under the 350 kHz condition, as shown in Figure 4.4. The ratio for LNCaPs is much larger than 1, indicating that the cells exhibited a strong pDEP response that resulted in significantly more cells being captured as compared to without DEP. In contrast, the ratio for PBMCs remains smaller than 1, indicating that the cells continued to exhibit a nDEP response that resulted in significantly fewer cells being captured as compared to without DEP. Once again, the conclusions drawn from these comparisons of captured cell densities are supported by tests of statistical significance (Figure 4.3). In summary, DEP-guided immunocapture of LNCaPs was diminished at 250 kHz and enhanced at 350 kHz, whereas the nonspecific adhesion of PBMCs with DEP was reduced at both 250 kHz and 350 kHz. Therefore, we have shown that by precisely selecting an appropriate frequency, LNCaPs can be enriched from PBMCs with DEP to improve immunocapture performance. Although the ratios presented here do not in themselves justify rare cell capture or enrichment, the device geometry and experimental conditions were chosen to purposely augment nonspecific PBMC adhesion; implementation of DEP conditions in a typical rare cell immunocapture device is expected to lead to significant improvement [126, 60].

Cell adhesion was not only affected by the addition of DEP, but also by the shear stress experienced by cells in the Hele-Shaw flow cell. Without DEP, captured cell densities generally decreased with increasing shear stress. When a nDEP force was applied to PBMCs, nonspecific adhesion was lower at high shear stresses, resulting in statisti-

cally insignificant differences between the no-DEP and nDEP conditions (Figure 4.3(b)). However, when a pDEP force was applied to LNCaPs, captured cell densities were consistently and statistically greater than the no-DEP condition across the entire shear stress range (Figure 4.3(a)). This result suggests that in designing future hybrid DEP-immunocapture devices for CTC capture [126, 152, 60], shear stress (as controlled by flow rate) is an adjustable parameter that can be optimized. For example, flow rate can be increased to minimize interactions between leukocytes and immunocapture surfaces, and the addition of DEP can further reduce nonspecific leukocyte adhesion and promote interactions between CTCs and immunocapture surfaces.

DEP is an advantageous technique because, in many cases, the applied frequency can be tuned to separate cell populations based on differences in their electrical properties. We have previously characterized the DEP response of LNCaPs [60] and, in this study, have shown that prostate cancer cells exhibit a distinct response as compared to PBMCs. Furthermore, in this study, we used a diluted PBS media that is 5–50 times less dilute and 2–7 times more conductive than media used in previous DEP studies [7, 43, 56, 140, 48, 4]. We used PBS as a model for whole blood and expect to demonstrate similar cancer cell capture and enrichment results in minimally diluted blood, which can potentially result in improved throughput and efficiency as compared to current DEP devices. Recently, Shim et al. introduced a media-deionizing region to the previously reported DEP-FFF device [43, 48]; depleting ions in the sample decreases the medium conductivity to a level at which differential DEP separation of cancer and blood cells is possible, and serves an alternative technique to diluting whole blood [150, 149].

Our characterization data of DEP-guided immunocapture of cancer cells as a function of shear stress can also be incorporated into computational fluid dynamics simulations of cancer cell and blood cell trajectories in a 3D immunocapture device to better

predict differential capture performance [45, 79, 152]. These simulations will inform the design of future hybrid DEP-immunocapture systems that have the potential to improve CTC capture purity while retaining the capture efficiency of previous immunocapture devices [113, 45, 155, 170]. The capability of producing a highly pure sample will in turn facilitate subsequent biological studies on captured CTCs, cancer metastasis, and drug therapies [91, 156, 79, 188].

4.5   Conclusions

This work characterizes the DEP-enhanced immunocapture of LNCaPs and nonspecific adhesion of PBMCs to antibody-functionalized surfaces as a function of shear stress. In a model system designed to make nonspecific PBMC adhesion readily apparent, we showed that LNCaPs can be enriched from PBMCs by precisely tuning the frequency of the applied electric field to attract cancer cells to and repel leukocytes from immuno-capture surfaces. This result is dependent on local shear stresses experienced by cells, and informs the design (e.g., geometric features) and optimization (e.g., flow rate, applied frequency) of future hybrid DEP-immunocapture devices for rare cell capture. We expect that such a combination will lead to improved capture performance relative to either technique alone, which will facilitate subsequent biological analyses of captured CTCs.

4.6   Acknowledgements

CHAPTER 5

CHARACTERIZATION OF MICROFLUIDIC SHEAR-DEPENDENT EPCAM IMMUNOCAPTURE AND ENRICHMENT OF PANCREATIC CANCER CELLS FROM BLOOD CELLS WITH DIELECTROPHORESIS

5.1 Abstract

Current microfluidic techniques for isolating circulating tumor cells (CTCs) from cancer patient blood are limited by low capture purity, and dielectrophoresis (DEP) has the potential to complement existing immunocapture techniques to improve capture performance. We present a hybrid DEP and immunocapture Hele-Shaw flow cell to characterize DEP's effects on immunocapture of pancreatic cancer cells (Capan-1, PANC-1, and BxPC-3) and peripheral blood mononuclear cells (PBMCs) with an anti-EpCAM antibody. By carefully specifying the applied electric field frequency, we demonstrate that pancreatic cancer cells are attracted to immunocapture surfaces whereas PBMCs are repelled. Using an exponential capture model to interpret our capture data, we show that immunocapture performance is dependent on the applied DEP force sign and magnitude, cell surface EpCAM expression level, and shear stress experienced by cells flowing in the capture device. Our work suggests that DEP can not only repel contaminating blood cells, but also enhance capture of cancer cell populations that are less likely to be captured by traditional immunocapture methods. This combination of DEP

and immunocapture techniques to potentially increase CTC capture purity can facilitate subsequent biological analyses of captured CTCs and research on cancer metastasis and drug therapies.

5.2   Introduction

Circulating tumor cells (CTCs) are cells that have been shed into the circulatory system from a tumor source, and it is hypothesized that a subpopulation contributes to cancer metstasis by forming secondary tumors elsewhere in the body [3]. Genetic and pharmacological evaluation of captured CTCs can lead to a better understanding of cancer metastasis as well as improved drug therapies [91, 156, 79, 132]. In particular, a high CTC capture purity—the percentage of all captured cells that are actually CTCs—can facilitate numerous subsequent biological analyses by reducing the amount of time and money that is potentially wasted on analyzing contaminating blood cells. For example, the yield from analyses that require single-cell sequencing, such as RNA sequencing to identify distinct CTC gene expression patterns [131, 188, 10, 79] and copy number variation analysis to characterize CTC provenance [136, 114, 125], is directly proportional to purity; a higher sample purity leads to more CTCs per sample that are analyzed, which results in less time and money spent per analysis of a single CTC.

Microfluidic techniques have been used successfully to capture rare CTCs from whole blood with high efficiency, although reported purities are often relatively low because of the nonspecific adhesion of leukocytes to capture surfaces [113, 45, 155, 170, 79]. A majority of immunocapture techniques use the epithelial marker EpCAM, which has been reported to have oncogenic potential [111], is correlated with proliferation in cancer cell lines [47], and has been used to identify CTCs in many cancers

81

[113, 146, 29, 31, 155, 161, 133, 126, 118]. However, EpCAM varies in expression level between cancers and potentially fails to capture more invasive CTCs that have undergone the epithelial-to-mesenchymal transition [103, 99, 116]. Despite differences in cell surface antigen expression levels, a majority of cancer cells are vastly different from blood cells in cellular composition and morphology, which leads to their distinct electrical properties and dielectrophoretic response [149]. Therefore, we hypothesize that dielectrophoresis can potentially be used to capture cancer cells that are less likely to be isolated by traditional immunocapture methods with epithelial markers such as EpCAM. In this work, we aim to study how cancer cell capture performance can be improved by (1) characterizing EpCAM capture as a function of flow conditions (e.g., shear stress) and cancer cell surface expression levels, and (2) incorporating dielectrophoretic effects to enhance cancer cell capture while reducing nonspecific adhesion of leukocytes.

Dielectrophoresis (DEP) is widely used in microfluidics to separate cell populations based on differences in their electrical properties [167, 52, 126]. Within certain applied electric field frequency ranges, cancer cells exhibit a positive DEP (pDEP) response, are attracted to regions of high electric field gradients, and can be separated from blood cells, which exhibit a negative DEP (nDEP) response and are repelled from regions of high electric field gradients [7, 43, 56, 48, 138, 149, 59, 44]. For applications in CTC capture, however, the use of DEP techniques alone have typically been limited by low capture efficiency and throughput owing to the rarity of CTCs in whole blood, as well as by restrictions of device and electrode design and difficulties with applying large enough electric field gradients near rare cells to capture them [126].

Given that existing immunocapture techniques typically report high capture efficiencies but low capture purities, and DEP methods have the potential for high-purity separation by cancer cells' pDEP and blood cells' nDEP responses but are limited by low

capture efficiencies in rare cell capture applications, we hypothesize that DEP may work best as a complement to existing immunocapture devices to act only near immunocapture surfaces where electric fields are strongest and antibody interactions occur to improve capture purity. We previously characterized how a hybrid DEP-immunocapture approach can enrich prostate cancer cells from blood cells by attracting cancer cells to immunocapture surfaces while repelling contaminating peripheral blood mononuclear cells (PBMCs) [60, 59]. However, these studies used an antibody, J591, that is highly specific to the prostate-specific membrane antigen (PSMA) expressed on the surface of prostate cancer cells [96]. As many cancers (e.g., pancreatic) do not have an organ-specific biomarker and therefore are more difficult to capture with EpCAM [161, 133], CTC immunocapture can be further optimized by characterizing capture performance as a function of EpCAM expression level and evaluating the potential benefits of incorporating DEP effects. We have also recently reported on a capture probability model that can be used to inform simulations of capture as a function of shear stress in existing immunocapture device geometries [153]; by characterizing immunocapture with DEP effects, we can predict enhanced CTC capture performance in a future hybrid DEP-immunocapture system.

In the current study, we characterized the DEP response of a panel of pancreatic cancer cell lines (Capan-1, PANC-1, BxPC-3)—which, to our knowledge, has not been described before—with varying levels of EpCAM expression and measured their immunocapture performance as a function of the local shear stress experienced by the cells. This work was performed using a Hele-Shaw flow cell and a protocol designed to make nonspecific adhesion of PBMCs readily apparent [59]. In addition, by precisely tuning the applied electric field frequency, we enriched the pancreatic cancer cells from blood cells by attracting cancer cells to and repelling PBMCs from immunocapture surfaces with pDEP and nDEP, respectively. In comparing immunocapture performance with and

without DEP effects, we also evaluated capture probability as a function of shear stress, cell surface chemistry, and normal force using the previously reported capture probability model [153]. We demonstrate that DEP can enhance immunocapture of cancer cells with lower EpCAM expression and that immunocapture purity can potentially be improved by repelling PBMCs with nDEP; this work informs the design of future hybrid DEP-immunocapture devices with increased CTC capture purity, which will facilitate subsequent functional and genetic analyses to elucidate cancer progression and develop more effective treatment options.

5.3   Materials and methods

5.3.1   Device fabrication and antibody functionalization

A Hele-Shaw flow cell with interdigitated gold electrodes, depicted in Figure 5.1, was used to characterize immunocapture with DEP effects as a function of shear stress. The design and fabrication of this Hele-Shaw DEP device is detailed in our previous work [60, 59, 142]. One major change to the device geometry from previous iterations is an elongation of the straight inlet channel to 45 mm, which allows for all cancer cells and PBMCs to settle to the bottom of the channel before entering the main chamber, and ensures that all cells are rolling on the immunocapture surface in the shear stress range where data is taken. This condition allows for cell capture to be quantified as a fraction of total cells entering the main chamber in subsequent data analysis steps.

The bottom surface of the Hele-Shaw DEP device was functionalized with NeutrAvidin (Thermo Fisher Scientific) following previously reported protocols [45, 142], then incubated with 10 μg/mL biotinylated goat anti-mouse antibody (Santa Cruz Biotech-
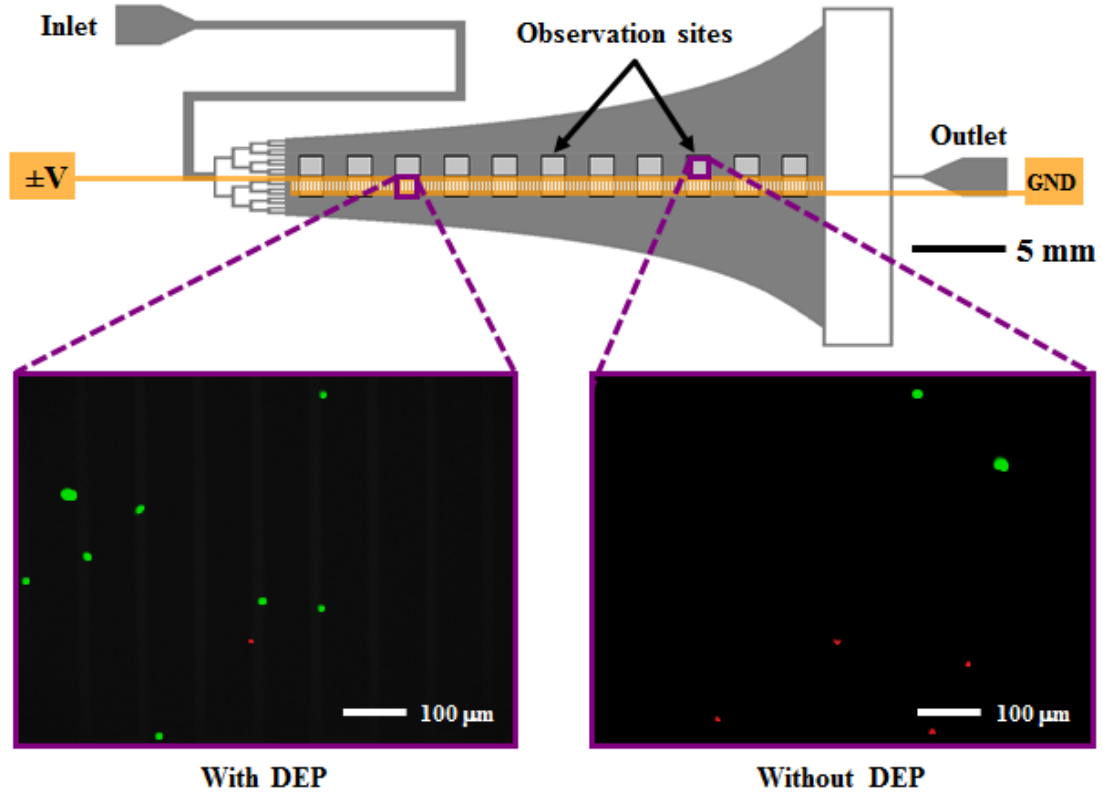
Figure 5.1: Schematic of the Hele-Shaw flow cell and its interdigitated electrodes with lead connections to an applied voltage ($\pm$V) and ground (GND), and elongated straight inlet channel compared to previous designs [60, 59]. The elongated straight inlet channel was 500 μm wide, the smaller branching channels were 156 μm wide, and all channels were 48 μm tall. The main chamber geometry leads to a monotonically decreasing shear stress along the device centerline, which allows for cell capture to be measured as a function of shear stress [163, 112, 142]. Inset images show fluorescently labeled PANC-1 cells (green) and PBMCs (red) adhered to the antibody-functionalized surface with and without DEP effects. These example images show that at an applied AC electric field frequency of 200 kHz, more PANC-1 cells and fewer PBMCs were captured with DEP compared to without DEP. Captured cells in each pair of 1-mm^2 observation windows were enumerated and compared at a series of observation sites corresponding to a range of shear stresses found in typical immunocapture devices [45, 79, 152, 153].

nology) for 1 hour, followed by incubation with 10 μg/mL anti-EpCAM antibody (Clone 158206, R&D Systems) for 1 hour [161]. All antibodies were prepared in 1% BSA in PBS.

5.3.2 Cell culture and preparation

Pancreatic cancer cell lines Capan-1, PANC-1, and BxPC-3 were purchased from the American Type Culture Collection and cultured at 37°C in a 5% CO_2 humidified environment. Capan-1 cells were cultured in 20% FBS in IMDM, PANC-1 cells were cultured in 10% FBS in DMEM, and BxPC-3 cells were cultured in 10% FBS in RPMI. All culture media was also supplemented with 1% penicillin-streptomycin. To prepare for experiments, cancer cells at >80% confluency were trypsinized from their culture flasks and incubated with 5 μM CellTracker^{TM} Green CMFDA (Invitrogen) for at least 30 minutes.

PBMCs were isolated from the blood of consenting colonoscopy screening patients with IRB approval from the University of Michigan School of Medicine. Whole blood was collected in BD Vacutainer$^{®}$ CPT^{TM} Cell Preparation Tubes with Sodium Heparin^{N}, and PBMCs were isolated after centrifugation and incubated with 5 μM CellTracker^{TM} Orange CMRA (Invitrogen) for at least 30 minutes.

After incubation with their respective fluorescent probes, pancreatic cancer cells and PBMCs were washed twice and resuspended in PBS diluted 20 times by volume in an isotonic sugar in DI H_2O solution consisting of 9.5% sucrose and 0.3% dextrose with conductivity 0.07 S/m; this medium was chosen because of the distinct DEP response that cancer cells and blood cells exhibit at the given conductivity [60, 59]. The final cell densities were approximately 5×10^5 cancer cells per mL and 2×10^6 PBMCs per

mL; the two populations were mixed together before injection into the Hele-Shaw DEP device for all experiments except for those with BxPC-3 cells and an applied electric field frequency of 200 kHz, in which blood samples were unavailable and only cancer cell capture was characterized.

5.3.3   Characterization of pancreatic cancer cells' DEP response

In order to separate cancer cells from blood cells, the DEP response of both populations must be characterized as a function of applied electric field frequency. In this study, as with our previous characterization of prostate cancer [60, 59], we measured the approximate DEP crossover frequency of each pancreatic cancer cell line and extrapolated electrical properties to predict their DEP responses. The sign and magnitude of the time-averaged DEP force, $\langle \mathbf{F}_{\text{DEP}} \rangle$, on a spherical particle in an infinite domain with a weakly varying electric field and homogeneous and isotropic complex permittivities is determined by the real part of the Clausius-Mossotti factor, $\Re(\tilde{f}_{\text{CM}})$:

$$\langle \mathbf{F}_{\text{DEP}} \rangle = \pi \varepsilon_{\text{m}} a^3 \Re(\tilde{f}_{\text{CM}}) \nabla (\mathbf{E}_0 \cdot \mathbf{E}_0) \tag{5.1}$$

$$\tilde{f}_{\text{CM}} = \frac{\tilde{\varepsilon}_{\text{p}} - \tilde{\varepsilon}_{\text{m}}}{\tilde{\varepsilon}_{\text{p}} + 2\tilde{\varepsilon}_{\text{m}}}, \tag{5.2}$$

where a is the particle radius, $\mathbf{E} = \mathbf{E}_0 \cos(\omega t)$ is the externally applied AC electric field, ω is the angular frequency of the electric field, $\tilde{\varepsilon} = \varepsilon - \mathrm{i}\sigma/\omega$ is the complex permittivity, $\mathrm{i} = (-1)^{1/2}$, ε is the electrical permittivity, σ is the electrical conductivity, the subscripts p and m denote the particle and the medium, respectively, and bolded letters denote vectors [78]. The frequency at which $\Re(\tilde{f}_{\text{CM}}) = 0$, i.e., when the particle transitions from nDEP to pDEP, or vice versa, is termed the crossover frequency.

To determine the crossover frequency range of the pancreatic cancer cell lines, each

cell population was manually flowed through the Hele-Shaw DEP device and observed above the interdigitated electrodes region on a Nikon LV100 upright microscope. The electrodes were energized by an Agilent 33200A function generator at 6 volts peak-to-peak (V_{pp}) and frequencies ranging from 100 kHz to 1 MHz, and the DEP response was determined at each applied frequency by observing if the cells were attracted to or repelled from the electrodes by pDEP and nDEP, respectively. The DEP response of PBMCs in our setup was characterized in a previous study [59]. After determining each cell population's crossover frequency, we predicted the magnitude of its DEP response as a function of frequency by modeling the cell as a single-shelled dielectric sphere; this approach facilitates the description of a cell's extrinsic electrical properties, as they are often difficult to infer directly from experimental measurments [167, 7, 43, 141]. The effective permittivity of the particle, $\tilde{\varepsilon}_p$, in Equation 5.2, was replaced by an effective permittivity of the cell, $\tilde{\varepsilon}_{cell}$, that describes its electrical properties in terms of a specific membrane capacitance, $C_{membrane}$, and the cytoplasmic permittivity and conductivity [78, 60, 59]:

$$\tilde{\varepsilon}_{cell} = \frac{C_{membrane}\, a\, \tilde{\varepsilon}_{cytoplasm}}{C_{membrane}\, a + \tilde{\varepsilon}_{cytoplasm}}. \tag{5.3}$$

Figure 5.2 shows the predicted DEP responses of Capan-1, PANC-1, BxPC-3 and PBMCs as a function of frequency as described by the dielectric shell model. We fixed the cytoplasmic permittivity and conductivity to $50\varepsilon_0$ ($\varepsilon_0 = 8.85 \times 10^{-12}$ F/m) and 1 S/m, respectively, because these values are within previously reported ranges [7, 141, 50, 149] and varying them did not significantly change the magnitude of $\Re(\tilde{f}_{CM})$ under our experimental conditions. The average cell diameters of Capan-1, PANC-1, and BxPC-3 were previously measured to be 15.8±3.2 μm, 17.3±2.7 μm, and 13.3±2.9 μm, respectively [161], and PBMCs were measured to have an average diameter of 10.1±2.1 μm. We selected 50 kHz and 200 kHz as the frequencies to apply in characterizing nDEP and pDEP effects on cell adhesion as a function of shear
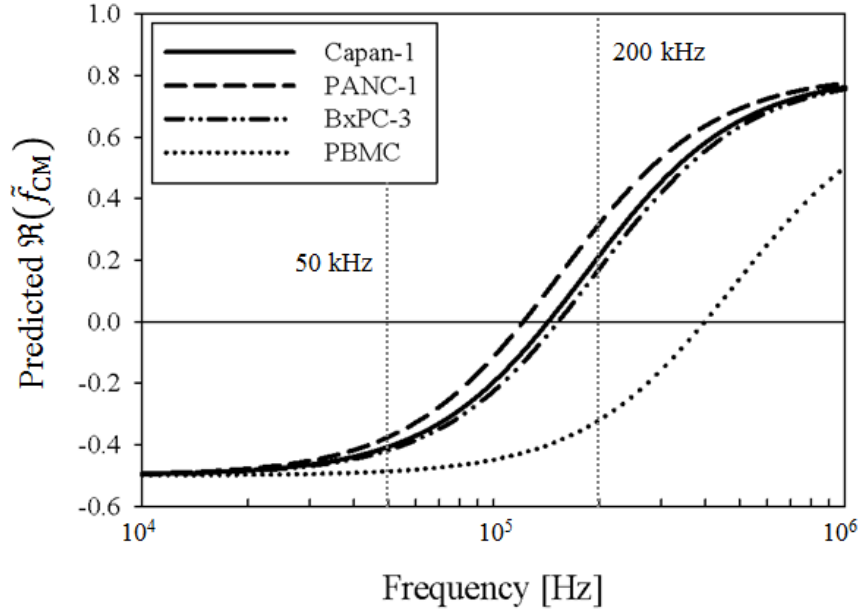
Figure 5.2: Predicted DEP response, as described by $\mathfrak{R}(\tilde{f}_{CM})$, of Capan-1 (solid line), PANC-1 (dashed line), BxPC-3 (dash-dotted line), and PBMCs (dotted line) as a function of applied electric field frequency. Cells were modeled as single-shelled dielectric spheres, described by Equations 5.2 and 5.3. In a diluted PBS suspending medium with $\sigma_m = 0.07$ S/m, the crossover frequency was experimentally determined to be approximately 140 kHz for Capan-1, 120 kHz for PANC-1, 140 kHz for BxPC-3, and 400 kHz for PBMCs. These empirical measurements, combined with Equation 5.3, corresponded to specific membrane capacitance values of $C_{membrane} = 13.5$ mF/m^2 for Capan-1, $C_{membrane} = 14.5$ mF/m^2 for PANC-1, and $C_{membrane} = 15$ mF/m^2 for BxPC-3, and $C_{membrane} = 7.5$ mF/m^2 for PBMCs in the dielectric shell model. At 50 kHz, cancer cells and blood cells both exhibit a nDEP response; at 200 kHz, however, cancer cells exhibit a pDEP response whereas PBMCs still exhibit a nDEP response.

stress. As shown in Figure 5.2, both cancer cells and PBMCs exhibit a nDEP response at 50 kHz, whereas at 200 kHz, cancer cells exhibit a pDEP response while PBMCs exhibit a nDEP response.

5.3.4 Characterization of EpCAM immunocapture with DEP

Capan-1, PANC-1, and BxPC-3 cells were each mixed with PBMCs and each mixture was flowed through the Hele-Shaw DEP device in separate experiments at 0.2 mL/hr

for 10 minutes using a Chemyx Fusion 400 syringe pump. The electrodes were energized at 6 V_{pp} and two frequencies (50 kHz and 200 kHz), with 3–4 experimental replicates each. Fluorescent images of cancer cells and PBMCs were taken with FITC and Texas Red® / Cy3.5™ Chroma filter cubes, respectively, at the observation window closest to the main chamber entrance every minute to quantify the amount of cells coming into the device (that are all rolling on the immunocapture surface). The total number of cells that entered the main chamber over the course of an experiment lasting t minutes was estimated as

$$\int_0^t \frac{\text{\# of cells at time } t}{\text{area of observation window}} \, dt \times (\text{width of observation window})$$
$$\times (\text{velocity in the channel at cell height}),$$
(5.4)

where the width of an observation window was 1 mm, the area of an observation window was 1 mm^2, and the integral was evaluated as a Riemann sum with the difference between upper and lower bounds equal to the number of subdivisions (i.e., the number of cells was counted at every minute):

$$\int_0^t f(t) \, dt = \sum_{i=0}^t f(t_i).$$
(5.5)

After each capture experiment, non-adherent cells were washed away with PBS, and images of captured cancer cells and PBMCs were taken at each observation window pair along the Hele-Shaw DEP device's central axis to directly compare capture with and without DEP as a function of shear stress. Captured cells were enumerated in each observation window and multiplied by a correction factor that was a function of shear stress to normalize for streamline divergence in the device [60, 59]. The number of cells captured in spaces between two adjacent capture windows was estimated as the average number of captured cells in the two adjacent windows and also multiplied by the correction factor. The local capture probability was calculated by dividing the number of cells captured in a capture window (i.e., at a given shear stress value) by the number of

cells that entered that particular window, which in turn was calculated by subtracting the number of cells captured in previous windows and those in the spaces between windows from the total number of cells that entered the device (determined by Equations 5.4 and 5.5).

5.3.5 Derivation of exponential capture model

An exponential fit was used to convert experimental data collected in the Hele-Shaw DEP device into a probabilistic model, suitable for use in immunocapture simulations. This model predicts the probability of adhesion, P_{capture}, as a function of receptor and ligand surface densities, m_r and m_a; the receptor–ligand association constant at zero load, K_a^0; the contact area, A_c; the characteristic receptor–ligand bond length, λ; the thermal energy, $k_B T$; and the dislodging force, F_{dislodge} [32, 169]:

$$P_{\text{capture}} = m_r m_l K_a^0 A_c \exp\left(-\frac{\lambda}{k_B T} \frac{F_{\text{dislodge}}}{m_r A_c}\right). \tag{5.6}$$

As values for these terms are often unavailable for rare cells in circulation, we grouped them into two lumped parameters, A and B, took F_{dislodge} as proportional to the shear stress τ, and discretized the equation as reported previously [153]:

$$dP_{\text{capture}}(\tau) = A \exp(-B\tau) \, dt. \tag{5.7}$$

We identified values for A and B as a function of cell type and the frequency of the applied electric field by integrating the discrete equation over the length of each Hele-Shaw observation window:

$$P_{\text{capture}}(\tau) = \int_{x_1}^{x_2} A \exp(-B\tau) \, dt. \tag{5.8}$$

Noting the relationship between distance x, characteristic velocity U, shear stress τ, and characteristic time t as $t = x/U = x/\tau a$ (where a is the cell radius), and discretizing as

$dt = dx/\tau a$, we found:

$$P_{\text{capture}}(\tau) = \int_{x_1}^{x_2} \frac{A}{\tau a} \exp(-B\tau) \, dx. \tag{5.9}$$

Integrating over each observation window with τ approximated as uniform yielded

$$P_{\text{capture}}(\tau) = \frac{A\Delta x}{\tau a} \exp(-B\tau), \tag{5.10}$$

where Δx is the length of each observation window (i.e., 1 mm) and $P_{\text{capture}}(\tau)$ is the fraction of cell captured that roll through each observation window. We fit our capture fraction versus shear stress data to a simple exponential model of the form

$$P_{\text{capture}}(\tau)\,\tau = A' \exp(-B\tau), \tag{5.11}$$

calculating B directly from our fit, and deriving A algebraically as $A = A'a/\Delta x$. Inserted into Equation 5.10, A and B provide a fit to our experimental data; used in Equation 5.7, A and B can be used to predict capture as cells are advected along a simulated capture surface [153].

5.4 Results and discussion

The immunocapture of pancreatic cancer cells and PBMCs was characterized with and without DEP effects as a function of shear stresses corresponding to those experienced by cells in typical immunocapture device geometries [79, 152, 153, 142, 60, 59]. We chose to characterize the cell lines Capan-1, PANC-1, and BxPC-3 because of differences in their tumor origin (Capan-1 from liver metastasis; PANC-1 and BxPC-3 from primary pancreatic tumors), differentiation state (Capan-1 is well differentiated; PANC-1 and BxPC-3 are moderately to poorly differentiated) [33], and EpCAM expression as measured by antibodies bound per cell [161]. In addition, although Pethig et

al. previously measured the membrane capacitance and conductance of pancreatic beta cells [119] and Shim et al. recently made DEP crossover frequency measurments of all NCI-60 cell lines [149], to our knowledge, the DEP response of these pancreatic cancer cells has not been characterized before. Therefore, in contrast to our previous work with prostate cancer and the highly organ-specific biomarker PSMA [142, 60, 59], we aim to study in this work how DEP and normal forces affect immunocapture of pancreatic cancer cells that have no organ-specific biomarker and varying levels of EpCAM expression with an exponential capture model.

Shear-dependent immunocapture was characterized in a Hele-Shaw flow cell, and cell concentrations were chosen to be high enough to make nonspecific adhesion of PBMCs readily apparent and facilitate comparison with cancer cell capture [59]. In addition, elongation of the straight inlet channel from previous designs [60, 59] led to all cells entering the main chamber to be rolling in contact with the immunocapture surface (Figure 5.1). This initial condition allowed for cell capture along the length of the device to be quantified as a fraction of the number of cells that entered a particular shear stress region (here termed the "capture probability"), which normalizes the data for variations in cell densities between experimental replicates. Figures 5.3(a), 5.3(b), 5.3(c), and 5.3(d) show the capture probability of cells at the Hele-Shaw DEP device's central axis (along which the shear stress is monotonically decreasing and observation windows are located) for Capan-1, PANC-1, BxPC-3, and PBMCs, respectively. With no DEP applied, capture across all cell types generally decreased with increasing shear stress; these trends are in line with our previous characterization work in a Hele-Shaw flow cell [142, 60, 59] as well as in a three-dimensional immunocapture device geometry [153, 161]. In addition, more Capan-1 cells were captured than PANC-1 and BxPC-3 cells at a majority of shear stress values. Previously measured EpCAM antibodies bound per cell (ABC) values by Thege et al. [161], as listed in Table 5.1, show that Capan-1
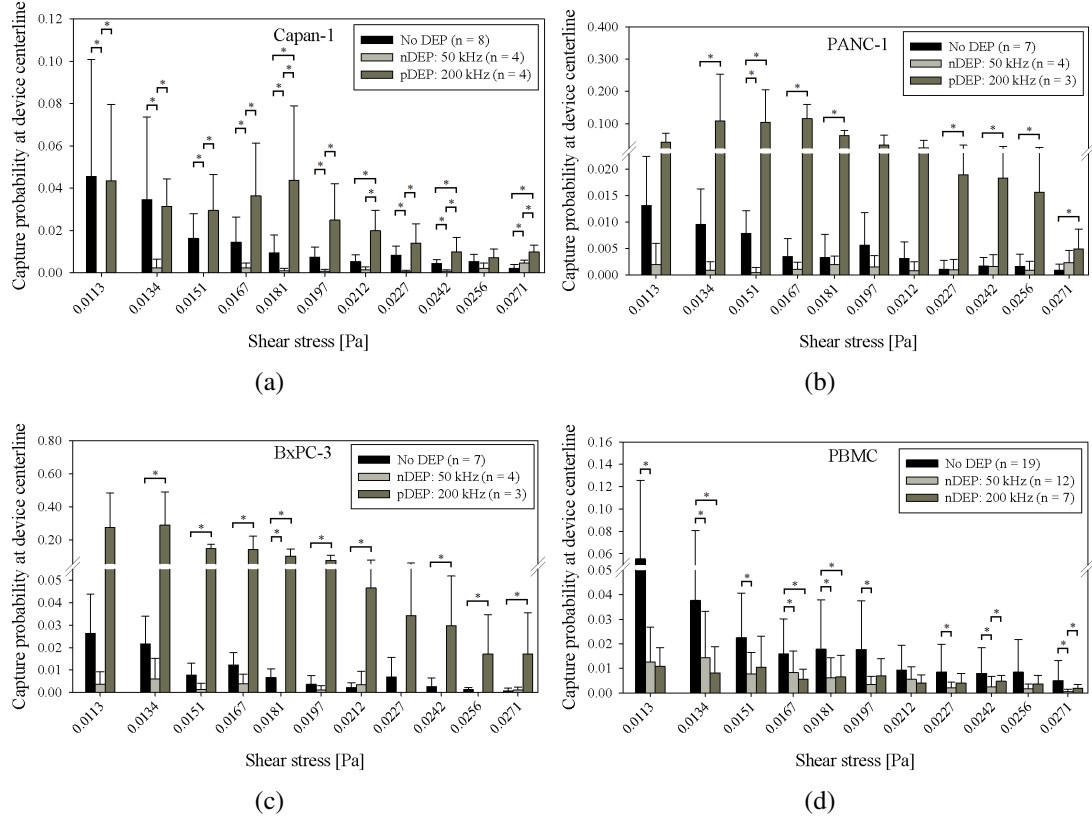
Figure 5.3: Capture probability of Capan-1 cells, 5.3(a), PANC-1 cells, 5.3(b), BxPC-3 cells, 5.3(c), and PBMCs, 5.3(d), at the central axis of the Hele-Shaw DEP device as a function of shear stress under experimental conditions of no DEP (black bars), 50 kHz (light gray bars), and 200 kHz (dark gray bars). Bars represent the mean capture of the indicated number of experimental replicates (n), and error bars represent standard deviation. A Wilcoxon rank-sum test was used to compare between each pair of DEP conditions, and asterisks (*) indicate significance of differences ($P < 0.05$).

cells have a higher expression of EpCAM, which explains the current study's higher Capan-1 capture without DEP effects.

At an applied electric field frequency of 50 kHz, pancreatic cancer cells and PBMCs both exhibit a nDEP response (Figure 5.2). For PBMCs, whose nonspecific adhesion to the immunocapture surface was purposely amplified by the device's geometric design and high input cell concentration to facilitate relative comparisons between capture with and without DEP, fewer cells were captured with nDEP at 50 kHz repelling them from the capture surface as compared to without DEP at a majority of shear stresses

Table 5.1: Ratios of pancreatic cancer cell capture probabilities with DEP to without DEP effects averaged across all reported shear stresses shown in Figure 5.3. Ratios are reported as mean $\pm$ standard error of the mean. EpCAM antibodies bound per cell (ABC) data were previously reported in [161].

Cell line	EpCAM ABC	nDEP (50 kHz) : no DEP	pDEP (200 kHz) : no DEP
Capan-1	71,807	0.33 ± 0.17	2.58 ± 1.04
PANC-1	21,247	0.63 ± 0.69	12.72 ± 7.59
BxPC-3	28,197	0.38 ± 0.55	15.21 ± 8.09

(Figure 5.3(d)). Similarly for the cancer cells, capture with nDEP was lower at a majority of shear stresses, as cells were repelled from immunocapture surfaces (Figure 5.3). Table 5.1 lists the ratios of cancer cell capture probabilities with DEP to without DEP averaged across all reported shear stresses shown in Figure 5.3. The ratio of capture with nDEP to without DEP was less than 1 for all three cell lines, although the errors were larger for PANC-1 and BxPC-3 cells, which indicate that in these cell lines, there were smaller differences between capture with nDEP and without DEP; this result can be explained by PANC-1 and BxPC-3 cells' low EpCAM expression, which already led to a low amount of capture without DEP.

At an applied electric field frequency of 200 kHz, pancreatic cancer cells exhibit a pDEP response whereas PBMCs exhibit a nDEP response (Figure 5.2). For PBMCs, there was a general trend of less capture with nDEP at 200 kHz repelling cells from the immunocapture surface compared to without DEP. For cancer cells, capture with pDEP attracting cells to the immunocapture surface was higher compared to without DEP (Figure 5.3). Interestingly, for PANC-1 and BxPC-3 cells, the magnitude of capture with pDEP was higher than that of Capan-1 cells. Table 5.1 shows that the ratio of capture with pDEP to without DEP is much higher for PANC-1 and BxPC-3 cells compared to Capan-1 cells, which is expected, as Capan-1 cells have a higher EpCAM ABC count and therefore higher capture without DEP. However, the magnitude of Capan-1 capture with pDEP is much lower than that of PANC-1 and BxPC-3 cells, which cannot be

attributed to differences in EpCAM ABC counts or DEP response magnitude, as our dielectric model predicts similar magnitudes of $\Re(\tilde{f}_{\mathrm{CM}})$ for all three cell lines (Figure 5.2). We hypothesize that differences in Capan-1 cells' tumor origin, differentiation state, and mutation status of key oncogenes [33] from those of PANC-1 and BxPC-3 cells may contribute to its observed weaker pDEP response that cannot be inferred from crossover frequency measurements alone. A more robust technique for measuring the magnitude of a cell's DEP response and magnitude is electrorotation [71, 173, 183, 143, 23], which can potentially be used to investigate the precise, absolute magnitudes of each cell line's DEP response as a function of frequency but is beyond the scope of this study. Nevertheless, our results show that pDEP enhances capture of all three pancreatic cancer cell lines, especially for PANC-1 and BxPC-3 cells, which are less differentiated; this suggests that DEP can potentially be used to enhance immunocapture of CTCs that (1) have lower EpCAM expression and are thus less likely to be captured without DEP, and (2) are less differentiated and metastatic, possibly leading to earlier detection of CTCs.

In comparing cancer cell capture with pDEP at 200 kHz to capture with nDEP at 50 kHz, there were more cancer cells captured across a majority of shear stresses for all three cell lines (Figures 5.3(a), 5.3(b), 5.3(c)), showing that DEP can be tuned to enhance or diminish cancer cell immunocapture by pDEP and nDEP, respectively. For PBMCs, capture with nDEP at 200 kHz and capture with nDEP at 50 kHz were similar across all shear stresses (Figure 5.3(d)), indicating that there was not a sigificant difference in the magnitude of the nDEP force experienced by PBMCs at 200 kHz and 50 kHz, as confirmed by the predicted $\Re(\tilde{f}_{\mathrm{CM}})$ magnitudes in Figure 5.2 and calculated $\langle \mathbf{F}_{\mathrm{DEP}} \rangle$ values in Table 5.2.

To further characterize capture probability as a function of shear stress, we fit our shear-dependent capture data for pancreatic cancer cells and PBMCs (Figure 5.3) to an

exponential capture model described in Section 5.3.5 and previously published work [153]. Curve fits to BxPC-3 capture data with no DEP, nDEP at 50 kHz, and pDEP at 200 kHz are shown in Figure 5.4; fit values for the other cell types are listed in Table 5.2. In the capture model, A represents the magnitude of capture and B represents the shear dependence. In our analysis, we found that fitting B as a free parameter under each separate DEP condition did not significantly change the quality of the fit (as measured by residual sum of squares and coefficient of determination calculations) when compared with fixing B to the same value for every DEP condition. Therefore, for each cell type, we fixed B for all DEP conditions to the same value obtained from fitting the capture data with no DEP effects applied (Table 5.2). This result suggests that although our capture data can be described by an exponential function that has a unique decay (determined by B) for each cell type, the decay was not significantly affected by DEP effects in the shear stress range that we tested, and therefore does not require further characterization for our purposes of rare cell capture applications. In this work, we characterize DEP's effect on the relative magnitudes of immunocapture and translate these data to capture probabilities that decay exponentially with increasing shear stress; this exponential capture model can then be used in simulations of a hybrid DEP-immunocapture device to predict capture performance as a function of applied DEP force and shear stress [153].
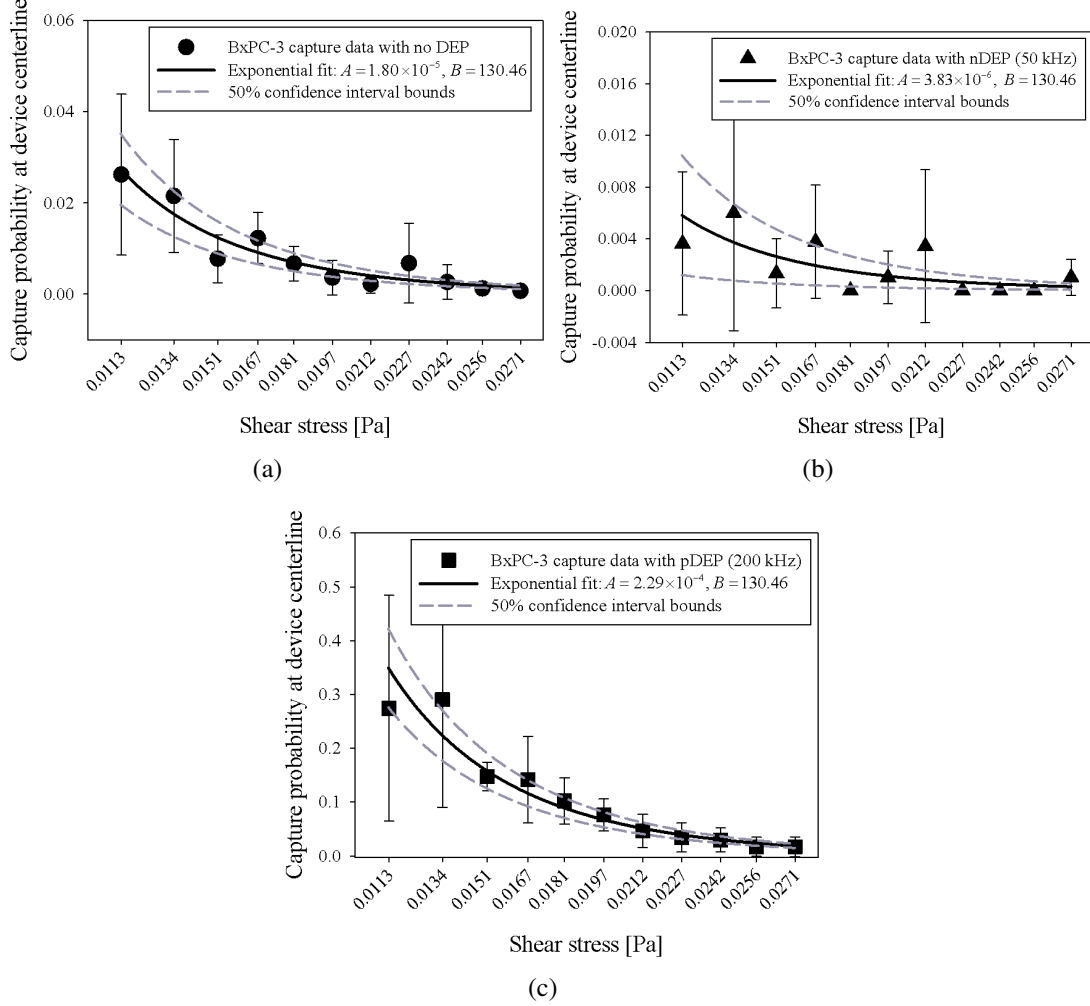
Figure 5.4: Exponential fits (solid line) to shear-dependent BxPC-3 capture data (symbols) shown in Figure 5.3(c) for experimental conditions with no DEP, 5.4(a), nDEP at 50 kHz, 5.4(b), and pDEP at 200 kHz, 5.4(c). The exponential capture model derivation is detailed in Section 5.3.5. A [Pa] and B [Pa^{-1}] values are calculated from the exponential fit described by $P_{\text{capture}}(\tau) = \frac{A\Delta x}{\tau a} \exp(-B\tau)$ (Equation 5.10), and 50% confidence interval upper and lower bounds for the A values are plotted as dashed lines. These fit values for Capan-1, PANC-1, BxPC-3, and PBMC capture data are also listed in Table 5.2.

Table 5.2: Exponential capture model fit values for A [Pa] and B [Pa^{-1}], described by $P_{\text{capture}}(\tau) = \frac{A\Delta r}{\tau a}\exp(-B\tau)$ (Equation 5.10), as a function of cell type and normal force, $\mathbf{F}$ [N], to the immunocapture surface. In a typical obstacle-array immunocapture geometry, the normal force (Stokes' drag, $\mathbf{F}_{\text{Stokes}} = 6\pi\mu a U$, where μ is the fluid viscosity, a is the cell radius, and U is the velocity of the cell normal to the obstacle) on a cell in contact with the obstacle varies from approximately zero to a maximum value reported in the table. With no DEP effects applied in the Hele-Shaw DEP device, the only normal force present is gravitational, $\mathbf{F}_{\text{g}}$. With DEP effects applied, however, the normal force is dominated by the time-averaged DEP force, $\langle\mathbf{F}_{\text{DEP}}\rangle$, described by Equations 5.1 and 5.2, with predicted $\Re(\tilde{f}_{\text{CM}})$ values taken from Figure 5.2 at 50 kHz and 200 kHz and the gradient of the electric field calculated by COMSOL simulation at a height equivalent to the cell radius above the immunocapture surface and electrodes. A positive force represents attraction to the immunocapture surface, whereas a negative force represents repulsion.

Cell type	No DEP				50 kHz			200 kHz		
	$\mathbf{F}_{\text{Stokes}}$	$\mathbf{F}_{\text{g}}$	A	B	$\langle\mathbf{F}_{\text{DEP}}\rangle$	A	B	$\langle\mathbf{F}_{\text{DEP}}\rangle$	A	B
Capan-1	1.40×10^{-11}	2.10×10^{-11}	2.58×10^{-5}	108.97	-1.48×10^{-9}	1.99×10^{-6}	108.97	1.25×10^{-9}	4.21×10^{-5}	108.97
PANC-1	1.62×10^{-11}	2.75×10^{-11}	5.53×10^{-6}	76.29	-1.76×10^{-9}	1.44×10^{-6}	76.29	9.70×10^{-10}	5.97×10^{-5}	76.29
BxPC-3	1.06×10^{-11}	1.25×10^{-11}	1.80×10^{-5}	130.46	-1.31×10^{-9}	3.83×10^{-6}	130.46	5.44×10^{-10}	2.29×10^{-4}	130.46
PBMC	6.66×10^{-12}	5.43×10^{-12}	1.24×10^{-5}	73.98	-1.14×10^{-9}	3.93×10^{-6}	73.98	-7.45×10^{-10}	3.96×10^{-6}	73.98

Figure 5.4 shows representative capture model fits to cancer cell (BxPC-3) capture data as a function of shear stress. For experimental conditions without DEP and especially with pDEP at 200 kHz (Figures 5.4a and 5.4c), cancer cell capture was generally high across the length of the device, resulting in good exponential fits to the data. The capture data with nDEP at 50 kHz (Figure 5.4b) was also fit well by an exponential function, but was noisier because there was comparatively lower capture compared to the other two experimental conditions (nDEP repelled cells across a majority of shear stresses). The magnitude of cancer cell capture with and without DEP effects is represented by A in the capture model, listed for each cell type under each DEP condition in Table 5.2. In general, A values were highest for cancer cell capture with pDEP at 200 kHz and lowest for cancer cell capture with nDEP at 50 kHz, as expected. For PBMCs, A was highest for capture with no DEP and similar for capture with nDEP at both 50 kHz and 200 kHz. In addition, we found that B values were unique for each cell type, indicating that the capture performance of each cell type was different and dependent on EpCAM expression levels and electrical properties.

To interpret our capture data as a function of normal force to an immunocapture surface (which is the key information needed for future simulation work on capture probability in a hybrid DEP-immunocapture device), we calculated the Stokes drag on each cell type when in contact with an obstacle in a typical obstacle-array immunocapture device (such as the one described in [45, 79, 46, 153]) from the normal component of the cell's velocity. In addition, we calculated each cell type's weight (gravitational force, $\mathbf{F}_g$, with no DEP effects) and predicted DEP response, $\langle \mathbf{F}_{DEP} \rangle$; these normal forces are all listed in Table 5.2. Although the equation for $\langle \mathbf{F}_{DEP} \rangle$ (Equation 5.1) assumes a linearly varying electric field (which is not the case near the electrodes in our device geometry) and is derived by only retaining the first term of a linear multipole expansion, Equation 5.1 provides a reasonable first-order approximation of the DEP force if the electric

field is approximately axisymmetric on the length scale of the cell and if the characteristic length scale of the electric field non-uniformity is large compared to the cell size [52]. For simplicity and to only compare normal forces directly, we also ignored tangential DEP forces that are present in the system, but acknowledge that such forces can potentially change immunocapture's shear dependence. The calculated $\langle \mathbf{F}_{DEP} \rangle$ values for all cell types were approximately 1–2 orders of magnitude larger than $\mathbf{F}_{Stokes}$ and $\mathbf{F}_g$, suggesting that under similar experimental conditions, DEP can be made the predominant normal force in a hybrid DEP-immunocapture geometry and actuate cell motion toward or away from immunocapture surfaces in the presence of other weaker fluid mechanical forces.

Interestingly, the cell size (whose cube is proportional to $\langle \mathbf{F}_{DEP} \rangle$ magnitude) does not appear to correlate with the amount of capture increase with pDEP or decrease with nDEP. For example, BxPC-3 cells are the smallest of the three cancer cell lines, had the lowest predicted $\langle \mathbf{F}_{DEP} \rangle$ magnitude, and expressed lower EpCAM levels than Capan-1 cells (Table 5.1), but had the highest *A* and *B* values with DEP (Table 5.2). These results show that BxPC-3 cells had higher capture with pDEP on average (which was unexpected given its lower EpCAM expression), but that this capture performance decayed faster with increasing shear stress compared to other cell lines, suggesting that pDEP enhancement may only work optimally at lower shear stresses and also depend on other factors such as differences in tumor origin, differentiation state, and mutation status of key oncogenes whose effects on DEP response are difficult to infer from our current measurements. Importantly, however, our data demonstrate that DEP can enhance the immunocapture of cancer cells regardless of their surface antigen expression levels, and therefore DEP has the potential not only to increase capture purity when used in combination with traditional immunocapture methods, but also to isolate cancer cells that are less likely to be captured by these immunocapture methods with epithelial

markers. DEP-enhanced capture of cancer cells that have undergone the epithelial-to-mesenchymal transition (EMT), for example, can provide access to a subpopulation of CTCs that is currently difficult to isolate and facilitate studies on EMT's role in cancer progression [100, 123].

5.5 Conclusions

This work characterizes shear-dependent EpCAM immunocapture of pancreatic cancer cells enhanced by pDEP and nonspecific adhesion of PBMCs reduced by nDEP. We interpret our capture data using an exponential capture model, and show that capture performance is dependent on the applied DEP force magnitude, cell surface EpCAM expression level, and shear stress experienced by cells flowing in the capture device. Importantly, our results show that DEP enhances immunocapture of cancer cells regardless of their surface epithelial antigen expression levels. Our characterization of DEP-controlled immunocapture inform the simulation of cancer cell and blood cell capture probabilities in a proposed hybrid DEP-immunocapture system for CTC capture, which we expect will increase capture purity and facilitate subsequent biological analyses of captured CTCs to better understand cancer metastasis and improve drug therapies.

5.6 Acknowledgements

CHAPTER 6

CONCLUSIONS

In this work, we used microfluidic devices to investigate and optimize relevant experimental parameters for DEP separation and immunocapture techniques operating in concert. In **Chapter 2**, we reviewed the state-of-the-art devices—both electrokinetic and non-electrokinetic—for microfluidic rare cell capture applications, and found that a majority of these devices have a performance tradeoff between high-efficiency and high-purity capture. We noted that DEP and immunocapture techniques have complementary strengths, and hypothesized that a combination of the two can potentially result in improved rare cell capture performance.

To test our hypotheses, we designed and fabricated a hybrid DEP and immunocapture microfluidic system to characterize adhesion of cancer cells and blood cells to immunocapture surfaces. In **Chapter 3** and **Chapter 4**, we made novel measurements of the DEP response of prostate cancer cells, and demonstrated that DEP and immunocapture techniques can work synergistically to enrich prostate cancer cells from PBMCs; at the same applied electric field frequency, immunocapture of prostate cancer cells was enhanced by positive DEP, and nonspecific adhesion of PBMCs was reduced by negative DEP. To our knowledge, these were the first reported studies of DEP effects on enhancing immunocapture of prostate cancer cells with a highly organ-specific biomarker.

In **Chapter 5**, we extended our characterization work to cancers with no organ-specific biomarkers, and investigated DEP's effects on anti-EpCAM immunocapture of pancreatic cancer cells. We made novel measurements of pancreatic cancer cells' DEP response, and showed that capture performance is dependent on the applied DEP force sign and magnitude, cell surface EpCAM expression level, and shear stress experienced by cells flowing in the capture device. Importantly, we demonstrated that DEP can en-

hance capture of cancer cells regardless of their surface antigen expression levels, therefore indicating that DEP has the potential to isolate cancer cells that are less likely to be captured by traditional immunocapture methods with epithelial markers. We concluded that DEP experimental parameters can be tuned and optimized to enhance capture of cancer cells and reduce nonspecific adhesion of blood cells, although precise measurements of factors affecting DEP response and capture performance (e.g., tumor origin, differentiation state, mutation status of key oncogenes) are difficult to infer from our current measurements and require further characterization.

The work presented in this thesis are the first reported studies of a hybrid DEP and immunocapture microfluidic system for characterization of cancer cell capture. To date, there has not been a reported study on isolation of CTCs from whole blood using DEP techniques alone; however, recent work has shown that DEP is capable of isolating cultured cancer cells from PBMCs in a low-conductivity solution similar to that used in this thesis [48, 150]. DEP techniques' limited ability to deliver high capture efficiencies at low cell concentrations remains a technical challenge [43, 150], and thus we believe that DEP may work best to increase CTC capture purity as a complement to existing immunocapture geometries that are already capable of high-efficiency capture. The need to use a low-conductivity solution to induce a pDEP response in cancer cells and nDEP response in blood cells at the same applied electric field frequency also introduces extra preparation steps to the CTC isolation protocol that hinders the simple, single-step capture of CTCs *from whole blood* that current state-of-the-art immunocapture devices employ.

To address the limitations of current DEP methods for rare cell capture applications, we believe that future work in this field should focus on incorporating DEP effects into existing immunocapture device geometries to increase CTC capture purity while re-

taining the immunocapture techniques' high capture efficiencies. Therefore, immediate future work should focus on two key areas: (1) characterization of cancerous and non-cancerous cells' DEP response with electrorotation techniques, and (2) simulation of DEP effects in immunocapture geometries to inform the design of future hybrid DEP-immunocapture devices.

Precise measurement of cells' DEP response can be made with electrorotation techniques [71, 173, 183, 143, 23] to precisely quantify differences in DEP force magnitudes as functions of applied frequency and other biological and experimental factors. In particular, if DEP is to be used in whole blood (a highly conductive medium), then the DEP response of cancer cells needs to be carefully measured in high-conductivity solutions. In unpublished data, we found that the predicted DEP response of cancer cells in these high-conductivity solutions (on the order of 1 S/m) is negative across the same applied frequencies tested with low-conductivity solutions. Therefore, it is important to verify these predictions (made using dielectric models) with biophysical measurements to confirm cancer cells' nDEP response in high-conductivity media such as blood; if the nDEP response is confirmed, then a frequency range must be selected in which cancer cells exhibit a weak nDEP response whereas blood cells exhibit a strong nDEP response to improve capture purity only with repulsion of contaminating blood cells from immunocapture surfaces using nDEP and no enhancement of cancer cell capture using pDEP.

Furthermore, precise measurements of DEP response with electrorotation techniques can elucidate the differences in DEP force magnitudes and electrical properties between cell populations that are difficult to measure in our current devices. By characterizing these differences between non-cancerous epithelial cells (e.g., hTERT-HPNE [89]) or cancer cells in various stages of the epithelial-to-mesenchymal transition, for example,

we can not only precisely tune the applied electric field for better separation performance from blood cells, but also make biophysical measurements and comparisons of cellular morphology and composition between cancerous and non-cancerous cells, cells in various differentiation states, or cells under physiological stress to better characterize and define CTCs and its subpopulations.

These precise DEP characterization data combined with the shear-dependent immunocapture data presented in this thesis can be incorporated into further computational fluid dynamics simulations of cancer cell and blood cell capture probabilities [46, 153] with DEP effects in an immunocapture device geometry. These simulations can not only inform experimental parameters for optimized CTC capture, but also the geometric design and fabrication of a first-generation hybrid DEP and immunocapture rare cell capture device capable of high capture efficiency *and* purity. We expect that such a device can eventually be used by clinical technicians to produce highly pure captured CTC samples to facilitate functional and genetic analyses for the development of improved cancer treatment options.

BIBLIOGRAPHY

[1] André A Adams, Paul I Okagbare, Juan Feng, Matuesz L Hupert, Don Patterson, Jost Göttert, Robin L McCarley, Dimitris Nikitopoulos, Michael C Murphy, and Steven A Soper. Highly efficient circulating tumor cell isolation from whole blood and label-free enumeration using polymer-based microfluidics with an integrated conductivity sensor. *Journal of the American Chemical Society*, 130(27):8633–41, July 2008.

[2] Anas Alazzam, Ion Stiharu, Rama Bhat, and Ari-Nareg Meguerditchian. Interdigitated comb-like electrodes for continuous separation of malignant cells from blood using dielectrophoresis. *Electrophoresis*, 32(11):1327–36, June 2011.

[3] W Jeffrey Allard, Jeri Matera, M Craig Miller, Madeline Repollet, Mark C Connelly, Chandra Rao, Arjan G J Tibbe, Jonathan W Uhr, and Leon W M M Terstappen. Tumor cells circulate in the peripheral blood of all major carcinomas but not in healthy subjects or patients with nonmalignant diseases. *Clinical Cancer Research*, 10(20):6897–904, October 2004.

[4] Mohammed Alshareef, Nicholas Metrakos, Eva Juarez Perez, Fadi Azer, Fang Yang, Xiaoming Yang, and Guiren Wang. Separation of tumor cells with dielectrophoresis-based microfluidic chip. *Biomicrofluidics*, 7(1):011803, 2013.

[5] Ning Bao, Jun Wang, and Chang Lu. Recent advances in electric analysis of cells in microfluidic systems. *Analytical and bioanalytical chemistry*, 391(3):933–42, 2008.

[6] Louise M Barrett, Andrew J Skulan, Anup K Singh, Eric B Cummings, and Gregory J Fiechtner. Dielectrophoretic manipulation of particles and cells using insulating ridges in faceted prism microchannels. *Analytical chemistry*, 77(21):6798–804, November 2005.

[7] F F Becker, P R Gascoyne, X B Wang, Y Huang, R Pethig, and J Vykoukal. Separation of human breast cancer cells from blood by differential dielectric affinity. *Proceedings of the National Academy of Sciences of the United States of America*, 92(3):860–4, January 1995.

[8] Sanchari Bhattacharya, Tzu-Chiao Chao, and Alexandra Ros. Insulator-based dielectrophoretic single particle and single cancer cell trapping. *Electrophoresis*, 32(18):2550–8, September 2011.

[9] Thomas Braschler, Nicolas Demierre, Elisabete Nascimento, Tiago Silva, Abel G Oliva, and Philippe Renaud. Continuous separation of cells by balanced dielectrophoretic forces at multiple frequencies. *Lab on a chip*, 8(2):280–6, 2008.

[10] Gordon M Cann, Zulfiqar G Gulzar, Samantha Cooper, Robin Li, Shujun Luo, Mai Tat, Sarah Stuart, Gary Schroth, Sandhya Srinivas, Mostafa Ronaghi, James D Brooks, and Amirali H Talasaz. mRNA-Seq of single prostate cancer circulating tumor cells reveals recapitulation of gene expression and pathways found in prostate cancer. *PLOS ONE*, 7(11):e49144, January 2012.

[11] Kelly E Caputo, Dooyoung Lee, Michael R King, and Daniel A Hammer. Adhesive dynamics simulations of the shear threshold effect for leukocytes. *Biophysical Journal*, 92(3):787–97, February 2007.

[12] Esther G Cen, Colin Dalton, Youlan Li, Sophia Adamia, Linda M Pilarski, and Karan V I S Kaler. A combined dielectrophoresis, traveling wave dielectrophoresis and electrorotation microchip for the manipulation and characterization of human malignant cells. *Journal of microbiological methods*, 58(3):387–401, September 2004.

[13] Wesley C Chang, Luke P Lee, and Dorian Liepmann. Adhesion-based capture and separation of cells for microfluidic devices. *Materials Research Society Proceedings*, 79, 2002.

[14] D F Chen and H Du. Simulation studies on electrothermal fluid flow induced in a dielectrophoretic microelectrode system. *Journal of Micromechanics and Microengineering*, 16(11):2411–2419, November 2006.

[15] P. Chen, X. Feng, W. Du, and B.F. Liu. Microfluidic chips for cell sorting. *Frontiers in Bioscience*, 2008.

[16] I-Fang Cheng, Hsien-Chang Chang, Diana Hou, and Hsueh-Chia Chang. An integrated dielectrophoretic chip for continuous bioparticle filtering, focusing, sorting, trapping, and detecting. *Biomicrofluidics*, 1(2):21503, 2007.

[17] I-Fang Cheng, Victoria E Froude, Yingxi Zhu, Hsueh-Chia Chang, and Hsien-Chang Chang. A continuous high-throughput bioparticle sorter based on 3D traveling-wave dielectrophoresis. *Lab on a chip*, 9(22):3193–201, 2009.

[18] Yoon-Kyoung Cho, Suhyeon Kim, Kyusang Lee, Chinsung Park, Jeong-Gun Lee, and Christopher Ko. Bacteria concentration using a membrane type insulator-based dielectrophoresis in a plastic chip. *Electrophoresis*, 30(18):3153–9, 2009.

[19] Sungyoung Choi, Seunjeong Song, Chulhee Choi, and Je-Kyun Park. Microfludic self-sorting of mammalian cells to achieve cell cycle synchrony by hydrophoresis. *Analytical Chemistry*, 81:1964–1968, 2009.

[20] C Chou, J O Tegenfeldt, O Bakajin, S Chan, E Cox, N Darnton, T Duke, and R Austin. Electrodeless Dielectrophoresis of Single- and Double-Stranded DNA. *Biophysical Journal*, 83(4):2170–2179, October 2002.

[21] Cheng-Hsin Chuang, Yao-Wei Huang, and Yao-Tung Wu. System-level biochip for impedance sensing and programmable manipulation of bladder cancer cells. *Sensors*, 11(11):11021–35, January 2011.

[22] Christopher Church, Junjie Zhu, Gaoyan Wang, Tzuen-Rong J. Tzeng, and Xiangchun Xuan. Electrokinetic focusing and filtration of cells in a serpentine microchannel. *Biomicrofluidics*, 3(4):044109, 2009.

[23] M Cristofanilli, G De Gasperis, L S Zhang, M C Hung, P R C Gascoyne, and G N Hortobagyi. Automated electrorotation to reveal dielectric variations related to HER-2/neu overexpression in MCF-7 sublines. *Clinical Cancer Research*, 8(2):615–619, February 2002.

[24] Massimo Cristofanilli, G Thomas Budd, Matthew J Ellis, Alison Stopeck, Jeri Matera, M Craig Miller, James M Reuben, Gerald V Doyle, W Jeffrey Allard, Leon W M M Terstappen, and Daniel F Hayes. Circulating tumor cells, disease progression, and survival in metastatic breast cancer. *The New England Journal of Medicine*, 351(8):781–91, August 2004.

[25] Massimo Cristofanilli, Savitri Krishnamurthy, Chandra M Das, James M Reuben, William Spohn, Jamileh Noshari, Frederick Becker, and Peter R Gascoyne. Dielectric cell separation of fine needle aspirates from tumor xenografts. *Journal of Separation Science*, 31(21):3732–9, 2008.

[26] L Cui and H Morgan. Design and fabrication of travelling wave dielectrophoresis structures. *Journal of Micromechanics and Microengineering*, 10(1):72–79, March 2000.

[27] Eric B. Cummings and Anup K. Singh. Dielectrophoresis in Microchips Containing Arrays of Insulating Posts: Theoretical and Experimental Results. *Analytical Chemistry*, 75(18):4724–4731, September 2003.

[28] Daniel C Danila, Martin Fleisher, and Howard I Scher. Circulating tumor cells as biomarkers in prostate cancer. *Clinical Cancer Research*, 17(12):3903–12, June 2011.

[29] Daniel C Danila, Glenn Heller, Gretchen A Gignac, Rita Gonzalez-Espinoza, Aseem Anand, Erika Tanaka, Hans Lilja, Lawrence Schwartz, Steven Larson, Martin Fleisher, and Howard I Scher. Circulating tumor cell number and prognosis in progressive castration-resistant prostate cancer. *Clinical Cancer Research*, 13(23):7053–8, December 2007.

[30] JA Davis, DW Inglis, KJ Morton, DA Lawrence, LR Huang, SY Chou, JC Sturm, and RH Austin. Deterministic hydrodynamics: Taking blood apart. *Proceedings of the National Academy of Sciences of the United States of America*, 103(40):14779–14784, 2006.

[31] Johann S de Bono, Howard I Scher, R Bruce Montgomery, Christopher Parker, M Craig Miller, Henk Tissing, Gerald V Doyle, Leon W W M Terstappen, Kenneth J Pienta, and Derek Raghavan. Circulating tumor cells predict survival benefit from treatment in metastatic castration-resistant prostate cancer. *Clinical Cancer Research*, 14(19):6302–9, October 2008.

[32] P Decuzzi and M Ferrari. The adhesive strength of non-spherical particles mediated by specific interactions. *Biomaterials*, 27(30):5307–14, October 2006.

[33] Emily L Deer, Jessica González-Hernández, Jill D Coursen, Jill E Shea, Josephat Ngatia, Courtney L Scaife, Matthew A Firpo, and Sean J Mulvihill. Phenotype and genotype of pancreatic cancer cell lines. *Pancreas*, 39(4):425–35, May 2010.

[34] Udara Dharmasiri, Subramanian Balamurugan, André A Adams, Paul I Okagbare, Annie Obubuafo, and Steven A Soper. Highly efficient capture and enumeration of low abundance prostate cancer cells using prostate-specific membrane antigen aptamers immobilized to a polymeric microfluidic device. *Electrophoresis*, 30(18):3289–300, September 2009.

[35] Udara Dharmasiri, Samuel K Njoroge, MaĆgorzata A Witek, Morayo G Adebiyi, Joyce W Kamande, Mateusz L Hupert, Francis Barany, and Steven A Soper. High-throughput selection, enumeration, electrokinetic manipulation, and molecular profiling of low-abundance circulating tumor cells using a microfluidic system. *Analytical Chemistry*, 83(6):2301–9, March 2011.

[36] Elan Diamond, Guang Yu Lee, Naveed H Akhtar, Brian J Kirby, Paraskevi Giannakakou, Scott T Tagawa, and David M Nanus. Isolation and characterization of circulating tumor cells in prostate cancer. *Frontiers in Oncology*, 2:131, January 2012.

[37] F Du, M Baune, and J Thoming. Insulator-based dielectrophoresis in viscous

media - Simulation of particle and droplet velocity. *Journal of Electrostatics*, 65(7):452–458, June 2007.

[38] C D Falokun, F Mavituna, and G H Markx. AC electrokinetic characterisation and separation of cells with high and low embryogenic potential in suspension cultures of carrot (Daucus carota). *Plant Cell Tissue and Organ Culture*, 75(3):261–272, December 2003.

[39] Henry O Fatoyinbo, Michael P Hughes, Stacey P Martin, Paul Pashby, and Fatima H Labeed. Dielectrophoretic separation of Bacillus subtilis spores from environmental diesel particles. *Journal of environmental monitoring : JEM*, 9(1):87–90, 2007.

[40] K R Foster, F A Sauer, and H P Schwan. Electrorotation and levitation of cells and colloidal particles. *Biophysical Journal*, 63(1):180–90, July 1992.

[41] Nitzan Gadish and Joel Voldman. High-throughput positive-dielectrophoretic bioparticle microconcentrator. *Analytical chemistry*, 78(22):7870–6, November 2006.

[42] Peter Gascoyne, Chulabhorn Mahidol, Mahidol Ruchirawat, Jutamaad Satayavivad, Piyajit Watcharasit, and Frederick F Becker. Microsample preparation by dielectrophoresis: isolation of malaria. *Lab on a chip*, 2(2):70–5, 2002.

[43] Peter R C Gascoyne, Jamileh Noshari, Thomas J Anderson, and Frederick F Becker. Isolation of rare cells from cell mixtures by dielectrophoresis. *Electrophoresis*, 30(8):1388–98, 2009.

[44] Peter R C Gascoyne, Sangjo Shim, Jamileh Noshari, Frederick F Becker, and Katherine Stemke-Hale. Correlations between the dielectric properties and exterior morphology of cells revealed by dielectrophoretic field-flow fractionation. *Electrophoresis*, 34(7):1042–50, April 2013.

[45] Jason P Gleghorn, Erica D Pratt, Denise Denning, He Liu, Neil H Bander, Scott T Tagawa, David M Nanus, Paraskevi A Giannakakou, and Brian J Kirby. Capture of circulating tumor cells from whole blood of prostate cancer patients using geometrically enhanced differential immunocapture (GEDI) and a prostate-specific antibody. *Lab on a Chip*, 10(1):27–9, January 2010.

[46] Jason P. Gleghorn, James P. Smith, and Brian J. Kirby. Transport and collision dynamics in periodic asymmetric obstacle arrays: Rational design of microfluidic rare-cell immunocapture devices. *Physical Review E*, 88(3):032136, September 2013.

[47] Johanna M Gostner, Dominic Fong, Oliver A Wrulich, Florian Lehne, Marion Zitt, Martin Hermann, Sylvia Krobitsch, Agnieszka Martowicz, Guenther Gastl, and Gilbert Spizzo. Effects of EpCAM overexpression on human breast cancer cell lines. *BMC Cancer*, 11:45, January 2011.

[48] Vishal Gupta, Insiya Jafferji, Miguel Garza, Vladislava O. Melnikova, David K. Hasegawa, Ronald Pethig, and Darren W. Davis. ApoStreamâĎć, a new dielectrophoretic device for antibody independent isolation and recovery of viable cancer cells from blood. *Biomicrofluidics*, 6(2):024133, 2012.

[49] D A Hammer and D A Lauffenburger. A dynamical model for receptor-mediated cell adhesion to surfaces. *Biophysical Journal*, 52(3):475–87, September 1987.

[50] Song-I Han, Young-Don Joo, and Ki-Ho Han. An electrorotation technique for measuring the dielectric properties of cells with simultaneous use of negative quadrupolar dielectrophoresis and electrorotation. *The Analyst*, 138(5):1529–37, March 2013.

[51] Masahiko Hashimoto, Hirokazu Kaji, and Matsuhiko Nishizawa. Selective capture of a specific cell type from mixed leucocytes in an electrode-integrated microfluidic device. *Biosensors & Bioelectronics*, 24(9):2892–7, 2009.

[52] Benjamin G Hawkins, Jason P Gleghorn, and Brian J Kirby. Dielectrophoresis for Particle and Cell Manipulations. In Jeffrey D. Zahn, editor, *Methods in Bioengineering: Biomicrofabrication and Biomicrofluidics*, chapter 6, pages 133–81. Artech House, Boston, MA, 2009.

[53] Benjamin G Hawkins, Chao Huang, Srinitya Arasanipalai, and Brian J Kirby. Automated dielectrophoretic characterization of Mycobacterium smegmatis. *Analytical Chemistry*, 83(9):3507–15, May 2011.

[54] Benjamin G Hawkins, A Ezekiel Smith, Yusef A Syed, and Brian J Kirby. Continuous-flow particle separation by 3D Insulative dielectrophoresis using coherently shaped, dc-biased, ac electric fields. *Analytical Chemistry*, 79(19):7291–300, October 2007.

[55] Daniel F Hayes, Massimo Cristofanilli, G Thomas Budd, Matthew J Ellis, Alison Stopeck, M Craig Miller, Jeri Matera, W Jeffrey Allard, Gerald V Doyle, and Leon W W M Terstappen. Circulating tumor cells at each follow-up time point during therapy of metastatic breast cancer patients predict progression-free and overall survival. *Clinical Cancer Research*, 12(14 Pt 1):4218–24, July 2006.

[56] Erin A Henslee, Michael B Sano, Andrea D Rojas, Eva M Schmelz, and Rafael V Davalos. Selective concentration of human cancer cells using contactless dielectrophoresis. *Electrophoresis*, 32(18):2523–9, September 2011.

[57] C T Ho, R Z Lin, W Y Chang, H Y Chang, and C H Liu. Rapid heterogeneous liver-cell on-chip patterning via the enhanced field-induced dielectrophoresis trap. *Lab on a Chip*, 6(6):724–734, June 2006.

[58] Lo-Chang Hsiung, Chi-Ling Chiang, Chen-Ho Wang, Yu-Hsu Huang, Ching-Te Kuo, Ji-Yen Cheng, Ching-Hung Lin, Victoria Wu, Hsien-Yeh Chou, De-Shien Jong, Hsinyu Lee, and Andrew M Wo. Dielectrophoresis-based cellular microarray chip for anticancer drug screening in perfusion microenvironments. *Lab on a Chip*, 11(14):2333–42, July 2011.

[59] Chao Huang, He Liu, Neil H Bander, and Brian J Kirby. Enrichment of prostate cancer cells from blood cells with a hybrid dielectrophoresis and immunocapture microfluidic system. *Biomedical Microdevices*, 15(6):941–8, December 2013.

[60] Chao Huang, Steven M Santana, He Liu, Neil H Bander, Benjamin G Hawkins, and Brian J Kirby. Characterization of a hybrid dielectrophoresis and immunocapture microfluidic system for cancer cell capture. *Electrophoresis*, 34(20-21):2970–9, November 2013.

[61] Jung-Tang Huang, Guo-Chen Wang, Kuang-Ming Tseng, and Shiuh-Bin Fang. A chip for catching, separating, and transporting bio-particles with dielectrophoresis. *Journal of industrial microbiology & biotechnology*, 35(11):1551–7, 2008.

[62] Y Huang, XB Wang, FF Becker, and PR Gascoyne. Introducing dielectrophoresis as a new force field for field-flow fractionation. *Biophysical Journal*, 73(2):1118–1129, August 1997.

[63] Y Huang, J Yang, X B Wang, F F Becker, and P R C Gascoyne. The removal of human breast cancer cells from hematopoietic CD34+ stem cells by dielectrophoretic field-flow-fractionation. *Journal of Hematotherapy & Stem Cell Research*, 8(5):481–90, 1999.

[64] Y Huang, J M Yang, P J Hopkins, S Kassegne, M Tirado, A H Forster, and H Reese. Separation of simulants of biological warfare agents from blood by a miniaturized dielectrophoresis device. *Biomedical Microdevices*, 5(3):217–225, September 2003.

[65] Andrew D Hughes and Michael R King. Use of naturally occurring halloysite

nanotubes for enhanced capture of flowing cells. *Langmuir*, 26(14):12155–64, July 2010.

[66] Andrew D Hughes, Jeff Mattison, Laura T Western, John D Powderly, Bryan T Greene, and Michael R King. Microtube device for selectin-mediated capture of viable circulating tumor cells from blood. *Clinical Chemistry*, 58(5):846–53, May 2012.

[67] Kyung-A Hyun and Hyo-Il Jung. Microfluidic devices for the isolation of circulating rare cells: A focus on affinity-based, dielectrophoresis, and hydrophoresis. *Electrophoresis*, 34(7):1028–41, February 2013.

[68] DW Inglis, JA Davis, TJ Zieziulewicz, DA Lawrence, RH Austin, and JC Sturm. Determining blood cell size using microfluidic hydrodynamics. *Journal of Immunological Methods*, 329(1-2):151–156, 2008.

[69] Chun-Ping Jen, Ho-Hsien Chang, Ching-Te Huang, and Kuang-Hung Chen. A microfabricated module for isolating cervical carcinoma cells from peripheral blood utilizing dielectrophoresis in stepping electric fields. *Microsystem Technologies*, 18(11):1887–1896, April 2012.

[70] HM Ji, V Samper, Y Chen, CK Heng, TM Lim, and L Yobas. Silicon-based microfilters for whole blood cell separation. *Biomedical Microdevices*, 10(2):251–257, 2008.

[71] T B Jones and M Washizu. Multipolar dielectrophoretic and electrorotation theory. *Journal of Electrostatics*, 37(1-2):121–134, May 1996.

[72] Thomas B Jones. *Electromechanics of Particles*. Cambridge University Press, New York, NY, 1995.

[73] Yuejun Kang and Dongqing Li. Electrokinetic motion of particles and cells in microchannels. *Microfluidics and Nanofluidics*, 6(4):431–460, 2009.

[74] Yuejun Kang, Dongqing Li, Spyros A Kalams, and Josiane E Eid. DC-Dielectrophoretic separation of biological cells by size. *Biomedical microdevices*, 10(2):243–9, 2008.

[75] Unyoung Kim, Jiangrong Qian, Sophia A Kenrick, Patrick S Daugherty, and H Tom Soh. Multitarget dielectrophoresis activated cell sorter. *Analytical chemistry*, 80(22):8656–61, 2008.

[76] Unyoung Kim, Chih-Wen Shu, Karen Y Dane, Patrick S Daugherty, Jean Y J Wang, and H T Soh. Selection of mammalian cells based on their cell-cycle phase using dielectrophoresis. *Proceedings of the National Academy of Sciences of the United States of America*, 104(52):20708–12, 2007.

[77] Unyoung Kim and H Tom Soh. Simultaneous sorting of multiple bacterial targets using integrated dielectrophoretic-magnetic activated cell sorter. *Lab on a Chip*, 9(16):2313–8, 2009.

[78] Brian J Kirby. *Micro- and Nanoscale Fluid Mechanics: Transport in Microfluidic Devices*. Cambridge University Press, New York, NY, 2010.

[79] Brian J Kirby, Mona Jodari, Matthew S Loftus, Gunjan Gakhar, Erica D Pratt, Chantal Chanel-Vos, Jason P Gleghorn, Steven M Santana, He Liu, James P Smith, Vicente N Navarro, Scott T Tagawa, Neil H Bander, David M Nanus, and Paraskevi Giannakakou. Functional characterization of circulating tumor cells with a prostate-cancer-specific microfluidic device. *PLOS ONE*, 7(4):e35976, January 2012.

[80] Ok Kyung Koo, Yishao Liu, Salamat Shuaib, Shantanu Bhattacharya, Michael R Ladisch, Rashid Bashir, and Arun K Bhunia. Targeted capture of pathogenic bacteria using a mammalian cell receptor coupled with dielectrophoresis on a biochip. *Analytical chemistry*, 81(8):3094–101, 2009.

[81] Leopold Kremser, Dieter Blaas, and Ernst Kenndler. Capillary electrophoresis of biological particles: viruses, bacteria, and eukaryotic cells. *Electrophoresis*, 25(14):2282–91, 2004.

[82] Robert T Krivacic, Andras Ladanyi, Douglas N Curry, H B Hsieh, Peter Kuhn, Danielle E Bergsrud, Jane F Kepros, Todd Barbera, Michael Y Ho, Lan Bo Chen, Richard A Lerner, and Richard H Bruce. A rare-cell detector for cancer. *Proceedings of the National Academy of Sciences of the United States of America*, 101(29):10501–4, July 2004.

[83] Chin Hock Kua, Yee Cheong Lam, Isabel Rodriguez, Chun Yang, and Kamal Youcef-Toumi. Dynamic cell fractionation and transportation using moving dielectrophoresis. *Analytical chemistry*, 79(18):6975–87, September 2007.

[84] T. Kulrattanarak, R. van der Sman, C. Schron, and R. Boom. Classification and evaluation of microfluidic devices for continuous suspension fractionation. *Advances in Colloid and Interface Science*, 2008.

[85] Sathyakumar Kuntaegowdanahalli, Ali Asgar S Bhagat, Girish Kumar, and Ian Papautsky. Inertial microfluidics for continuous particle separation in spiral microchannels. *Lab on a Chip*, 9:2973–2980, 2009.

[86] Blanca H Lapizco-Encinas, Rafael V Davalos, Blake A Simmons, Eric B Cummings, and Yolanda Fintschenko. An insulator-based (electrodeless) dielectrophoretic concentrator for microbes in water. *Journal of microbiological methods*, 62(3):317–26, September 2005.

[87] Blanca H Lapizco-Encinas, Blake A Simmons, Eric B Cummings, and Yolanda Fintschenko. Dielectrophoretic concentration and separation of live and dead bacteria in an array of insulators. *Analytical chemistry*, 76(6):1571–9, March 2004.

[88] Blanca H Lapizco-Encinas, Blake A Simmons, Eric B Cummings, and Yolanda Fintschenko. Insulator-based dielectrophoresis for the selective concentration and separation of live bacteria in water. *Electrophoresis*, 25(10-11):1695–704, June 2004.

[89] K.M Lee, C Nguyen, A.B Ulrich, P.M Pour, and M.M Ouellette. Immortalization with telomerase of the Nestin-positive cells of the human pancreas. *Biochemical and Biophysical Research Communications*, 301(4):1038–1044, February 2003.

[90] U Lei, C W Huang, James Chen, C Y Yang, Y J Lo, Andrew Wo, C F Chen, and T W Fung. A travelling wave dielectrophoretic pump for blood delivery. *Lab on a chip*, 9(10):1349–56, 2009.

[91] Margaret A Leversha, Jialian Han, Zahra Asgari, Daniel C Danila, Oscar Lin, Rita Gonzalez-Espinoza, Aseem Anand, Hans Lilja, Glenn Heller, Martin Fleisher, and Howard I Scher. Fluorescence in situ hybridization analysis of circulating tumor cells in metastatic prostate cancer. *Clinical Cancer Research*, 15(6):2091–7, March 2009.

[92] H Li and R Bashir. Dielectrophoretic separation and manipulation of live and heat-treated cells of Listeria on microfabricated devices with interdigitated electrodes. *Sensors and Actuators B: Chemical*, 86(2-3):215–221, September 2002.

[93] Che-Hsin Lin, Cheng-Yan Lee, Chien-Hsiung Tsai, and Lung-Ming Fu. Novel continuous particle sorting in microfluidic chip utilizing cascaded squeeze effect. *Microfludics and Nanofluidics*, 7:499–508, 2009.

[94] Henry K Lin, Siyang Zheng, Anthony J Williams, Marija Balic, Susan Groshen, Howard I Scher, Martin Fleisher, Walter Stadler, Ram H Datar, Yu-Chong Tai,

and Richard J Cote. Portable filter-based microdevice for detection and characterization of circulating tumor cells. *Clinical Cancer Research*, 16(20):5011–8, October 2010.

[95] C X Liu, L Lagae, and G Borghs. Manipulation of magnetic particles on chip by magnetophoretic actuation and dielectrophoretic levitation. *Applied Physics Letters*, 90(18):–, April 2007.

[96] H Liu, P Moy, S Kim, Y Xia, A Rajasekaran, V Navarro, B Knudsen, and N H Bander. Monoclonal antibodies to the extracellular domain of prostate-specific membrane antigen also react with tumor vascular endothelium. *Cancer Research*, 57(17):3629–34, September 1997.

[97] Yi-Shao Liu, T M Walter, Woo-Jin Chang, Kwan-Seop Lim, Liju Yang, S W Lee, A Aronson, and R Bashir. Electrical detection of germination of viable model Bacillus anthracis spores in microfluidic biochips. *Lab on a chip*, 7(5):603–10, 2007.

[98] S. Loire and I. Mezic. *Separation of bioparticles using the travelling wave dielectrophoresis with multiple frequencies*, volume 6. IEEE, Maui, Hawaii, USA, 2003.

[99] Shyamala Maheswaran and Daniel A Haber. Circulating tumor cells: a window into cancer biology and metastasis. *Current Opinion in Genetics & Development*, 20(1):96–9, February 2010.

[100] Sendurai A Mani, Wenjun Guo, Mai-Jing Liao, Elinor Ng Eaton, Ayyakkannu Ayyanan, Alicia Y Zhou, Mary Brooks, Ferenc Reinhard, Cheng Cheng Zhang, Michail Shipitsin, Lauren L Campbell, Kornelia Polyak, Cathrin Brisken, Jing Yang, and Robert A Weinberg. The epithelial-mesenchymal transition generates cells with properties of stem cells. *Cell*, 133(4):704–15, May 2008.

[101] G. H. Marks, Y. Huang, X.-F. Zhou, and R. Pethig. Dielectrophoretic characterization and separation of micro-organisms. *Microbiology*, 140(3):585–591, March 1994.

[102] G H Markx and R Pethig. Dielectrophoretic separation of cells: Continuous separation. *Biotechnology and bioengineering*, 45(4):337–43, February 1995.

[103] M Mego, U De Giorgi, K Broglio, S Dawood, V Valero, E Andreopoulou, B Handy, J M Reuben, and M Cristofanilli. Circulating tumour cells are associated with increased risk of venous thromboembolism in metastatic breast cancer patients. *British Journal of Cancer*, 101(11):1813–6, December 2009.

[104] Jitendra N. Mehrishi and Johann Bauer. Electrophoresis of cells and the biological relevance of surface charge. *Electrophoresis*, 23(13):1984, 2002.

[105] Petra Mela, Albert van Den Berg, Yolanda Fintschenko, Eric B Cummings, Blake A Simmons, and Brian J Kirby. The zeta potential of cyclo-olefin polymer microchannels and its effects on insulative (electrodeless) dielectrophoresis particle trapping devices. *Electrophoresis*, 26(9):1792–9, May 2005.

[106] Hisham Mohamed, Leslie D. McCurdy, Donald H. Szarowski, Salvatore Duva, James N. Turner, and Michele Caggana. Development of a rare cell fractionation device: Application for cancer detection. *IEEE Transactions on Nanobioscience*, 3(4):251–256, 2004.

[107] Hisham Mohamed, James N. Turner, and Michele Caggana. Biochip for separating fetal cells from mathernal circulation. *Journal of Chromatography A*, 1162:187–192, 2007.

[108] Hui-Sung Moon, Kiho Kwon, Seung-Il Kim, Hyunju Han, Joohyuk Sohn, Soohyeon Lee, and Hyo-Il Jung. Continuous separation of breast cancer cells from blood samples using multi-orifice flow fractionation (MOFF) and dielectrophoresis (DEP). *Lab on a Chip*, 11(6):1118–25, March 2011.

[109] Hywell Morgan and Nicholas Green. *AC Electrokinetics: Colloids and Nanoparticles*. Research Studies Press, Ltd., Baldock, Hertfordshire, England, 2002.

[110] H J Mulhall, F H Labeed, B Kazmi, D E Costea, M P Hughes, and M P Lewis. Cancer, pre-cancer and normal oral cells distinguished by dielectrophoresis. *Analytical and bioanalytical chemistry*, 401(8):2455–63, November 2011.

[111] M. Munz, P. A. Baeuerle, and O. Gires. The Emerging Role of EpCAM in Cancer and Stem Cell Signaling. *Cancer Research*, 69(14):5627–5629, July 2009.

[112] Shashi K Murthy, Aaron Sin, Ronald G Tompkins, and Mehmet Toner. Effect of flow and surface conditions on human lymphocyte isolation using microfluidic chambers. *Langmuir*, 20(26):11649–55, December 2004.

[113] Sunitha Nagrath, Lecia V Sequist, Shyamala Maheswaran, Daphne W Bell, Daniel Irimia, Lindsey Ulkus, Matthew R Smith, Eunice L Kwak, Subba Digumarthy, Alona Muzikansky, Paula Ryan, Ulysses J Balis, Ronald G Tompkins, Daniel A Haber, and Mehmet Toner. Isolation of rare circulating tumour cells in cancer patients by microchip technology. *Nature*, 450(7173):1235–9, December 2007.

[114] Nicholas Navin, Jude Kendall, Jennifer Troge, Peter Andrews, Linda Rodgers, Jeanne McIndoo, Kerry Cook, Asya Stepansky, Dan Levy, Diane Esposito, Lakshmi Muthuswamy, Alex Krasnitz, W Richard McCombie, James Hicks, and Michael Wigler. Tumour evolution inferred by single-cell sequencing. *Nature*, 472(7341):90–4, April 2011.

[115] Kazuhiro Okahara, Bing Sun, and Jun ichi Kambayashi. Upregulation of prostacyclin synthesisŰrelated gene expression by shear stress in vascular endothelial cells. *Arteriosclerosis, Thrombosis, and Vascular Biology*, 1998.

[116] Klaus Pantel and Catherine Alix-Panabières. Circulating tumour cells in cancer patients: challenges and perspectives. *Trends in Molecular Medicine*, 16(9):398–406, September 2010.

[117] D Pappas and K Wang. Cellular separations: A review of new challenges in analytical chemistry. *Analytica Chimica Acta*, 601(1):26–35, October 2007.

[118] David R Parkinson, Nicholas Dracopoli, Brenda Gumbs Petty, Carolyn Compton, Massimo Cristofanilli, Albert Deisseroth, Daniel F Hayes, Gordon Kapke, Prasanna Kumar, Jerry Sh Lee, Minetta C Liu, Robert McCormack, Stanislaw Mikulski, Larry Nagahara, Klaus Pantel, Sonia Pearson-White, Elizabeth A Punnoose, Lori T Roadcap, Andrew E Schade, Howard I Scher, Caroline C Sigman, and Gary J Kelloff. Considerations in the development of circulating tumor cell technology for clinical use. *Journal of Translational Medicine*, 10(1):138, July 2012.

[119] R Pethig, L M Jakubek, R H Sanger, E Heart, E D Corson, and P J S Smith. Electrokinetic measurements of membrane capacitance and conductance for pancreatic beta-cells. *IEE Proceedings - Nanobiotechnology*, 152(6):189–93, December 2005.

[120] Brian D Plouffe, Danson N Njoka, Joscelyn Harris, Jiahui Liao, Nora K Horick, Milica Radisic, and Shashi K Murthy. Peptide-mediated selective adhesion of smooth muscle and endothelial cells in microfluidic shear flow. *Langmuir*, 23:7, 2007.

[121] Brian D Plouffe, Milica Radisic, and Shashi K Murthy. Microfluidic depletion of endothelial cells, smooth muscle cells, and fibroblasts from heterogeneous suspensions. *Lab on a Chip*, 8:11, 2008.

[122] Herbert A Pohl. *Dielectrophoresis: The behavior of neutral matter in nonuniform electric fields*. Cambridge University Press, New York, NY, 1978.

[123] Kornelia Polyak and Robert A Weinberg. Transitions between epithelial and mesenchymal states: acquisition of malignant and stem cell traits. *Nature Reviews Cancer*, 9(4):265–73, April 2009.

[124] Matthew S Pommer, Yanting Zhang, Nawarathna Keerthi, Dong Chen, James A Thomson, Carl D Meinhart, and Hyongsok T Soh. Dielectrophoretic separation of platelets from diluted whole blood in microfluidic channels. *Electrophoresis*, 29(6):1213–8, 2008.

[125] Erica D Pratt, James Hicks, Asya Stepansky, and Brian J. Kirby. Copy Number Analysis of Prostate Cancer Cells using GEDI Microdevice. *submitted*, 2014.

[126] Erica D Pratt, Chao Huang, Benjamin G Hawkins, Jason P Gleghorn, and Brian J Kirby. Rare Cell Capture in Microfluidic Devices. *Chemical Engineering Science*, 66(7):1508–22, April 2011.

[127] Sittisak Pui-ock, Mathuros Ruchirawat, and Peter Gascoyne. Dielectrophoretic field-flow fractionation system for detection of aquatic toxicants. *Analytical chemistry*, 80(20):7727–34, 2008.

[128] Michele D Pysher and Mark A Hayes. Electrophoretic and dielectrophoretic field gradient technique for separating bioparticles. *Analytical chemistry*, 79(12):4552–7, June 2007.

[129] Emilian Racila, David Euhus, Arthur J. Weiss, Chandra Rao, John McConnell, Leon W. M. M. Terstappen, and Jonathan W. Uhr. Detection and characterization of carcinoma cells in the blood. *Proceedings of the National Academy of Sciences of the United States of America*, 95(8):4589–94, 1998.

[130] Javier Ramón-Azcón, Tomoyuki Yasukawa, and Fumio Mizutani. Immunodevice for simultaneous detection of two relevant tumor markers based on separation of different microparticles by dielectrophoresis. *Biosensors & Bioelectronics*, 28(1):443–9, October 2011.

[131] Daniel Ramsköld, Shujun Luo, Yu-Chieh Wang, Robin Li, Qiaolin Deng, Omid R Faridani, Gregory A Daniels, Irina Khrebtukova, Jeanne F Loring, Louise C Laurent, Gary P Schroth, and Rickard Sandberg. Full-length mRNA-Seq from single-cell levels of RNA and individual circulating tumor cells. *Nature Biotechnology*, 30(8):777–82, August 2012.

[132] Andrew D Rhim, Emily T Mirek, Nicole M Aiello, Anirban Maitra, Jennifer M Bailey, Florencia McAllister, Maximilian Reichert, Gregory L Beatty, Anil K

Rustgi, Robert H Vonderheide, Steven D Leach, and Ben Z Stanger. EMT and dissemination precede pancreatic tumor formation. *Cell*, 148(1-2):349–61, January 2012.

[133] Andrew D Rhim, Fredrik I Thege, Steven M Santana, Timothy B Lannin, Trisha N Saha, Shannon Tsai, Lara R Maggs, Michael L Kochman, Gregory G Ginsberg, John G Lieb, Vinay Chandrasekhara, Jeffrey A Drebin, Nuzhat Ahmad, Yu-Xiao Yang, Brian J Kirby, and Ben Z Stanger. Detection of circulating pancreas epithelial cells in patients with pancreatic cystic lesions. *Gastroenterology*, 146(3):647–51, March 2014.

[134] Elizabeth R Rhoades, Rachel E Geisel, Barbara A Butcher, Sean McDonough, and David G Russell. Cell wall lipids from Mycobacterium bovis BCG are inflammatory when inoculated within a gel matrix: characterization of a new model of the granulomatous response to mycobacterial components. *Tuberculosis (Edinburgh, Scotland)*, 85(3):159–76, May 2005.

[135] J Rousselet, GH Markx, and R Pethig. Separation of erythrocytes and latex beads by dielectrophoretic levitation and hyperlayer field-flow fractionation. *Colloids and Surfaces A: Physicochemical and Engineering Aspects*, 140(1-3):209–216, September 1998.

[136] Hege G Russnes, Hans Kristian Moen Vollan, Ole Christian Lingjaerde, Alexander Krasnitz, Pär Lundin, Bjø rn Naume, Therese Sø rlie, Elin Borgen, Inga H Rye, Anita Langerø d, Suet-Feung Chin, Andrew E Teschendorff, Philip J Stephens, Susanne Må nér, Ellen Schlichting, Lars O Baumbusch, Rolf Kå resen, Michael P Stratton, Michael Wigler, Carlos Caldas, Anders Zetterberg, James Hicks, and Anne-Lise Bø rresen Dale. Genomic architecture characterizes tumor progression paths and fate in breast cancer patients. *Science Translational Medicine*, 2(38):38ra47, June 2010.

[137] Alireza Salmanzadeh, Lina Romero, Hadi Shafiee, Roberto C Gallo-Villanueva, Mark A Stremler, Scott D Cramer, and Rafael V Davalos. Isolation of prostate tumor initiating cells (TICs) through their dielectrophoretic signature. *Lab on a Chip*, 12(1):182–9, January 2012.

[138] Alireza Salmanzadeh, Michael B. Sano, Roberto C. Gallo-Villanueva, Paul C. Roberts, Eva M. Schmelz, and Rafael V. Davalos. Investigating dielectric properties of different stages of syngeneic murine ovarian cancer cells. *Biomicrofluidics*, 7(1):011809, 2013.

[139] A Sanchis, A P Brown, M Sancho, G Martínez, J L Sebastián, S Muñoz, and J M

Miranda. Dielectric characterization of bacterial cells using dielectrophoresis. *Bioelectromagnetics*, 28(5):393–401, July 2007.

[140] Michael B Sano, John L Caldwell, and Rafael V Davalos. Modeling and development of a low frequency contactless dielectrophoresis (cDEP) platform to sort cancer cells from dilute whole blood samples. *Biosensors & Bioelectronics*, 30(1):13–20, December 2011.

[141] Michael B Sano, Erin A Henslee, Eva Schmelz, and Rafael V Davalos. Contactless dielectrophoretic spectroscopy: examination of the dielectric properties of cells found in blood. *Electrophoresis*, 32(22):3164–71, November 2011.

[142] Steven M Santana, He Liu, Neil H Bander, Jason P Gleghorn, and Brian J Kirby. Immunocapture of prostate cancer cells by use of anti-PSMA antibodies in microdevices. *Biomedical Microdevices*, 14(2):401–7, April 2012.

[143] T Schnelle, T Muller, C Reichle, and G Fuhr. Combined dielectrophoretic field cages and laser tweezers for electrorotation. *Applied Physics B-Lasers and Optics*, 70(2):267–274, February 2000.

[144] Palaniappan Sethu, Aaron Sin, and Mehmet Toner. Microfluidic diffusive filter for apheresis (leukapheresis). *Lab on a Chip*, 6:83–89, 2005.

[145] Palaniappan Sethu, Aaron Sin, and Mehmet Toner. Microfluidic diffusive filter for apheresis (leukapheresis). *Lab on a Chip*, 6(1):83–9, January 2006.

[146] David R Shaffer, Margaret A Leversha, Daniel C Danila, Oscar Lin, Rita Gonzalez-Espinoza, Bin Gu, Aseem Anand, Katherine Smith, Peter Maslak, Gerald V Doyle, Leon W M M Terstappen, Hans Lilja, Glenn Heller, Martin Fleisher, and Howard I Scher. Circulating tumor cell analysis in patients with progressive castration-resistant prostate cancer. *Clinical Cancer Research*, 13(7):2023–9, April 2007.

[147] Hadi Shafiee, Michael B Sano, Erin A Henslee, John L Caldwell, and Rafael V Davalos. Selective isolation of live/dead cells using contactless dielectrophoresis (cDEP). *Lab on a Chip*, 10(4):438–45, 2010.

[148] Sangjo Shim, Peter Gascoyne, Jamileh Noshari, and Katherine Stemke Hale. Dynamic physical properties of dissociated tumor cells revealed by dielectrophoretic field-flow fractionation. *Integrative Biology*, 3(8):850–62, August 2011.

[149] Sangjo Shim, Katherine Stemke-Hale, Jamileh Noshari, Frederick F. Becker, and

Peter R. C. Gascoyne. Dielectrophoresis has broad applicability to marker-free isolation of tumor cells from blood by microfluidic systems. *Biomicrofluidics*, 7(1):011808, 2013.

[150] Sangjo Shim, Katherine Stemke-Hale, Apostolia M. Tsimberidou, Jamileh Noshari, Thomas E. Anderson, and Peter R. C. Gascoyne. Antibody-independent isolation of circulating tumor cells by continuous-flow dielectrophoresis. *Biomicrofluidics*, 7(1):011807, 2013.

[151] Aaron Sin, Shashi K Murthy, Alexander Revzin, Ronald G Tompkins, and Mehmet Toner. Enrichment using antibody-coated microfluidic chambers in shear flow: model mixtures of human lymphocytes. *Bioengineering and Biotechnology*, 91(7):816–826, 2005.

[152] James P Smith, Alexander C Barbati, Steven M Santana, Jason P Gleghorn, and Brian J Kirby. Microfluidic transport in microdevices for rare cell capture. *Electrophoresis*, 33(21):3133–42, July 2012.

[153] James P Smith, Timothy B Lannin, Yusef Syed, Steven M Santana, and Brian J Kirby. Parametric control of collision rates and capture rates in geometrically enhanced differential immunocapture (GEDI) microfluidic devices for rare cell capture. *Biomedical Microdevices*, 16(1):143–51, February 2014.

[154] Jeffrey SooHoo and Glenn Walker. Microfluidic liquid filters for leukocyte isolation. *Proceedings of the 29th Annual International Conference of the IEEE EMBS*, 2007.

[155] Shannon L Stott, Chia-Hsien Hsu, Dina I Tsukrov, Min Yu, David T Miyamoto, Belinda A Waltman, S Michael Rothenberg, Ajay M Shah, Malgorzata E Smas, George K Korir, Frederick P Floyd, Anna J Gilman, Jenna B Lord, Daniel Winokur, Simeon Springer, Daniel Irimia, Sunitha Nagrath, Lecia V Sequist, Richard J Lee, Kurt J Isselbacher, Shyamala Maheswaran, Daniel A Haber, and Mehmet Toner. Isolation of circulating tumor cells using a microvortex-generating herringbone-chip. *Proceedings of the National Academy of Sciences of the United States of America*, 107(43):18392–7, October 2010.

[156] Shannon L Stott, Richard J Lee, Sunitha Nagrath, Min Yu, David T Miyamoto, Lindsey Ulkus, Elizabeth J Inserra, Matthew Ulman, Simeon Springer, Zev Nakamura, Alessandra L Moore, Dina I Tsukrov, Maria E Kempner, Douglas M Dahl, Chin-Lee Wu, A John Iafrate, Matthew R Smith, Ronald G Tompkins, Lecia V Sequist, Mehmet Toner, Daniel A Haber, and Shyamala Maheswaran. Isolation and characterization of circulating tumor cells from patients with localized and

metastatic prostate cancer. *Science Translational Medicine*, 2(25):25ra23, March 2010.

[157] Shannon L. Stott, Richard J. Lee, Sunitha Nagrath, Min Yu, David T. Miyamoto, Lindsey Ulkus, Elizabeth J. Inserra, Matthew Ulman, Simeon Springer, Zev Nakamura, Alessandra L. Moore, Dina I. Tsukrov, Maria E. Kempner, Douglas M. Dahl, Chin-Lee Wu, A. John Iafrate, Matthew R. Smith, Ronald G. Tompkins, Lecia V. Sequist, Mehmet Toner, Daniel A. Haber, and Shyamala Maheswara. Isolation and characterization of circulating tumor cells from patients with localized and metastatic prostate cancer. *Science and Translational Medicine*, 2010.

[158] Tao Sun, Hywel Morgan, and Nicolas Green. Analytical solutions of ac electrokinetics in interdigitated electrode arrays: Electric field, dielectrophoretic and traveling-wave dielectrophoretic forces. *Physical Review E*, 76(4), October 2007.

[159] Chien-Hsuan Tai, Suz-Kai Hsiung, Chih-Yuan Chen, Mei-Lin Tsai, and Gwo-Bin Lee. Automatic microfluidic platform for cell separation and nucleus collection. *Biomedical microdevices*, 9(4):533–43, August 2007.

[160] M S Talary, J P H Burt, J A Tame, and R Pethig. Electromanipulation and separation of cells using travelling electric fields. *Journal of Physics D-Applied Physics*, 29(8):2198–2203, August 1996.

[161] Fredrik I Thege, Timothy B Lannin, Trisha N Saha, Shannon Tsai, Michael L Kochman, Michael A Hollingsworth, Andrew D Rhim, and Brian J Kirby. Microfluidic immunocapture of circulating pancreatic cells using parallel EpCAM and MUC1 capture: characterization, optimization and downstream analysis. *Lab on a Chip*, 14(10):1775–84, May 2014.

[162] Ryan T Turgeon and Michael T Bowser. Micro free-flow electrophoresis: theory and applications. *Analytical and bioanalytical chemistry*, 394(1):187–98, 2009.

[163] S Usami, H H Chen, Y Zhao, S Chien, and R Skalak. Design and construction of a linear shear stress flow chamber. *Annals of Biomedical Engineering*, 21(1):77–83, January 1993.

[164] M D Vahey and J Voldman. An equilibrium method for continuous-flow cell sorting using dielectrophoresis. *Analytical chemistry*, 80(9):3135–43, May 2008.

[165] V VanDelinder and A Groisman. Separation of plasma from whole human blood in a continuous cross-flow in a molded microfluidic device. *Analytical Chemistry*, 78(11):3765–3771, 2006.

[166] V VanDelinder and A Groisman. Perfusion in microfluidic cross-flow: Separation of white blood cells from whole blood and exchange of medium in a continuous flow. *Analytical Chemistry*, 79(5):2023–2030, 2007.

[167] Joel Voldman. Electrical forces for microscale cell manipulation. *Annual Review of Biomedical Engineering*, 8:425–54, January 2006.

[168] Jody Vykoukal, Daynene M Vykoukal, Susanne Freyberg, Eckhard U Alt, and Peter R C Gascoyne. Enrichment of putative stem cells from adipose tissue using dielectrophoretic field-flow fractionation. *Lab on a chip*, 8(8):1386–93, 2008.

[169] Yuan Wan, Jifu Tan, Waseem Asghar, Young-tae Kim, Yaling Liu, and Samir M Iqbal. Velocity effect on aptamer-based circulating tumor cell isolation in microfluidic devices. *The Journal of Physical Chemistry B*, 115(47):13891–6, December 2011.

[170] Shutao Wang, Kan Liu, Jian Liu, Zeta T-F Yu, Xiaowen Xu, Libo Zhao, Tom Lee, Eun Kyung Lee, Jean Reiss, Yi-Kuen Lee, Leland W K Chung, Jiaoti Huang, Matthew Rettig, David Seligson, Kumaran N Duraiswamy, Clifton K-F Shen, and Hsian-Rong Tseng. Highly efficient capture of circulating tumor cells by using nanostructured silicon substrates with integrated chaotic micromixers. *Angewandte Chemie International Edition*, 50(13):3084–8, March 2011.

[171] Shutao Wang, Hao Wang, Jing Jiao, Kuan-Ju Chen, Gwen E Owens, Ken-ichiro Kamei, Jing Sun, David J Sherman, Christian P Behrenbruch, Hong Wu, and Hsian-Rong Tseng. Three-dimensional nanostructured substrates toward efficient capture of circulating tumor cells. *Angewandte Chemie International Edition*, 48(47):8970–3, January 2009.

[172] X B Wang, Y Huang, J P H Burt, G H Markx, and R Pethig. Selective Dielectrophoretic Confinement of Bioparticles in Potential-Energy Wells. *Journal of Physics D-Applied Physics*, 26(8):1278–1285, August 1993.

[173] X J Wang, X B Wang, and P R C Gascoyne. General expressions for dielectrophoretic force and electrorotational torque derived using the Maxwell stress tensor method. *Journal of Electrostatics*, 39(4):277–295, August 1997.

[174] X J Wang, J Yang, and P R C Gascoyne. Role of peroxide in AC electrical field exposure effects on Friend murine erythroleukemia cells during dielectrophoretic manipulations. *Biochimica Et Biophysica Acta-General Subjects*, 1426(1):53–68, January 1999.

[175] XB Wang, Y Huang, X Wang, FF Becker, and PR Gascoyne. Dielectrophoretic manipulation of cells with spiral electrodes. *Biophysical Journal*, 72(4):1887–1899, April 1997.

[176] Xiao-Bo Wang, Jun Yang, Ying Huang, Jody Vykoukal, Frederick F. Becker, and Peter R. C. Gascoyne. Cell Separation by Dielectrophoretic Field-flow-fractionation. *Analytical Chemistry*, 72(4):832–839, 2000.

[177] Zuankai Wang, Sau Yin Chin, Curtis D Chin, John Sarik, Martiza Harper, Jessica Justman, and Samuel K Sia. Microfluidic cd4+ t-cell counting device using chemiluminescence-based detection. *Analytical Chemistry*, 82:39–40, 2010.

[178] Florian Wernig, Manuel Mayr, and Qingbo Xu. Mechanical stretch-induced apoptosis in smooth muscle cells is mediated by SS1-integrin signaling pathways. *Hypertension*, 2003.

[179] Liqun Wu, Lin-Yue Lanry Yung, and Kian-Meng Lim. Dielectrophoretic capture voltage spectrum for measurement of dielectric properties and separation of cancer cells. *Biomicrofluidics*, 6(1):14113, March 2012.

[180] Zhigang Wu, Ben Willing, Joakim Bjerketorp, Janet K. Jansson, and Klas Hjort. Soft inertial microfluidics for high throughput separation of bacteria from human blood cells. *Lab on a Chip*, 9:1193–1199, 2009.

[181] Ye Xu, Joseph A Philips, Jilin Yan, Qingge Li, Z. Hugh Fan, and Weihong Tan. Aptamer-based microfluidic device for enrichment, sorting, and detection of multiple cancer cells. *Analytical Chemistry*, 81:7436–7442, 2009.

[182] Fang Yang, Xiaoming Yang, Hong Jiang, and Guiren Wang. Cascade and staggered dielectrophoretic cell sorters. *Electrophoresis*, 32(17):2377–84, August 2011.

[183] J Yang, Y Huang, X J Wang, X B Wang, F F Becker, and P R C Gascoyne. Dielectric properties of human leukocyte subpopulations determined by electrorotation as a cell separation criterion. *Biophysical Journal*, 76(6):3307–3314, June 1999.

[184] J Yang, Y Huang, XB Wang, FF Becker, and PRC Gascoyne. Differential Analysis of Human Leukocytes by Dielectrophoretic Field-Flow-Fractionation. *Biophysical Journal*, 78(5):2680–2689, 2000.

[185] Jun Yang, Ying Huang, Xiao-Bo Wang, Frederick F. Becker, and Peter R. C. Gascoyne. Cell Separation on Microfabricated Electrodes Using Di-

electrophoretic/Gravitational Field-Flow Fractionation. *Analytical Chemistry*, 71(5):911–918, March 1999.

[186] Liju Yang. Dielectrophoresis assisted immuno-capture and detection of food-borne pathogenic bacteria in biochips. *Talanta*, 80(2):551–8, 2009.

[187] Liju Yang, Padmapriya P Banada, Mohammad R Chatni, Kwan Seop Lim, Arun K Bhunia, Michael Ladisch, and Rashid Bashir. A multifunctional micro-fluidic system for dielectrophoretic concentration coupled with immuno-capture of low numbers of Listeria monocytogenes. *Lab on a Chip*, 6(7):896–905, 2006.

[188] Min Yu, David T Ting, Shannon L Stott, Ben S Wittner, Fatih Ozsolak, Suchis-mita Paul, Jordan C Ciciliano, Malgorzata E Smas, Daniel Winokur, Anna J Gilman, Matthew J Ulman, Kristina Xega, Gianmarco Contino, Brinda Alage-san, Brian W Brannigan, Patrice M Milos, David P Ryan, Lecia V Sequist, Nabeel Bardeesy, Sridhar Ramaswamy, Mehmet Toner, Shyamala Maheswaran, and Daniel A Haber. RNA sequencing of pancreatic circulating tumour cells implicates WNT signalling in metastasis. *Nature*, 487(7408):510–3, July 2012.

[189] C Zhang, K Khoshmanesh, A Mitchell, and K Kalantar-Zadeh. Dielectrophoresis for manipulation of micro/nano particles in microfluidic systems. *Analytical and bioanalytical chemistry*, 396(1):401–20, January 2010.

[190] Y T Zhang, F Bottausci, M P Rao, E R Parker, I Mezic, and N C MacDonald. Titanium-based dielectrophoresis devices for microfluidic applications. *Biomed-ical Microdevices*, 10(4):509–517, January 2008.

[191] Siyang Zheng, Henry Lin, Jing-Quan Liu, Marija Balic, Ram Datar, Richard J Cote, and Yu-Chong Tai. Membrane microfilter device for selective capture, electrolysis and genomic analysis of human circulating tumor cells. *Journal of Chromatography A*, 1162(2):154–61, August 2007.

[192] Siyang Zheng, Jing-Quan Liu, and Yu-Chong Tai. Streamline-based microfluidic devices for erythrocytes and leukocytes separation. *Journal of Microelectrome-chanical systems*, 17:1029–1038, 2008.